NASA Contractor Report 198449

# Prediction of Characteristics of Two Dimensional Turbulent Wakes Under the Influence of Streamline Curvature and Zero, Positive, and Negative Pressure Gradients, Part II

M. T. Schobeiri and K.R. Pappu
*Texas A&M University*
*College Station, Texas*

January 1996

Prepared for
Lewis Research Center
Under Grant NAG3–1256


National Aeronautics and
Space Administration

## PREFACE TO FINAL REPORTS, PART II

The present report constitutes Part II of a three part research report that deals with experimental and theoretical investigations of steady and unsteady wakes and their influence on boundary layer transition. The experimental research was performed in the recently established Turbomachinery Performance and Flow Research Laboratory, a division of the Turbomachinery Laboratory of Texas A&M University.

In this part, a theoretical framework has been developed that precisely predicts the development and decay of steady and unsteady wake flows through curved as well as straight channels at positive, zero and negative pressure gradients. To compare the theory with the experiment, the results of comprehensive experimental investigations of steady and unsteady wake flows reported in Part I are utilized.

Part III reports the effects of periodic unsteady wake flow and pressure gradient on boundary layer transition along the concave surface of a curved plate. The measurements were performed on an unsteady flow research facility using a rotating cascade of rods positioned upstream of the curved plate. Boundary layer measurements using a hot-wire probe were analyzed by the ensemble-averaging technique.

*M. T. Schobeiri*
*College Station, Texas*
*March 1994*

## ABSTRACT

The development of a wake flow downstream of a cylindrical rod within a curved channel under turbomachinery flow conditions (streamline curvature, and zero, positive and negative pressure gradients) has been investigated theoretically. The theoretical framework is based on the equations of continuity and motion that are transformed into an orthogonal curvilinear coordinate system. These equations describing the wake phenomenon are solved for mean velocities, and Reynolds normal and shear stresses. The theory also describes the straight wake as a special case, for which the radius of curvature approaches infinity. To demonstrate its general validity, the theory has been compared with experimental measurements made available from the Turbomachinery Performance Laboratory at Texas A&M University as well as from the current literature.

## ACKNOWLEDGEMENT

The principal investigator and his students would like to express their sincere thanks and appreciations to Dr. R. Simoneau, Chief of Heat Transfer Branch, and Mrs. B. Lucci and the administration of the NASA Lewis Research Center for the continuous cooperation and support of this project.

## TABLE OF CONTENTS

Page

## LIST OF TABLES

## LIST OF FIGURES

Page

Page

Page

Page

Page

## NOMENCLATURE

| | | |
|---|---|---|
| b | = | wake width |
| B | = | half the height of the test section (refer to Fig.4) |
| c | = | constant of integration |
| $C_w$ | = | drag coefficient |
| d | = | diameter of cylinder, the wake generating body |
| erf | = | error function |
| $\vec{g}^i$ | = | contravariant base vectors |
| $\vec{g}_i$ | = | covariant base vectors |
| $g^{ij}$, $g_{ij}$ | = | contravariant and covariant metric coefficients |
| h | = | height of the curved channel (refer to Fig.3) |
| $p_i$ | = | static pressure at station i |
| $\frac{\partial \bar{p}}{\partial \xi_1}$ | = | mean streamwise pressure gradient |
| $\vec{r}$ | = | radius vector for wake development |
| R | = | radius of curvature of wake centerline |
| $u$ | = | time dependent physical component in $\xi_1$ direction |
| $\bar{U}$ | = | time averaged physical component in $\xi_1$ direction = $\bar{V}^1$ |
| $U_\infty$ | = | potential flow velocity in $\xi_1$ direction |
| $\bar{U}_1$ | = | wake velocity defect = $U_\infty - \bar{U}$ |
| $\bar{U}_{1m}$ | = | maximum wake velocity defect |
| $\bar{U}_1^2$ | = | wake momentum defect = $2\ U_\infty \bar{U}_1 - \bar{U}_1^2$ |
| $\bar{U}_{1m}^2$ | = | maximum wake momentum defect |

$U_{P_0}$ = hypothetical potential flow velocity at the wake center

$\bar{U}\bar{V}$ = total impulse

$\bar{U}\bar{V}$ = partial impulse

$\overline{uv}$ = Reynolds shear stress

$\bar{u}^2$ = mean longitudinal turbulent fluctuation impulse

$\bar{u}_m^2$ = mean longitudinal turbulent fluctuation impulse at the wake center

$v$ = time dependent physical component in $\xi_2$ direction

$\bar{v}^2$ = mean lateral turbulent fluctuation impulse

$\vec{V}$ = velocity vector

$\bar{\vec{V}}$ = time averaged mean velocity vector

$\tilde{\vec{V}}$ = time dependent fluctuating velocity vector

$\bar{V}_i^*$ = time averaged covariant physical components

$\bar{V}^{i*}$ = time averaged contravariant physical components

$\bar{V}$ = time averaged physical component in $\xi_2$ direction = $\bar{V}^{2*}$

$V^1$ = contravariant velocity component in $\xi_1$ direction

$V^2$ = contravariant velocity component in $\xi_2$ direction

$\bar{w}^2$ = mean spanwise turbulent fluctuation impulse

$\vec{W}$ = drag force

x/d = measurement stations located downstream of wake, identical with $\frac{\xi_1}{d}$

$\nabla = \vec{g}^i \frac{\partial}{\partial \xi_i}$

$\xi_i$ = curvilinear coordinate system

$\rho$ = density of air

$\Gamma^k_{ij}$ = Christoffel symbols

$\zeta$ = dimensionless variable, $\xi_2 / b$

$\varphi_1$ = nondimensional wake velocity defect

$\varphi^2$ = nondimensional wake momentum defect

$\psi$ = nondimensional longitudinal turbulent fluctuation impulse

**Subscripts, superscripts**

i, j, k = tensor indices

# 1. INTRODUCTION

The turbulent wake flow constitutes a special case of free turbulent shear flow with wide ranging applications in the fields of science and engineering. In turbomachinery, the wakes shed by upstream blade rows considerably influence the boundary layer development and the heat transfer characteristics of the blades downstream of the wake. The wake flow at the entrance of the diffuser, initiated by an obstruction in the flow field such as a blade or a strut, greatly affects the overall performance of the diffuser, depending upon the wake development. If the pressure gradient is sufficiently high, the wake flow could lead to stagnation-pressure variations resulting in diffuser stall (Hill, 1963). The wake flow also considerably influences the pressure distribution on airfoils and thus is of great practical interest, especially on wings made of multi-element airfoils. Due to a significant impact on efficiency and performance of turbomachines, the wake development associated with inherent unsteadiness induced by mutual interaction between stator and rotor has naturally attracted the interest of many researchers and resulted in an abundance of publications. However, there is little literature concerning the theoretical framework for cylinder wake characteristics under turbomachinery flow conditions, aside from cases dealing with straight channel and no streamwise pressure gradient.

Under turbomachinery flow conditions, the wakes undergo massive distortion due to the effects of streamline curvature of blades and pressure gradients. The curvature and pressure gradient greatly influence the growth of wake width, maximum wake velocity defect, mean velocities, and turbulent characteristics of wakes. Because of the significant impact of curvature and pressure gradients on the wake development phenomenon, the results of research on 2-dimensional turbulent wakes in straight channel under zero streamwise pressure gradient are not readily applicable to turbomachinery flow situations.

---

The format of this document follows the ASME *Journal of Turbomachinery*.

This situation has given rise to a need for investigating the wake characteristics under turbomachinery flow conditions. The present investigation, under the supervision of Dr. T. Schobeiri, provides a theoretical basis for better understanding of wake phenomenon under the influence of streamline curvature and pressure gradients.

## 2. LITERATURE REVIEW

The study of 2-dimensional wakes dates back to the 1930's, when the phenomenon was first investigated by Schlichting (1930), based on Prandtl's mixing length hypothesis. Assuming that 1) the mixing length is proportional to the wake width, and 2) velocity profiles are similar for larger downstream distances, and by making some assumptions in agreement with the power laws for wake width and maximum wake defect velocity, Schlichting derived expressions for the wake width and defect velocity in a straight channel. The theoretical calculations have been compared with the measurements done by Schlichting, in the wake behind a circular cylinder. There is excellent agreement between the theory and experimental results.

Reichardt (1942) carried out both the experimental and theoretical study of the wake flow downstream of cylinder wakes and free jet flows. The measurements are in agreement with theoretical predictions. The predictions of Reichardt match quite well with the predictions of Schlichting. Reichardt (1962) also carried out the experimental investigation on wakes behind bodies of revolution in order to test the similarity of velocity profiles behind bodies of different shapes, and determined the downstream location at which the onset of similarity occurred. It was concluded that velocity distribution in a wake became independent of the shape of the body sufficiently far downstream from the body, and that the downstream location at which similarity occurred varied with the body.

Townsend (1947a) studied the turbulent wake behind a cylinder in a straight square working section, and measured the mean velocity distribution, distribution of streamwise ($u$), transverse ($v$) and spanwise ($w$) fluctuation components, as well as the statistical distribution of turbulent velocity components. The measurements indicated a rapid development and stabilization of a characteristic shape of distribution. The turbulent intensities were found to be nearly equal, except at the center of the wake where $v$ had

higher intensity than $u$ and $w$. This was explained on the qualitative grounds that the turbulent intensity at the wake center came from the conversion of energy of mean flow by diffusion from regions of shearing motion, and that this diffusion took place by movement of small bodies of fluid in the y-direction. These movements in the y-direction consequently resulted in faster transport of transverse fluctuations than the streamwise or spanwise fluctuations. From the calculations of energy in both the mean flow and the turbulent motion, Townsend concluded that complete dynamic similarity in the wake, if ever attained, occurs beyond 1000 cylinder diameters downstream where the ratio of turbulent and mean flow energies approach a constant value.

Roshko (1953), in his note on the development of turbulent wakes from vortex streets, studied wake development behind cylinders at Reynolds numbers (Re) ranging from 40 to 10000. The Reynolds number range of periodic vortex shedding is divided into two distinct sub ranges, 40-150 being the stable range where regular vortex streets are formed with no development of turbulent motion, and 150-300 being the transition range to the regime of turbulent motion called the irregular range, where turbulent velocity fluctuations accompany periodic formation of vortices. Studying the velocity fluctuations from the spectrum and statistical measurements, Roshko reported that in the stable range, the vortices decay by viscous diffusion, while in the irregular range, the diffusion is turbulent and the wake becomes fully turbulent in 40-50 cylinder diameters downstream.

Eifler (1975) carried out both the theoretical and experimental study of cylinder wake for a wide range of downstream locations and also for different diameters of cylinders in a straight channel. He derived analytical expressions for the Reynolds shear stress and the mean velocities by making use of the time-averaged continuity equation and the momentum equation. From the definition of mean velocity in the x-direction and from the continuity equation, Eifler obtained an expression for partial impulse, while integration of the x-momentum equation resulted in an expression for the total impulse. Shear stress is defined as the difference between the total impulse and partial impulse.

The theoretical predictions agree with the measurements by Eifler for defect velocity and all Reynolds stresses.

Fabris (1979) studied the far turbulent wake of a slightly heated cylinder using a specially developed four-wire probe. Full, nonlinear response equations for all four sensors, reflecting the influence of all three components of velocity and temperature, are solved simultaneously yielding instantaneous values of the three components of velocity and temperature at a given point. The streamwise fluctuating component, $u$, has a maximum at the position of maximum mean shear, $\partial U/\partial y$, where the turbulence production is the highest. The conditional average of the lateral fluctuating component is observed to have a shallow valley between two small peaks, in agreement with Eifler (1975) and in contradiction to what has been reported by Townsend (1946), who reported a single maximum at the wake center and values about two times higher than $\overline{u}^2$, $\overline{w}^2$. Of all the three fluctuating components, the streamwise component has the highest peak, since it absorbs energy directly from the mean flow, while $\overline{v}^2$, $\overline{w}^2$ are much lower, but approaching the $\overline{u}^2$ level at the center of the wake. At the wake edge, fluctuations in the lateral direction are higher than the other directions, in agreement with Phillips' (1955) theory for potential fluctuations. According to Phillips, outside a stationary 2D turbulent flow region, the intensity of each of three components of induced potential fluctuations decays as lateral distance to the "one-fourth" power. But in the intermittent region, lateral fluctuations were not found to be equal to the sum of the streamwise and spanwise fluctuations.

Hebbar (1986) carried out measurements for defect velocity and Reynolds stresses of boundary layer development on a symmetric airfoil, subsequent merging of the boundary layer into a wake, and the development of wake downstream of the trailing edge, with the focus of study on the change over of wall turbulence to free turbulence. A careful observation of the distributions of streamwise and lateral intensities reveal that the characteristic peaks close to the center of the wake disappear beyond a downstream

distance of 50 times the momentum thickness of the trailing edge, and so he predicted that a value of 50 for the momentum thickness of the trailing edge as the limit beyond which the wake structure changes from wall turbulence to free turbulence. He also noticed initial overshoots in turbulent intensities and no tendency towards similarity in wake characteristics over the range of experimental study.

Turbulent flow with streamline curvature finds many applications in the field of turbomachinery, especially in knowing the heat and momentum transfer in boundary layers noticeable on turbomachine blades. This has been systematically investigated by Wattendorf (1935), Thomann (1968), and many others. Thomann (1968), in his study of streamline wall curvature on heat transfer in a turbulent boundary layer, showed a considerable increase in heat transfer on a concave surface compared to that on a convex surface.

Wattendorf (1935) in his study on the effect of curvature on fully developed turbulent flow, carried out experiments in two different curved channels of different curvatures. Strong influence of curvature on velocity distributions has been reported. Rayleigh's (1916) stability criteria are considered valid, as evidenced by the calculations of mixing length and exchange factor. According to Rayleigh's stability criterion, instability and increased mixing at the outer walls of the curved channels, and stability and decreased mixing at the inner walls occur in a flow along a curved path which has been explained on a theoretical basis. If a fluid particle is displaced towards the outer walls due to a disturbing force in radial direction, then the centrifugal force of the displaced fluid element is greater than the centripetal pressure gradient. Since such a motion is unstable, the fluid particle has a tendency to move further in the same direction. Conversely, if the displacement is inward, the centrifugal force will be less than the centripetal pressure gradient, and the fluid element will be forced further inward. Similar observations have been reported by other researchers (Koyama, Savill, and others). The near and far wake characteristics of a cascade of airfoils has been studied both experimentally and analytically by Raj and Lakshminarayana (1973). From the

experimental study for three different incidence angles, they reported wake asymmetry and strong dependence of the decay of the wake defect on the variation of wake edge velocity, solidity, and incidence. Also presented were some semi-theoretical expressions for the wake profile, decay of the defect velocity, turbulence intensity, and Reynolds stress.

Bradshaw, Muck and Hoffmann (1985), in their study on the sensitivity of the boundary layer to streamline curvature, observed that convex (stabilizing) curvature tends to attenuate the pre-existing turbulence while the concave (destabilizing) curvature results in the generation of Taylor-Görtler vortices. Study of this curvature effect on turbulent wakes has been undertaken by several other researchers.

The study of the wake characteristics by Ramjee and Neelakandan (1989) involved a rectangular cylinder wake in both the straight and curved channels. The test section was such that a longitudinally curved duct was attached at the end of a straight duct with flow deflected by 90 degrees in a gradual manner. The sensitivity of wake flow to the curvature is quite evident from the pronounced changes between the straight and curved wakes in the maximum defect velocity and Reynolds stress intensities noted in the downstream side. Larger maximum defect velocity and asymmetry of the mean velocity profile were quite evident in the case of a curved duct. The lateral fluctuations are found to be more sensitive to curvature than the streamwise fluctuations. Of all the Reynolds stresses, shear stress exhibited pronounced changes with downstream distance being the most sensitive to the streamline curvature. The convex curvature has been found to exert a stabilizing influence on shear stress while the concave surface tends to attenuate the shear stress, resulting in strong asymmetry in shear stress distribution.

Koyama (1983) studied the stabilizing, destabilizing, and secondary flow effects of the streamwise curvature of a cylinder wake in a curved channel in the absence of the streamwise pressure gradient. When the wake generating cylinder was located normal to the streamline curvature (spanwise), Koyama observed asymmetry about the wake centerline in the mean velocity and turbulent intensity profiles, owing to the destabilizing

effects on inner side of the wake and stabilizing effects on the outer side. In his terminology of a curved shear flow, the motion of fluid particles is stabilized if transverse velocity gradient is positive, and destabilized if transverse velocity gradient is negative. However, the symmetry about the wake centerline is preserved when the wake generating body is placed along the streamline curvature. In this case, the radial pressure gradient produces a secondary flow, which draws fluid towards the center of the curvature from a destabilized boundary layer on the outer wall toward a stabilized boundary layer on the inner wall.

The sensitivity of the flow to the curvature and pressure gradient can best be realized from the study by Schobeiri (1976), which involved viscous flows with low Reynolds numbers in symmetric convex and concave channels. The investigation shows that the flow separation through the symmetric channel with the convex wall is more sensitive to an adverse pressure gradient than the flow through a channel with concave walls. Other investigations by Schobeiri (1980, 1990b) in asymmetric channels also show that the flow has a higher tendency to separate on the convex wall than on the concave wall in the presence of adverse pressure gradient.

Hill, Schaub and Senoo (1963) investigated the effect of an adverse pressure gradient on turbulent wakes, produced by obstructions in a flow field. Using a two dimensional diffuser of variable divergence angles, they measured time-averaged, transverse velocity and pressure distribution at five different axial locations with different axial pressure distributions. They showed experimentally that if the pressure gradient was sufficiently rapid, the wake size grew instead of decayed, leading to the stagnation flow at the center portion of the diffuser. Employing momentum integral equations and an eddy viscosity, which is uniform across the wake, they developed an expression for the wake width and also a criterion for the limiting value of a pressure gradient to prevent wake growth.

Gartshore (1967) performed the experimental investigation of the effect of adverse pressure gradients on two dimensional turbulent wakes. The data measured for the mean

velocity, longitudinal and lateral turbulence intensities, and shear stress distributions have been compared with Townsend's (1956a) data for small-deficit undistorted wake that resulted in slightly lower levels of turbulence intensities and much less shear stress. The pressure gradient in the straight channel was adjusted to get a constant ratio between the maximum wake defect velocity, $\bar{U}_{1m}$, and potential flow velocity, $U_{\infty}$, in order to study the effect of increasing the ratio on turbulent intensities and shear stress distributions. Though, in general, the effect of increasing the ratio is to lower the turbulent intensity ratios, large discrepancies were observed between measured values and those of Townsend's for the zero pressure gradient case.

Savill (1983) carried out the study of a cylinder wake that was deflected about 90 degrees by means of a back plate so that it was under the influence of both the streamwise curvature and streamwise pressure gradients. The measured data for the mean velocity and all Reynolds stress intensities indicated a strong effect due to the streamline curvature. He concluded that the study of the flow was complex owing to the coexistence of the stabilized and destabilized regions across the wake, and a strong interaction between them.

The mild curvature, in the case of Nakayama (1987), is established by placing an airfoil-like thin plate at a small angle to the free-stream direction while the qualitative separation between the effects due to the curvature and pressure gradient is achieved by placing the thin plate at both positive and negative angles to the free-stream direction. Despite the presence of a mild pressure gradient and curvature, the measured data indicate a strong sensitivity of turbulence quantities, especially the Reynolds shear stress values to the curvature and pressure gradient.

Unsteady wake flow has considerable impact on the aerodynamic and heat-transfer performance of turbomachinery blades. The aerodynamic fluctuations due to the passage of wakes shed from upstream blade rows greatly affect the heat transfer rate to the blade surface, especially in cooled gas turbines.

Pfeil and Schröder (1981) studied the wake decay downstream of a cylinder moving transverse to the main flow. Based on the laws for decay processes behind stationary cylinders, they developed a method for the computation of velocity components of a 2-dimensional cylinder wake, as a function of space coordinates and time. The results from their calculations are in agreement with their measurements, performed in a low speed wind tunnel.

Doorly and Oldfield (1985) developed a technique for the simulation of wake-passing in a turbine stage by using a rotating wake generator in front of a stationary turbine cascade. Their study revealed that the wakes undergo massive distortion due to high velocity gradients in the rotor blade passages, and there is also a very high rate of transient heat transfer because of the production of a boundary layer patch on the suction surface and subsequent sweeping along the blade surface.

O'Brien and Capp (1989) carried out an experimental study for the axial and tangential components of velocity in an unsteady turbulent flow downstream of a rotating spoked-wheel wake generator, with the focus of study on the wake response to Reynolds and Strouhal numbers. Mean axial velocities were found to be independent of Reynolds and bar-passing Strouhal numbers, while the tangential component has a stronger dependence on bar-passing Strouhal numbers.

## 3. OBJECTIVES

The objective of this research is to establish a theoretical framework for the description of two-dimensional turbulent wake development phenomena. The present theoretical framework is based on the fundamental concept developed by Schobeiri (1990a) and Schobeiri et al. (1993). Except for some theoretical work in the case of a straight channel in the absence of a streamwise pressure gradient, published by Schlichting, Reichardt and Eifler, as reviewed in the previous chapter, there has been no major attempt to explain the wake phenomenon in a curved channel under the influence of zero, positive and negative pressure gradients from a theoretical point of view.

Using tensor analysis tools, the conservation laws of fluid mechanics, such as the equation of continuity and motion, have been transformed into an orthogonal curvilinear coordinate system. The wake structure described by these equations can then be solved for the required wake characteristics, i.e. mean defect velocity, mean longitudinal and lateral velocities, and Reynolds shear and normal stresses, under the influence of streamline curvature and zero, positive and negative pressure gradients. Straight channel wake flow is to be treated as a special case of curved channel wake flow for which the radius of curvature approaches infinity. To show general validity of the theory, it has to be verified with experimental measurements carried out at the Turbomachinery Performance Laboratory at Texas A&M University, as well as appropriate selections from literature.

## 4. COORDINATE TRANSFORMATIONS

In order to transform the coordinate invariant conservation laws of fluid mechanics into an orthogonal curvilinear coordinate system, it is necessary to build up necessary transformation parameters such as covariant, contravariant base vectors, metric coeffcients, and Christoffel symbols using tensor analysis tools. The derivation of these parameters has been dealt with in this chapter, based on the concept laid out by Schobeiri (1990).

In Fig. 1, the radius vector for the wake development is described by:

$$\vec{r} = (R+\xi_2)\cos(\theta_0-\frac{\xi_1}{R})\,\vec{e}_1 + (R+\xi_2)\sin(\theta_0-\frac{\xi_1}{R})\,\vec{e}_2 \tag{4.1}$$

where $\xi_i$ is the curvilinear coordinate system and $\theta_0$ an arbitrary initial angle. The co- and contravariant base vectors in $\xi_i$ directions are calculated from Eq. (4.1) as:

$$\vec{g}_1 = \frac{\partial \vec{r}}{\partial \xi_1} = (\frac{R+\xi_2}{R})\sin(\theta_0-\frac{\xi_1}{R})\vec{e}_1 - (\frac{R+\xi_2}{R})\cos(\theta_0-\frac{\xi_1}{R})\vec{e}_2 \tag{4.2}$$

$$\vec{g}_2 = \frac{\partial \vec{r}}{\partial \xi_2} = \cos(\theta_0-\frac{\xi_1}{R})\vec{e}_1 + \sin(\theta_0-\frac{\xi_1}{R})\vec{e}_2 \tag{4.3}$$

$$\vec{g}^{\,1} = (\frac{R}{R+\xi_2})\sin(\theta_0-\frac{\xi_1}{R})\vec{e}_1 - (\frac{R}{R+\xi_2})\cos(\theta_0-\frac{\xi_1}{R})\vec{e}_2 \tag{4.4}$$

$$\vec{g}^{\,2} = \cos(\theta_0-\frac{\xi_1}{R})\vec{e}_1 + \sin(\theta_0-\frac{\xi_1}{R})\vec{e}_2 \tag{4.5}$$

The metric coefficients and Christoffel symbols are defined as:

$$g^{ij} = \vec{g}^{\,i} \cdot \vec{g}^{\,j} \tag{4.6}$$

$$g_{ij} = \vec{g}_i \cdot \vec{g}_j \tag{4.7}$$

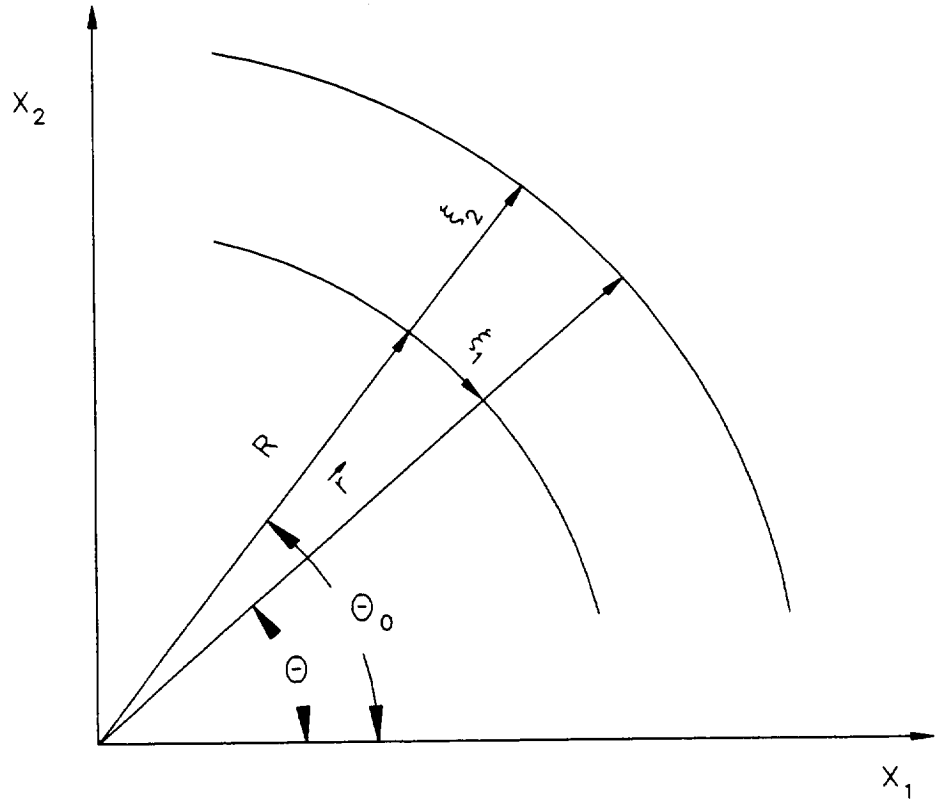


Fig. 1 Radius vector for wake development in curvilinear coordinate system

$$\Gamma^{i}_{jk} = \vec{g}_{jk} \cdot \vec{g}^{\,i} = \frac{\partial \vec{g}_j}{\partial \xi_k} \cdot \vec{g}^{\,i} \tag{4.8}$$

A direct relation between the covariant and contravariant base vectors exists. They are related with each other through metric coefficients as shown below:

$$\vec{g}^{\,i} = g^{ij}\, \vec{g}_j \tag{4.9}$$

Using Eqs. (4.2-4.5), and the definitions from Eqs. (4.6-4.8), the metric coefficients, as well as the Christoffel symbols are obtained as:

$$g_{ij} = \begin{pmatrix} (\frac{R+\xi_2}{R})^2 & 0 \\ 0 & 1 \end{pmatrix}, \quad g^{ij} = \begin{pmatrix} (\frac{R}{R+\xi_2})^2 & 0 \\ 0 & 1 \end{pmatrix} \tag{4.10}$$

$$\Gamma^{1}_{ij} = \begin{pmatrix} 0 & \frac{1}{R+\xi_2} \\ \frac{1}{R+\xi_2} & 0 \end{pmatrix}, \quad \Gamma^{2}_{ij} = \begin{pmatrix} -\frac{R+\xi_2}{R^2} & 0 \\ 0 & 0 \end{pmatrix} \tag{4.11}$$

## 5. TRANSFORMATION OF CONSERVATION LAWS

The focus of this chapter is on transformation of the equation of continuity and motion into an orthogonal curvilinear coordinate system by making use of the transformations derived in Chapter 4. The development of theory is based on the assumptions that the free turbulent flow under investigation is both two dimensional and incompressible. The molecular viscosity has been neglected in comparison to turbulent eddy viscosity, as has been verified from the experimental investigations. The conservation laws are first presented in coordinate invariant form and are then transformed to a special orthogonal curvilinear coordinate system under investigation. Starting with the law of conservation of mass, the equation of continuity in coordinate invariant form is:

$$\nabla . \vec{V} = 0 \tag{5.1}$$

As stated earlier, the molecular viscosity can be neglected in comparison with the turbulent eddy viscosity, so the equation of motion in coordinate invariant form is:

$$\vec{V} \cdot (\nabla \vec{V}) = -\frac{1}{\rho} \nabla p \tag{5.2}$$

Combining Eqs. (5.1) and (5.2) results in an appropriate version :

$$\nabla \cdot (\vec{V}\ \vec{V}) = -\frac{1}{\rho} \nabla p \tag{5.3}$$

This version is particularly useful for comparing the order of magnitude of individual terms and their contributions. For further treatment of the conservation laws, the velocity vector is decomposed into a time averaged mean and a time dependent fluctuation, i.e.

$$\vec{V} = \bar{\vec{V}} + \tilde{\vec{V}} \tag{5.4}$$

Using the above decomposition and the corresponding index notation for the curvilinear coordinate system, Eqs. (5.1)-(5.3) can be treated in a time averaged sense as discussed below.

### 5.1. Equation of Continuity

Continuity equation, governing the conservation of mass, is quite useful in deriving expressions for velocity components of the flow under investigation. Substituting $\nabla = \vec{g}^i \frac{\partial}{\partial \xi_i}$, $\vec{V} = V^j \vec{g}_j$, and the decomposition of velocity vector from Eq. (5.4) into the equation of continuity, and then time averaging the resulting equation gives rise to:

$$\nabla . \bar{V} = (\vec{g}^i \frac{\partial}{\partial \xi_i}) . (\bar{V}^j \vec{g}_j) = 0$$

The continuity equation in index notation can now be written as:

$$\nabla . \bar{V} = \bar{V}^i_{,i} + \bar{V}^i \Gamma^j_{ij} = 0 \tag{5.5}$$

For further analytical treatment of the problem, contravariant velocity components in $\xi_i$ direction are replaced with corresponding physical components which are defined as:

$$V^{i*} = \sqrt{g_{ii}}\ V^i , \qquad V_i^* = \sqrt{g^{ii}}\ V_i \tag{5.6}$$

Expanding the Eq. (5.5) over the indices results in:

$$\bar{V}^1_{,1} + \bar{V}^2_{,2} + \bar{V}^1 \Gamma^1_{11} + \bar{V}^1 \Gamma^2_{12} + \bar{V}^2 \Gamma^1_{21} + \bar{V}^2 \Gamma^2_{22} = 0$$

Using the physical components, as defined in Eq. (5.6), and Christoffel symbols from Eq. (4.11) yields:

$$\frac{\partial}{\partial \xi_1}[(\frac{R}{R+\xi_2})\ \bar{V}^{1*}] + \frac{\partial}{\partial \xi_2}(\bar{V}^{2*}) + (\frac{1}{R+\xi_2})\ \bar{V}^{2*} = 0$$

Introducing $\bar{U}$ and $\bar{V}$ for time averaged physical components of $V^i$ results in:

$$\frac{R}{R+\xi_2}\,\bar{U}_{,1} + \bar{V}_{,2} + \frac{1}{R+\xi_2}\,\bar{V} = 0$$

$$\frac{\partial \bar{U}}{\partial \xi_1} + \frac{\partial}{\partial \xi_2}\left[(1+\frac{\xi_2}{R})\bar{V}\right] = 0 \qquad (5.7)$$

Given one of the velocity components, the above equation is quite useful in obtaining an expression for the other component of velocity.

**5.2. Equation of Motion, Version 1**

Using Eq. (5.4) in Eq. (5.2) and time averaging the resulting equation yields:

$$\bar{V}.\nabla\bar{V} + \overline{\tilde{V}.\nabla\tilde{V}} = -\frac{1}{\rho}\nabla\bar{p} \qquad (5.8)$$

From the continuity equation:

$$\nabla.\vec{V} = 0, \text{ i.e. } \nabla.(\bar{V} + \tilde{V}) = 0$$

Multiplying the above equation with $\vec{V}$ on both sides and then averaging the resulting equation gives rise to:

$$\bar{V}(\nabla.\bar{V}) + \overline{\tilde{V}(\nabla.\tilde{V})} = 0 \qquad (5.9)$$

Again from continuity:

$$\nabla.\vec{V} = \nabla.\bar{V} + \nabla.\tilde{V} = 0 \qquad (5.10)$$

The above equation on time averaging yields:

$$\nabla.\bar{V} = 0 \qquad (5.11)$$

Making use of Eq. (5.11) in Eq. (5.9) leads to:

$$\overline{\tilde{V}(\nabla.\tilde{V})} = 0 \tag{5.12}$$

Now, adding Eq. (5.12) to Eq. (5.8) gives rise to:

$$\bar{V}.\nabla\bar{V} + \overline{\tilde{V}.\nabla\tilde{V}} + \overline{\tilde{V}(\nabla.\tilde{V})} = -\frac{1}{\rho}\nabla\bar{p}$$

This can be rewritten in concise form as:

$$\bar{V}.\nabla\bar{V} + \nabla.(\overline{\tilde{V}\tilde{V}}) = -\frac{1}{\rho}\nabla\bar{p} \tag{5.13}$$

Introducing the index notation, the equation of motion can now be written as:

$$\vec{g}_i\,[\bar{V}^j\bar{V}^i_{,j} + \bar{V}^j\bar{V}^k\,\Gamma^i_{kj}] = -\frac{1}{\rho}\vec{g}_i\,g^{ij}\bar{p}_j - [(\overline{\tilde{V}^m\tilde{V}^i})_{,m} + \overline{\tilde{V}^m\tilde{V}^i}\,\Gamma^j_{mj} + \overline{\tilde{V}^m\tilde{V}^n}\,\Gamma^i_{mn}]\,\vec{g}_i \tag{5.14}$$

Using Christoffel symbols from Eq. (4.11), the above equation in $\xi_1$, $\xi_2$ directions can be written as:

$$\bar{V}^1\bar{V}^1_{,1} + \bar{V}^2\bar{V}^1_{,2} + \frac{2}{R+\xi_2}\bar{V}^1\bar{V}^2 = -\frac{1}{\rho}\left(\frac{R}{R+\xi_2}\right)^2\bar{p}_{,1} - (\overline{\tilde{V}^1\tilde{V}^1})_{,1} - (\overline{\tilde{V}^1\tilde{V}^2})_{,2} - \frac{3}{R+\xi_2}\overline{\tilde{V}^1\tilde{V}^2}$$

$$\bar{V}^1\bar{V}^2_{,1} + \bar{V}^2\bar{V}^2_{,2} - \frac{(R+\xi_2)}{R^2}\bar{V}^1\bar{V}^1 = -\frac{1}{\rho}\bar{p}_{,2} - (\overline{\tilde{V}^1\tilde{V}^2})_{,1} - (\overline{\tilde{V}^2\tilde{V}^2})_{,2} - \frac{(\overline{\tilde{V}^2\tilde{V}^2})}{R+\xi_2} + \frac{R+\xi_2}{R^2}\overline{\tilde{V}^1\tilde{V}^1}$$

Introducing the physical components, as defined earlier in Eq. (5.6), and introducing $\bar{U}$ and $\bar{V}$ for the time averaged physical components of $V^i$, and $\overline{u^2}$, $\overline{v^2}$ and $\overline{uv}$ for the time averaged physical components of the fluctuation impulse $\overline{\tilde{V}^I\tilde{V}^J}$, the equation of motion in $\xi_1$ direction in final form is:

$$\frac{R}{R+\xi_2}\bar{U}\bar{U}_{,1} + \bar{V}\bar{U}_{,2} + \frac{\bar{U}\bar{V}}{R+\xi_2} = -\frac{1}{\rho}\left(\frac{R}{R+\xi_2}\right)\bar{p}_{,1} - \frac{R}{R+\xi_2}(\overline{u^2})_{,1} - (\overline{uv})_{,2} - \frac{2}{R+\xi_2}\overline{uv} \tag{5.15}$$

Similarly in $\xi_2$ direction:

$$\frac{R}{R+\xi_2}\,\overline{U}\overline{V}_{,1} + \overline{V}\overline{V}_{,2} - \frac{\overline{U}^2}{R+\xi_2} = -\frac{1}{\rho}\,\overline{p}_{,2} - \frac{R}{R+\xi_2}\,(\overline{uv})_{,1} - (\overline{v}^2)_{,2} - \frac{1}{R+\xi_2}\,(\overline{v}^2 - \overline{u}^2) \tag{5.16}$$

### 5.3. Equation of Motion, Version 2

The equation of continuity has been added to the equation of motion to obtain a modified version of the equation of motion, as presented in Eq. (5.3). This version is quite useful to carry out the order of magnitude of analysis of individual terms and their contributions. Introducing Eq. (5.4) into Eq. (5.3) and then time averaging the whole equation leads to second version of equation of motion in index notation:

$$\vec{g}_j\,[(\overline{V}^m\overline{V}^j)_{,m} + \overline{V}^m\overline{V}^j\,\Gamma^i_{mi} + \overline{V}^m\overline{V}^n\,\Gamma^j_{mn}] =$$

$$-\frac{1}{\rho}\,\vec{g}_j\,g^{ij}\,\overline{p}_{,i} - \vec{g}_j\,[(\overline{\tilde{V}^m\tilde{V}^j})_{,m} + \overline{\tilde{V}^m\tilde{V}^j}\,\Gamma^i_{mi} + \overline{\tilde{V}^m\tilde{V}^n}\,\Gamma^j_{mn}]$$

Expanding over the indices, the second version of equation of motion in $\xi_1$, $\xi_2$ directions respectively is:

$$(\overline{V}^1\overline{V}^1)_{,1} + (\overline{V}^2\overline{V}^1)_{,2} + \frac{3\,\overline{V}^1\overline{V}^2}{R+\xi_2} = -\frac{1}{\rho}\,\left(\frac{R}{R+\xi_2}\right)^2\overline{p}_{,1} - (\overline{\tilde{V}^1\tilde{V}^1})_{,1} - (\overline{\tilde{V}^2\tilde{V}^1})_{,2} - \frac{3\,\overline{\tilde{V}^1\tilde{V}^2}}{R+\xi_2}$$

$$(\overline{V}^1\overline{V}^2)_{,1} + (\overline{V}^2\overline{V}^2)_{,2} + \overline{V}^1\overline{V}^1\left(-\frac{R+\xi_2}{R^2}\right) + \frac{\overline{V}^2\overline{V}^2}{R+\xi_2} =$$

$$-\frac{1}{\rho}\,\overline{p}_{,2} - (\overline{\tilde{V}^1\tilde{V}^2})_{,1} - (\overline{\tilde{V}^2\tilde{V}^2})_{,2} - \frac{\overline{\tilde{V}^2\tilde{V}^2}}{R+\xi_2} - \overline{\tilde{V}^1\tilde{V}^1}\left(-\frac{R+\xi_2}{R^2}\right)$$

Introducing physical components defined in Eq. (5.6) and using Christoffel symbols from Eq. (4.11), the final form of second version of the equation of motion in $\xi_1$ direction is:

$$\frac{R}{R+\xi_2}(\bar{U}^2)_{,1} + (\bar{U}\bar{V})_{,2} + \frac{2\bar{U}\bar{V}}{R+\xi_2} = -\frac{1}{\rho}\frac{R}{R+\xi_2}\bar{p}_{,1} - \frac{R}{R+\xi_2}(\overline{u^2})_{,1} - (\overline{uv})_{,2} - \frac{2\,\overline{uv}}{R+\xi_2} \qquad (5.17)$$

Similarly in $\xi_2$ direction:

$$\frac{R}{R+\xi_2}(\bar{U}\bar{V})_{,1} + (\bar{V}^2)_{,2} - \frac{1}{R+\xi_2}(\bar{U}^2 - \bar{V}^2) = -\frac{1}{\rho}\bar{p}_{,2} - \frac{R}{R+\xi_2}(\overline{uv})_{,1} - (\overline{v^2})_{,2} - \frac{1}{R+\xi_2}(\overline{v^2} - \overline{u^2}) \qquad (5.18)$$

Bringing terms with similar derivatives together in Eqs. (5.17) and (5.18):

$$\frac{R}{R+\xi_2}\left(\frac{\bar{p}}{\rho} + \bar{U}^2 + \overline{u^2}\right)_{,1} + (\bar{U}\bar{V} + \overline{uv})_{,2} + \frac{2}{R+\xi_2}(\bar{U}\bar{V} + \overline{uv}) = 0 \qquad (5.19)$$

$$\frac{R}{R+\xi_2}(\bar{U}\bar{V} + \overline{uv})_{,1} + \left(\frac{\bar{p}}{\rho} + \bar{V}^2 + \overline{v^2}\right)_{,2} - \frac{1}{R+\xi_2}(\bar{U}^2 - \bar{V}^2 + \overline{u^2} - \overline{v^2}) = 0 \qquad (5.20)$$

Eqs. (5.19) and (5.20) are of practical interest for estimating the order of magnitude of individual terms. The longitudinal fluctuation velocity $|u|$ is considerably smaller than the mean velocity $\bar{U}$, as has been verified from experiments. The lateral fluctuation velocity $|v|$, however, has the same order of magnitude as the mean lateral velocity $\bar{V}$, while it is negligible compared to $\bar{U}$. From this comparison it is evident that the contributions of the fluctuation velocity momenta are negligibly small compared to the contribution of the longitudinal mean velocity momentum $\bar{U}^2$. However, the above mentioned contributions are not neglected in the present investigation.

# 6. NONDIMENSIONAL PARAMETERS

Once the differential equations governing the problem under investigation are known, the next task is to determine appropriate dimensionless parameters. Nondimensionalization of wake characteristics is useful whenever a comparison is to be done with the measurements carried out by others, as well as to check if similarity of characteristics exists or not. Similarity of characteristics means that the characteristics such as velocity profiles assume similar shapes when normalized by local velocity and width. It will be evident from following discussion that the wake width, b, has been chosen as the reference length scale in defining the dimensionless variable $\zeta$, while the maximum wake velocity defect, $\bar{U}_{1m}$, has been chosen as the reference velocity scale to normalize velocities and impulses.

## 6.1. Assumptions and Definitions

It has been assumed that from a definite distance downstream of the wake region, the velocity and momentum defect profiles are similar. This assumption implies that for arbitrarily located points on the wake center with longitudinal coordinate $\xi_1$, corresponding length scale $b = b(\xi_1)$ on the lateral coordinate, $\xi_2$ can be found to generate a dimensionless variable: $\zeta = \xi_2 / b$. Furthermore, the wake velocity defect, shown in Fig. 2, is defined as :

$$\bar{U} = U_\infty - \bar{U}_1 \tag{6.1}$$

$$\bar{U}^2 = U_\infty^2 - \bar{U}_I^2 \text{ with } \bar{U}_I^2 = 2\, U_\infty\, \bar{U}_1 - \bar{U}_1^2$$

Here, $U_\infty$ represents the hypothetical velocity distribution, which is an extension of the undisturbed wake-external velocity into the wake. In the vicinity of the wake center, the potential velocity $U_\infty$ can be approximated, the derivation of which follows from

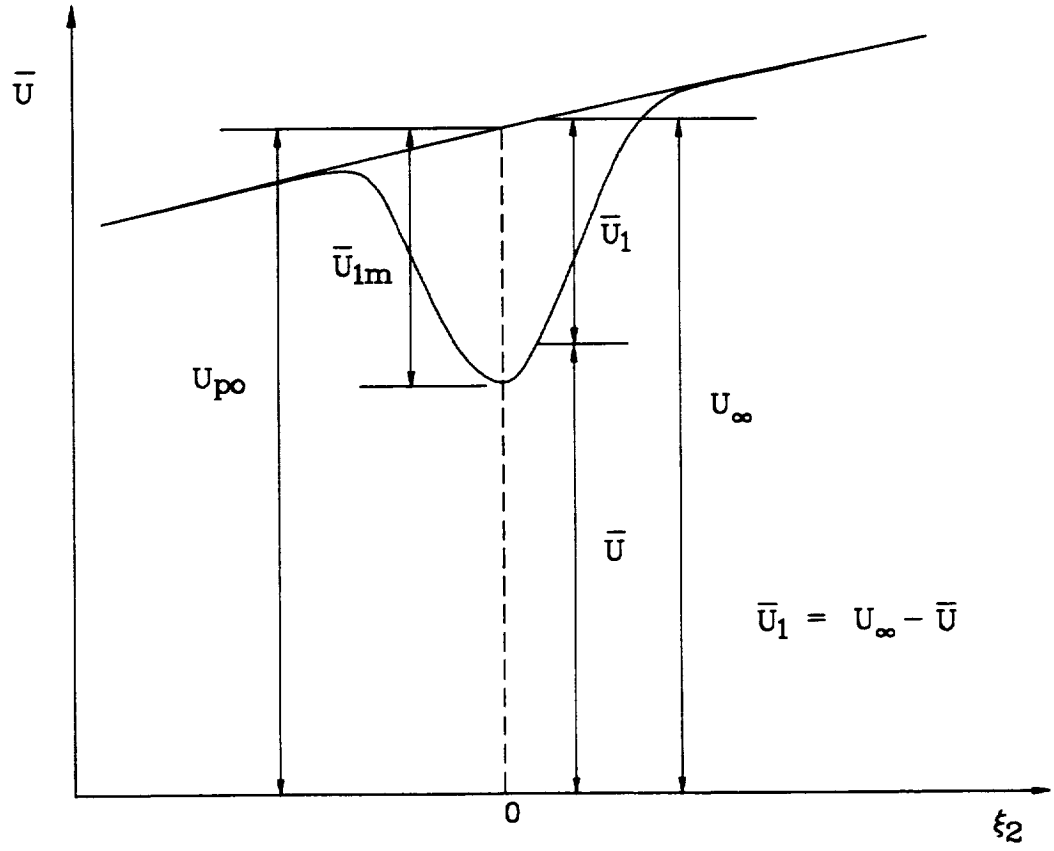


Fig. 2 Definition of nondimensional variables

equation of motion for inviscid flow. Thus, neglecting turbulent quantities for inviscid flow and for the case of zero streamwise pressure gradient, the equation of motion in $\xi_1$ direction can be written as:

$$\frac{R}{R+\xi_2}\,\bar{U}\,\frac{\partial \bar{U}}{\partial \xi_1} + \bar{V}\,\frac{\partial \bar{U}}{\partial \xi_2} + \frac{\bar{U}\bar{V}}{R+\xi_2} = 0 \tag{6.2}$$

Further assuming that variations of $\bar{U}$ in $\xi_1$ direction are quite small in comparison to the variations in $\xi_2$ direction, and $U_\infty$ represents the potential flow velocity, the above equation simplifies to:

$$\bar{V}\,\frac{\partial U_\infty}{\partial \xi_2} + \frac{U_\infty \bar{V}}{R+\xi_2} = 0 \tag{6.3}$$

Further simplification and separation into variables leads to:

$$\frac{\partial U_\infty}{U_\infty} = -\frac{\partial \xi_2}{R+\xi_2}$$

Integrating and denoting the value of the velocity at the wake center, $\xi_2 = 0$, by $U_{p0}$, in order to evaluate the constant of integration, yields:

$$U_\infty = U_{p_0}\,(1+\frac{\xi_2}{R})^{-1} \tag{6.4}$$

Expanding the expression in parenthesis as a Taylor series and neglecting higher order terms, the final expression for $U_\infty$ in the vicinity of wake center can be written as:

$$U_\infty = U_{p_0}\,(1-\frac{\xi_2}{R}) \tag{6.5}$$

Here, $U_{p0}$ is the hypothetical velocity at the wake center, $\xi_2 = 0$, thus $U_\infty$ is a function of $\xi_2$ only. The similarity assumption stated earlier requires the dimensionless wake velocity, as well as the momentum defect functions that are functions of $\zeta$ only:

$$\varphi_1 = \frac{\bar{U}_1}{\bar{U}_{1m}}, \qquad \varphi^2 = \frac{\bar{U}_I^2}{\bar{U}_{Im}^2} \tag{6.6}$$

The similarity assumption has been strongly confirmed by comprehensive experimental investigations that will be discussed later. In the above expressions, $\bar{U}_{1m}$ , $\bar{U}_{Im}^2$ represent the maximum wake velocity and momentum defects at the wake center. A definition for wake width follows from the following assumption. Setting

$\int_{-h/2}^{h/2} \bar{U}_1 \, d\xi_2 \cong \int_{-\infty}^{+\infty} \bar{U}_1 \, d\xi_2 \sim \bar{U}_{1m} \, b$ leads to the generation of an equation as:

$$\int_{-\infty}^{+\infty} \bar{U}_1 \, d\xi_2 = \gamma \, \bar{U}_{1m} b \quad \text{with } \gamma = \frac{\int_{-\infty}^{+\infty} \bar{U}_1 \, d\xi_2}{\bar{U}_{1m} b}.$$

$$\gamma = \int_{-\infty}^{+\infty} \frac{\bar{U}_1}{\bar{U}_{1m}} \frac{d\xi_2}{b} = \int_{-\infty}^{+\infty} \varphi_1 \, d\zeta = 2 \int_0^{\infty} e^{-\zeta^2} \, d\zeta = 2 \, \Gamma = 1.772$$

Thus, the definition of wake width turns out to be: $b = \frac{1}{2\Gamma} \int_{-\infty}^{+\infty} \frac{\bar{U}_1}{\bar{U}_{1m}} \, d\xi_2$ , $\zeta = \frac{\xi_2}{b}$

### 6.2. Derivation of Drag Coefficient, Curved Channel

Drag coefficient is representative of the momentum loss due to friction. Here, an expression for the drag coefficient due to the wake generating body in a curved channel is presented. This calculation enables one to establish a course for the product of maximum wake velocity defect and wake width quite easily. Of course, this is dependent upon the drag coefficient remaining constant within the channel for the case under

investigation. For the case of zero streamwise pressure gradient, it has been found to be constant from experimental investigations. The procedure for the derivation of drag coefficient in a curved channel is as follows.

With reference to Fig. 3, the drag force exerted in x-direction on the walls by the fluid for inviscid flow (outside the wake) is obtained by applying momentum balance to the control volume as:

$$(W_x)_{inviscid} = \rho V_1^2 h - \rho \int_0^h V_2^2 \cos\alpha \, dy + p_1 h - \int_0^h p_2 \cos\alpha \, dy \tag{6.7}$$

Here, $V_i$ denotes the velocity at station i, $p_i$ denotes the pressure at station i, h is the height of the channel and $\alpha$ is the inclination of the outward normal at station 2 to the horizontal. Now, considering the drag force in the x-direction by taking the wake into account gives:

$$(W_x)_{wake} = \rho V_1^2 h - \rho \int_0^h (U_2 - u_2)^2 \cos\alpha \, dy + p_1 h - \int_0^h p_2 \cos\alpha \, dy \tag{6.8}$$

$U_2$ denotes the mean velocity at station 2 that is assumed to be uniform across the control volume, while $u_2$ represents the wake velocity defect at station 2. So, the drag force due to the wake generating body, a cylinder in this case, can be obtained by subtracting Eq. (6.7) from Eq. (6.8). Thus:

$$(W_x)_{cyl} = (\rho V_1^2 h)_{wake} - (\rho V_1^2 h)_{inviscid} - \rho \int_0^h [(U_2 - u_2)^2 - V_2^2] \cos\alpha \, dy$$
$$+ [(p_1 h)_{wake} - (p_1 h)_{inviscid}] - [(\int_0^h p_2 \, dy)_{wake} - (\int_0^h p_2 \, dy)_{inviscid}] \cos\alpha \tag{6.9}$$

Assuming that the static pressure distribution within the wake is similar to that in the potential flow, which is true far downstream of the wake, and also that velocity at the inlet of the control volume is same in both the cases, the above equation simplifies to:

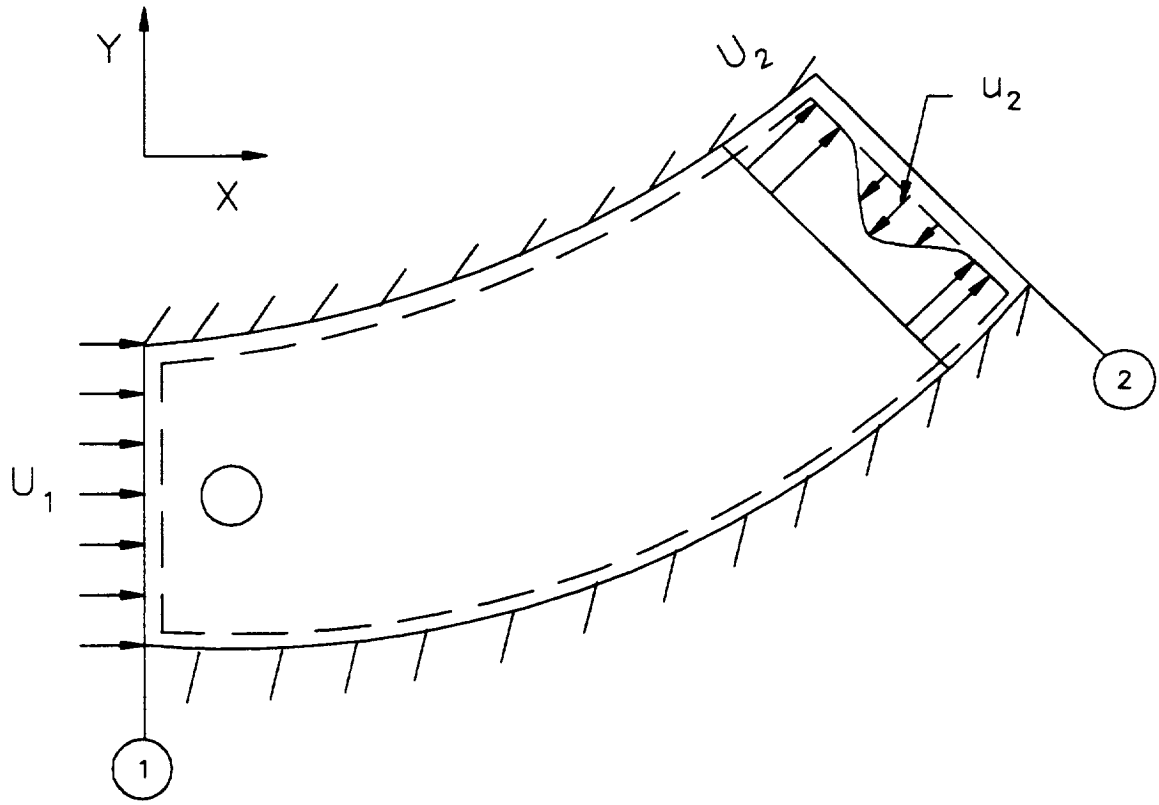


Fig. 3 Control volume for drag coefficient in curved channel

$$(W_x)_{cyl} \cong -\rho \int_0^h (U_2^2 + u_2^2 - 2U_2\, u_2 - V_2^2)\, \cos\alpha \tag{6.10}$$

Further assuming that the wake velocity defect is small in comparison with the potential flow velocity, which implies $V_2 \cong U_2$, the drag force due to the cylinder in the x-direction is:

$$(W_x)_{cyl} \cong \rho \int_0^h (2U_2\, u_2 + u_2^2)\, \cos\alpha\, dy \tag{6.11}$$

Similarly, the drag force due to the cylinder in the y-direction can be written as:

$$(W_y)_{cyl} \cong \rho \int_0^h (2U_2\, u_2 + u_2^2)\, \sin\alpha\, dy \tag{6.12}$$

If W denotes the magnitude of the total drag force due to the cylinder, the drag coefficient is given by:

$$C_W = \frac{W}{\frac{\rho}{2} U_{2max}^2\, d} = \frac{1}{d} \int_0^h \left( \frac{4U_2\, u_2}{U_{2max}^2} + \frac{2u_2^2}{U_{2max}^2} \right) dy$$

As assumed earlier, the wake velocity defect is quite small in comparison with the potential flow velocity, the above expression further simplifies to:

$$C_W = \frac{1}{d} \int_0^h \frac{4U_2\, u_2}{U_{2max}^2}\, dy = \frac{1}{d} \int_0^h 4 \frac{u_2}{U_2} \frac{U_2^2}{U_{2max}^2}\, dy \tag{6.13}$$

Introducing:

$$\varphi_2 = \frac{u_2}{u_{2m}} \text{ and } \zeta = \frac{y}{b}$$

which follow from similarity assumption, Eq. (6.13) modifies to:

$$C_W = \frac{4}{d}\, b\, \frac{u_{2m}}{U_2}\, \frac{U_2^2}{U_{2max}^2} \int_0^{\infty} \varphi_2\, d\zeta$$

The above expression shows the relation between the drag coefficient and velocity distribution inside the wake.

### 6.3. Derivation of Drag Coefficient, Straight Channel

The procedure of deriving drag coefficient for straight channel is same as that for curved channel. Applying mass balance to the control volume shown in the Fig. 4 gives:

$$2\, B\, U_1 = 2 \int_0^B (U_2 - u_2)\, dy$$

Here, $U_1$, $U_2$ represent mean velocities, assumed uniform, at inlet and exit of the control volume, while $u_2$ denotes wake velocity defect at the exit, and B represents half the height of the test section. Rewriting the above equation:

$$U_1 = U_2 - \frac{1}{B} \int_0^B u_2\, dy \tag{6.14}$$

Applying momentum balance to the same control volume results in the drag force as follows:

$$\vec{W} = \int_{S_1} d\dot{m}_1\, \vec{V}_1 + \int_{S_1} -p_1\, \vec{n}_1\, ds_1 - \int_{S_2} d\dot{m}_2\, \vec{V}_2 + \int_{S_2} -p_2\, \vec{n}_2\, ds_2 \tag{6.15}$$

Since $V_1 = U_1$ , $V_2 = U_2 - u_2$ and also $d\dot{m}_1 = \rho(U_1)h\, dy$ , $d\dot{m}_2 = \rho(U_2 - u_2)h\, dy$ Eq. (6.15) modifies to:

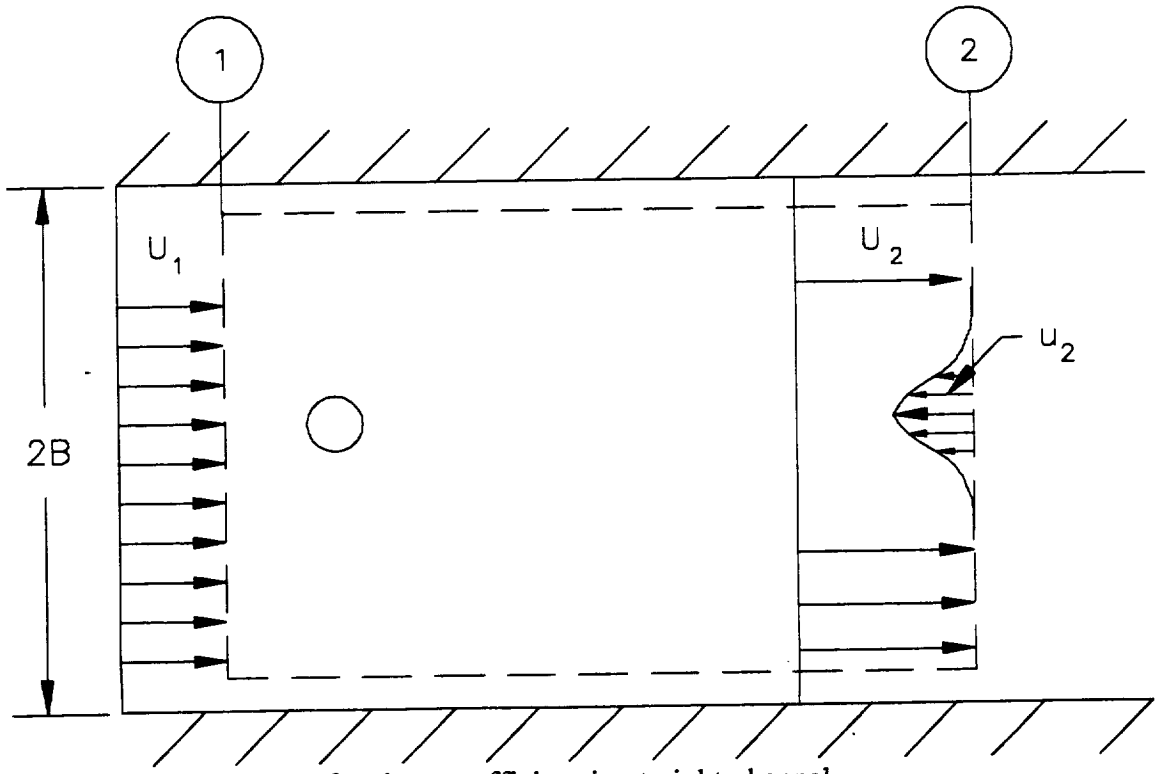


Fig. 4 Control volume for drag coefficient in straight channel

$$\vec{W} = 2\,\rho U_1^2 h\,B + 2\,p_1\,B - 2\int_0^B \rho(U_2 - u_2)h\,dy - 2\int_0^B p_2\,dy \tag{6.16}$$

Now, applying energy balance for the region outside the wake yields:

$$p_1 - p_2 = \frac{1}{2}\,\rho\,(U_2^2 - U_1^2) \tag{6.17}$$

Introducing Eqs. (6.14) and (6.17) into Eq. (6.16), and further simplifying, the resulting equation leads to:

$$\vec{W} = \rho\,[\frac{1}{B}\,(\int_0^B u_2\,dy)^2 - 2\int_0^B u_2^2\,dy + 2\,U_2\int_0^B u_2\,dy\,]$$

The drag coefficient is defined as: $C_w = \dfrac{2\,\vec{W}}{\rho\,U_2^2\,d}$ which implies:

$$C_w = \frac{2}{B\,d}\int_0^B (\frac{u_2}{U_2}\,dy)^2 - \frac{4}{d}\int_0^B (\frac{u_2}{U_2})^2\,dy + \frac{4}{d}\int_0^B \frac{u_2}{U_2}\,dy \tag{6.18}$$

For x/d > 80, contribution from the first two terms of the above equation is very small and thus Eq. (6.18) can be approximated as:

$$C_w \approx \frac{4}{d}\int_0^B \frac{u_2}{U_2}\,dy \tag{6.19}$$

Introducing the dimensionless parameter $\varphi_2 = \dfrac{u_2}{u_{2m}}$ and $\zeta = \dfrac{y}{b}$ with b as a function of

$\xi_1$, but basing only on the assumption of similarity, Eq. (6.19) is modified as:

$$C_w = \frac{4\,b}{d}\,\frac{u_{2m}}{U_2}\int_0^{\infty} \varphi_2\,d\zeta \tag{6.20}$$

# 7. WAKE CHARACTERISTICS WITHOUT PRESSURE GRADIENT

Deriving expressions for mean velocities, total impulse, partial impulse, Reynolds shear stress, and longitudinal turbulent fluctuation impulse for the wake flow under the sole influence of streamline curvature with no streamwise pressure gradient will be dealt with in this chapter. This task is based on making use of the derived transformed conservation laws and assumptions stated earlier in Chapter 5. This case of curved wake flow with zero pressure gradient is benign from a theoretical perspective, as it leads to simplified expressions for wake characteristics because of negligible contributions from many terms that appear from analytical treatment of the problem. Finally, at the end of this chapter, a summary of the expressions for wake characteristics in a straight channel is given. The straight channel wake flow is a special case of wake flow under the influence of streamline curvature in the sense that the radius of curvature approaches infinity.

## 7.1. Expression for Mean Lateral Velocity

Continuity equation dictating mass balance is used to obtain an expression for mean lateral velocity. This is possible once the velocity distribution in the streamwise direction is known. An expression for the mean velocity in longitudinal direction has already been presented in Chapter 6, i.e. in Eq. (6.1). The continuity equation in an orthogonal curvilinear coordinate system under investigation, as derived in Chapter 5, is:

$$\frac{\partial \bar{U}}{\partial \xi_1} + \frac{\partial}{\partial \xi_2}\left[\left(1+\frac{\xi_2}{R}\right)\bar{V}\right] = 0 \tag{7.1}$$

Separating the variables and integrating the above equation:

$$\left(1+\frac{\xi_2}{R}\right)\bar{V} = -\int \frac{\partial \bar{U}}{\partial \xi_1}\,\partial \xi_2 + c \tag{7.2}$$

Making use of the nondimensional parameters defined in Chapter 6, the above equation

becomes:

$$(1 + \frac{\xi_2}{R})\ \bar{V} = -\int \frac{\partial}{\partial \xi_1}[U_{P_o}(1-\frac{\xi_2}{R}) - \bar{U}_{1m}\varphi_1]\ b\ \partial\zeta + c \tag{7.3}$$

The partial derivative $\partial\varphi_1/\partial\xi_1$ can be rewritten by the chain rule as:

$$\frac{\partial\varphi_1}{\partial\xi_1} = \frac{\partial\varphi_1}{\partial\zeta}\frac{\partial\zeta}{\partial b}\frac{\partial b}{\partial\xi_1}; \qquad \frac{\partial\zeta}{\partial b} = -\frac{\zeta}{b} \tag{7.4}$$

Substituting Eq. (7.4) into Eq. (7.3) results in:

$$(1+\frac{\xi_2}{R})\ \bar{V} = \int\varphi_1\ \frac{\partial\bar{U}_{1m}}{\partial\xi_1}\ b\ d\zeta - \int\bar{U}_{1m}\ \zeta\ \frac{\partial b}{\partial\xi_1}\ \frac{\partial\varphi_1}{\partial\zeta}\ \partial\zeta - \int b\ (1-\frac{\xi_2}{R})\ \frac{\partial U_{P_o}}{\partial\xi_1}\ \partial\zeta + c \tag{7.5}$$

Adding and subtracting a term to Eq. (7.5), the above expression modifies to:

$$(1+\frac{\xi_2}{R})\ \bar{V} = -\int b\frac{\partial U_{P_o}}{\partial\xi_1}\ (1-\frac{\zeta b}{R})\ d\zeta + [\int\varphi_1\ \frac{\partial\bar{U}_{1m}}{\partial\xi_1}\ b\ d\zeta + \int\varphi_1\ \bar{U}_{1m}\frac{\partial b}{\partial\xi_1}\ \partial\zeta]$$
$$- \int\varphi_1\ \bar{U}_{1m}\frac{\partial b}{\partial\xi_1}\ \partial\zeta - \int\bar{U}_{1m}\ \zeta\ \frac{\partial b}{\partial\xi_1}\ \frac{\partial\varphi_1}{\partial\zeta}\ \partial\zeta + c \tag{7.6}$$

After some rearrangement of terms, Eq. (7.6) simplifies to:

$$(1+\frac{\xi_2}{R})\ \bar{V} = \frac{d(\bar{U}_{1m}b)}{d\xi_1}\ \int\varphi_1\ d\zeta - \frac{db}{d\xi_1}\ \bar{U}_{1m}\ \varphi_1\ \zeta - \frac{dU_{P_o}}{d\xi_1}\ b\ \int(1-\frac{\zeta\ b}{R})\ d\zeta + c \tag{7.7}$$

The development of maximum wake velocity defect, the wake width and especially their product, $\bar{U}_{1m}\ b$, is dictated by governing streamwise pressure gradient. Comprehensive experimental and theoretical investigations by Reichardt (1942), Eifler (1975) and Schobeiri et al. (1993) indicate that for wake development downstream of a single cylinder with negligible streamwise pressure gradient, the above mentioned product remains constant. For positive and negative pressure gradients, however, a pronounced

longitudinal dependency of this product has been observed. Also for the present case of zero streamwise pressure gradient, the variations of $U_{p0}$ in $\xi_1$ direction are quite small and can be neglected. Since the mean lateral velocity is zero at the wake center, it implies that the constant of integration in Eq. (7.7) becomes zero. Thus, the final form of expression for mean lateral velocity is:

$$\bar{V} = - \frac{R}{R+\xi_2} \frac{db}{d\xi_1} \bar{U}_{1m} \varphi_1 \zeta \tag{7.8}$$

### 7.2. Expression for Nondimensional Wake Velocity Defect

Assumption of similarity in wake velocity defect profiles implies that the velocity defect profiles become similar in shape when normalized by local velocity and width. Using the local length and velocity scales chosen in Chapter 6, the above assumption leads to: $\frac{\bar{U}_1}{U_{1m}} = f(\frac{\xi_2}{b}) = f(\zeta)$.

It has been shown by authors like Reichardt, Eifler and others from experimental and theoretical investigations, in a straight channel with zero streamwise pressure gradient, that the velocity distribution inside the wake can be represented by Gaussian distribution. Now, the task is to derive an expression for nondimensional wake velocity defect function by employing the equation of motion in the streamwise direction with the implementation of order of magnitude analysis carried out in Chapter 5:

$$\frac{R}{R+\xi_2} \bar{U} \frac{\partial \bar{U}}{\partial \xi_1} + \bar{V} \frac{\partial \bar{U}}{\partial \xi_2} + \frac{\bar{U}\,\bar{V}}{R+\xi_2} = -\frac{\partial(\overline{uv})}{\partial \xi_2}$$

Using the nondimensional parameters, from Chapter 6, in the above equation in addition to the following relations:

$$\frac{\partial \bar{U}}{\partial \xi_1} \equiv -\frac{\partial \bar{U}_1}{\partial \xi_1}, \qquad \frac{\partial \bar{U}}{\partial \xi_2} = -\frac{U_{P_0}}{R} - \frac{\partial \bar{U}_1}{\partial \xi_2}$$

leads to:

$$-\frac{R}{R+\xi_2}\left[U_{p_o}\left(1-\frac{\xi_2}{R}\right)-\bar{U}_1\right]\frac{\partial \bar{U}_1}{\partial \xi_1}+\bar{V}\left[\frac{-U_{p_o}}{R}-\frac{\partial \bar{U}_1}{\partial \xi_2}\right]+\frac{\left[U_{p_o}\left(1-\frac{\xi_2}{R}\right)-\bar{U}_1\right]}{R+\xi_2}\bar{V}=-\frac{\partial(\overline{uv})}{\partial \xi_2}$$

Substituting for $\bar{V}$ from Eq. (7.8) gives rise to:

$$\frac{R}{R+\zeta b}\left[-U_{p_o}\left(1-\frac{\zeta b}{R}\right)\frac{\partial(\bar{U}_{1m}\varphi_1)}{\partial \xi_1}+\bar{U}_{1m}\varphi_1\frac{\partial(\bar{U}_{1m}\varphi_1)}{\partial \xi_1}\right]+\frac{R}{R+\zeta b}\left(\frac{db}{d\xi_1}\bar{U}_{1m}\zeta\varphi_1\right)\frac{U_{p_o}}{R}+$$

$$\frac{R}{R+\zeta b}\left(\frac{db}{d\xi_1}\bar{U}_{1m}\zeta\varphi_1\right)\frac{\partial(\bar{U}_{1m}\varphi_1)}{\partial \xi_2}+\frac{R}{(R+\zeta b)^2}\left(\frac{db}{d\xi_1}\bar{U}_{1m}\zeta\varphi_1\right)\left[-U_{p_o}\left(1-\frac{\zeta b}{R}\right)+\bar{U}_{1m}\varphi_1\right]=-\frac{\partial(\overline{uv})}{\partial \xi_2} \tag{7.9}$$

From the earlier stated assumption that the variation of $\bar{U}_{1m}\,b$ is negligible for a zero streamwise pressure gradient case, the following rearrangement can be applied:

$$\frac{\partial \bar{U}_{1m}}{\partial \xi_1}=\frac{\partial(\bar{U}_{1m}\frac{b}{b})}{\partial \xi_1}=\bar{U}_{1m}\,b\,\frac{\partial(\frac{1}{b})}{\partial \xi_1}=-\frac{\bar{U}_{1m}}{b}\frac{db}{d\xi_1}$$

Using Eq. (7.4) in conjunction with the above relation, and also with the following approximation:

$$0\le\varphi_1\le 1;\qquad \varphi_1^2\ll\varphi_1;\qquad \frac{\partial\varphi_1^2}{\partial \xi_1}\ll\frac{\partial\varphi_1}{\partial \xi_1}$$

Eq. (7.9) can be treated, term by term, to get an expression for the wake velocity defect. The first term of Eq. (7.9) gets modified as:

$$\frac{R}{R+\zeta b}\left[-U_{p_o}\left(1-\frac{\zeta b}{R}\right)\frac{\partial(\bar{U}_{1m}\varphi_1)}{\partial \xi_1}+\bar{U}_{1m}\,\varphi_1\,\frac{\partial(\bar{U}_{1m}\varphi_1)}{\partial \xi_1}\right]=$$

$$\frac{R}{R+\zeta b}\left[-U_{p_o}\left(1-\frac{\zeta b}{R}\right)\varphi_1\frac{\partial \bar{U}_{1m}}{\partial \xi_1}-U_{p_o}\left(1-\frac{\zeta b}{R}\right)\bar{U}_{1m}\frac{\partial \varphi_1}{\partial \xi_1}+\frac{1}{2}\frac{\partial(\bar{U}_{1m}^{\,2}\varphi_1^2)}{\partial \xi_1}\right]=$$

$$\frac{R}{R+\zeta b}\left[-U_{p_o}\left(1-\frac{\zeta b}{R}\right)\left(\varphi_1\frac{\partial \bar{U}_{1m}}{\partial \xi_1}+\bar{U}_{1m}\frac{\partial \varphi_1}{\partial \xi_1}\right)\right]=$$

$$\frac{R}{R+\zeta b}\left[-U_{p_o}\left(1-\frac{\zeta b}{R}\right)\left(-\bar{U}_{1m}\frac{\partial \varphi_1}{\partial \zeta}\frac{\zeta}{b}\frac{db}{d\xi_1}-\frac{\bar{U}_{1m}}{b}\frac{db}{d\xi_1}\varphi_1\right)\right]=$$

$$\frac{R}{R+\zeta b}\left(\frac{\bar{U}_{1m}}{b}\frac{db}{d\xi_1}\right)\left[U_{p_o}\left(1-\frac{\zeta b}{R}\right)\frac{\partial(\zeta\varphi_1)}{\partial \zeta}\right]$$

Similarly rearranging the second term in Eq. (7.9) gives rise to:

$$\frac{R}{R+\zeta b}\left(\frac{db}{d\xi_1}\bar{U}_{1m}\zeta\varphi_1\right)\left[\frac{U_{p_o}}{R}+\frac{\partial(\bar{U}_{1m}\varphi_1)}{\partial \xi_2}\right]=$$

$$\frac{R}{R+\zeta b}\left(\frac{db}{d\xi_1}\bar{U}_{1m}\zeta\varphi_1\right)\left[\frac{U_{p_o}}{R}+\frac{\bar{U}_{1m}}{b}\frac{\partial \varphi_1}{\partial \zeta}\right]=$$

$$\frac{R}{R+\zeta b}\left(\frac{db}{d\xi_1}\frac{\bar{U}_{1m}}{b}\right)\left[\frac{U_{p_o}\,b\,\zeta\varphi_1}{R}+\bar{U}_{1m}\zeta\varphi_1\frac{\partial \varphi_1}{\partial \zeta}\right]$$

Similarly, the third term of Eq. (7.9) modifies to:

$$\frac{R}{(R+\zeta b)^2}\left(\frac{db}{d\xi_1}\bar{U}_{1m}\zeta\varphi_1\right)\left[-U_{p_o}\left(1-\frac{\zeta b}{R}\right)+\bar{U}_{1m}\varphi_1\right]=$$

$$\frac{R}{(R+\zeta b)^2}\left(\frac{db}{d\xi_1}\frac{\bar{U}_{1m}}{b}\right)\left[-U_{p_o}\left(1-\frac{\zeta b}{R}\right)b\,\zeta\varphi_1+\bar{U}_{1m}\,b\,\zeta\varphi_1^2\right]$$

Assuming that, $\overline{uv} = f_1(\xi_1)\, f_2(\varphi_1)$ , where

$$f_1(\xi_1)=\frac{1}{3}U_{p_o}\bar{U}_{1m}\frac{db}{d\xi_1};\qquad f_2(\varphi_1)=\frac{3}{2}\frac{R}{R+\zeta b}\frac{\partial \varphi_1}{\partial \zeta}$$

the fourth term in the Eq. (7.9) modifies to:

$$-\frac{\partial(\overline{uv})}{\partial\xi_2} = -\frac{\partial}{b\,\partial\zeta}\left[\frac{1}{2}\,U_{P_o}\,\bar{U}_{1m}\,\frac{db}{d\xi_1}\,\frac{R}{R+\zeta b}\,\frac{\partial\varphi_1}{\partial\zeta}\right] =$$

$$-\frac{1}{2}\,U_{P_o}\left(\frac{\bar{U}_{1m}}{b}\,\frac{db}{d\xi_1}\right)\left(\frac{R}{R+\zeta b}\right)\left[\frac{\partial^2\varphi_1}{\partial\zeta^2} - \frac{b}{R+\xi_2}\,\frac{\partial\varphi_1}{\partial\zeta}\right]$$

Bringing all portions together and neglecting non linear terms in $\varphi_1$, Eq. (7.9) takes the form:

$$U_{P_o}\left(1-\frac{\zeta b}{R}\right)\frac{\partial(\zeta\varphi_1)}{\partial\zeta} + \frac{U_{P_o}}{R}\,b\,\zeta\varphi_1 - \frac{1}{R+\zeta b}\left[U_{P_o}\left(1-\frac{\zeta b}{R}\right)b\,\zeta\varphi_1\right] =$$

$$-\frac{1}{2}\,U_{P_o}\left[\frac{\partial^2\varphi_1}{\partial\zeta^2} - \frac{b}{R+\zeta b}\,\frac{\partial\varphi_1}{\partial\zeta}\right]$$

Simplifying and rewriting:

$$\frac{\partial^2\varphi_1}{\partial\zeta^2} + \frac{\partial\varphi_1}{\partial\zeta}\left[-\frac{\frac{b}{R}}{1+\frac{b}{R}\zeta} + 2\zeta\left(1-\frac{b}{R}\zeta\right)\right] + 2\varphi_1\left[\frac{1+\frac{b^2}{R^2}\zeta^2}{1+\frac{b}{R}\zeta}\right] = 0 \qquad (7.10)$$

Setting: $\zeta=x$, $\varphi_1=y$; $\dfrac{\partial\varphi_1}{\partial\zeta} = y'$, $\dfrac{\partial^2\varphi_1}{\partial\zeta^2} = y''$

transforms Eq. (7.10) to the following ordinary differential equation:

$$y'' + y'\left[2x\left(1-\frac{b}{R}x\right) - \frac{\frac{b}{R}}{\left(1+\frac{b}{R}x\right)}\right] + 2\,y\left[\frac{1+\frac{b^2}{R^2}x^2}{1+\frac{b}{R}x}\right] = 0 \qquad (7.11)$$

The above second order ordinary differential equation has been solved numerically using the Runge-Kutta fourth order scheme. The results for different locations downstream of

the wake generating body are shown, by symbols, in Fig. 5.

For the case of a straight channel, which implies $R \rightarrow \infty$, the above differential equation in terms of $\varphi_1$ becomes:

$$\frac{\partial}{\partial \zeta}(\zeta \varphi_1) = -\frac{1}{2}\frac{\partial^2 \varphi_1}{\partial \zeta^2}$$

Integration with respect to $\zeta$ gives $\frac{\partial \varphi_1}{\partial \zeta} = -2\,\zeta \varphi_1$ .

Using the method of separation of variables and again integrating results in $\varphi_1 = e^{-\zeta^2}$.

The constant of integration is evaluated from the condition that at $\zeta = 0$, $\varphi_1 = 1$, which gives rise to:

$$\varphi_1 = e^{-\zeta^2} \tag{7.12}$$

In Fig. 5, the legend theory denotes the result of implementation of the above expression. Thus, it is obvious that Eq. (7.12) is valid within the curved channel also. It has been verified from experimental investigations that curvature and pressure gradient have little effect on this nondimensional wake velocity defect distribution and thus the validity of the expression in Eq. (7.12) in all the cases is established.

### 7.3. Expression for Partial Impulse

Partial impulse is simply the product of time-averaged mean velocities in streamwise and lateral directions. Since expressions for both these mean velocities have already been established, expression for partial impulse is obtained by taking the product of those two expressions. Therefore using Eqs. (6.1) and (7.8), the expression for the partial impulse can be written as:

$$\overline{UV} = -(U_\infty - \bar{U}_{1m}\,\varphi_1)\,\bar{U}_{1m}\,\frac{db}{d\xi_1}\zeta\varphi_1\,\frac{R}{R+\xi_2}$$

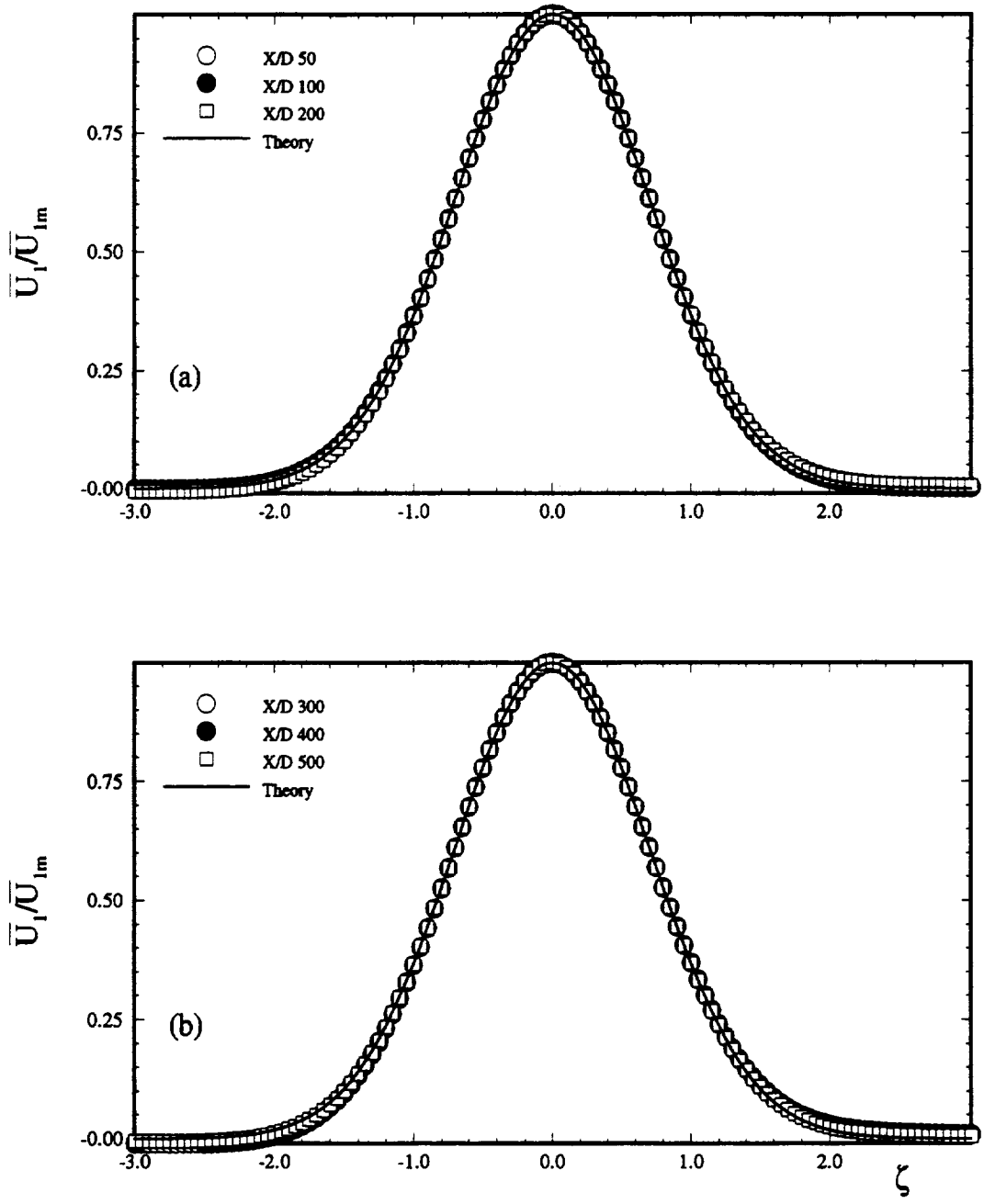


Fig. 5 Numerical solution for nondimensional wake velocity defect function in curved channel

With the approximation from Eq. (6.5), i.e. $U_\infty = U_{p_o}(1-\frac{\zeta b}{R})$, the above expression modifies to:

$$\bar{U}\bar{V} = \frac{R}{R+\xi_2}\left[- U_{p_o}\bar{U}_{1m}\frac{db}{d\xi_1}(1-\frac{\zeta b}{R})\zeta\varphi_1 + \bar{U}_{1m}^2\varphi_1^2\frac{db}{d\xi_1}\zeta\right]$$

Nondimensionalizing the above equation with square of the maximum wake velocity defect, the final expression for the partial impulse can be written as:

$$\frac{\bar{U}\bar{V}}{\bar{U}_{1m}^2} = -\frac{R}{R+\xi_2}\frac{db}{d\xi_1}\frac{U_{p_o}}{\bar{U}_{1m}}(1-\frac{\zeta b}{R})\zeta\varphi_1 + \frac{R}{R+\xi_2}\frac{db}{d\xi_1}\zeta\varphi_1^2 \qquad (7.13)$$

### 7.4. Expression for Total Impulse

Expression for total impulse is obtained by utilizing the transformed equation of motion in $\xi_1$ direction as follows. Using Eq. (5.16) with usual approximations already stated yields:

$$\frac{R}{R+\xi_2}(\bar{U}^2+\bar{u}^2)_{,1} + (\bar{U}\bar{V})_{,2} + \frac{2}{R+\xi_2}(\bar{U}\bar{V}) = -\frac{1}{\rho}\frac{R}{R+\xi_2}\frac{\partial\bar{p}}{\partial\xi_1} \qquad (7.14)$$

Let $\bar{U} = U_\infty - \bar{U}_1$

$\bar{U}^2 = U_\infty^2 - \bar{U}_I^2$ where $\bar{U}_I^2 = 2\,U_\infty\,\bar{U}_1 - \bar{U}_1^2$.

For the present case of zero streamwise pressure gradient, the term on right hand side of Eq. (7.14) vanishes. Assuming that the longitudinal turbulent fluctuation impulse is negligible in comparison with the mean momentum in streamwise direction of the flow and also that the fluctuations of the potential flow velocity in $\xi_1$ direction are very small in comparison to those in $\xi_2$ direction, i.e. $\frac{\partial U_\infty^2}{\partial\xi_1} \ll \frac{\partial U_\infty^2}{\partial\xi_2}$, $\bar{u}^2 \ll \bar{U}^2$, Eq. (7.14)

simplifies to:

$$\frac{R}{R+\xi_2}\frac{\partial}{\partial\xi_1}\left(-\bar{U}_I^2\right) = -\left(\bar{UV}\right)_{,2} - \frac{2}{R+\xi_2}\left(\bar{UV}\right)$$

This can be rewritten by some rearrangement of the terms as:

$$\frac{\partial}{\partial\xi_1}\left(\bar{U}_I^2\right) = \frac{\partial}{\partial\xi_2}\left[\left(1+\frac{\xi_2}{R}\right)\bar{UV}\right] + \frac{\left(\bar{UV}\right)}{R}$$

Assuming that $\frac{\bar{UV}}{R} \ll \frac{\partial}{\partial\xi_2}\left[\left(1+\frac{\xi_2}{R}\right)\bar{UV}\right]$ and integrating the resulting equation leads to:

$$\left(1+\frac{\xi_2}{R}\right)\bar{UV} = \int\frac{\partial}{\partial\xi_1}\left(\bar{U}_I^2\right)\partial\xi_2 + c = \int\frac{\partial}{\partial\xi_1}\left(\bar{U}_I^2\right) b\,\partial\zeta + c \qquad (7.15)$$

Now consider further treatment of the above equation by considering the term within the integration symbol, i.e.

$$\frac{\partial}{\partial\xi_1}\left(\bar{U}_I^2\right) b = \frac{\partial}{\partial\xi_1}\left(\bar{U}_{Im}^2\,\varphi^2\right) b, \text{ where } \bar{U}_{Im}^2 = 2\,U_\infty\,\bar{U}_{1m} - \bar{U}_{1m}^2\,,\quad \varphi^2 \approx \varphi_1$$

The nondimensional wake velocity (denoted by $\text{Phi}_1$ in legend table) and momentum defect (denoted by $\text{Phi}^2$ in legend table) distributions were found to be almost equal, i.e. $\varphi^2 \approx \varphi_1$, as shown in Fig. 6(a) for the zero pressure gradient case. This fact has been implemented in the following analytical treatment. This is also true for positive (Fig. 6(b)) and negative pressure gradient cases.

$$\frac{\partial}{\partial\xi_1}\left(\bar{U}_I^2\right) b = \bar{U}_{Im}^2\, b\,\frac{\partial\varphi_1}{\partial\xi_1} + b\,\varphi_1\,\frac{\partial\bar{U}_{Im}^2}{\partial\xi_1} \qquad (7.16)$$

Expanding $\partial\varphi_1/\partial\xi_1$ by chain rule and adding and subtracting a term, Eq. (7.16) modifies to:

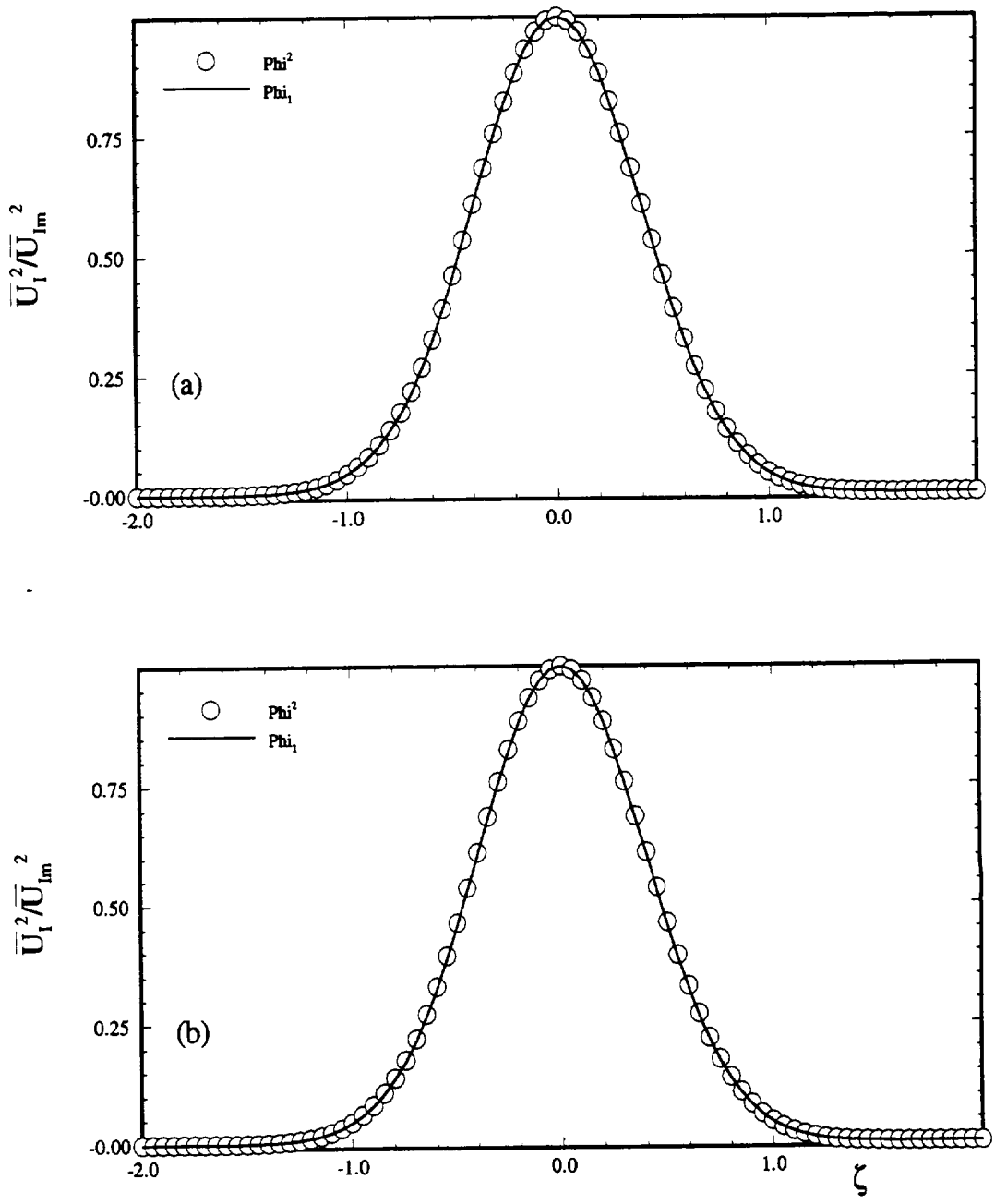


Fig. 6 Nondimensional momentum defect function for (a) zero pressure gradient and (b) positive pressure gradient cases

$$\frac{\partial}{\partial \xi_1}(\bar{U}_I^2)\, b = -\bar{U}_{Im}^2\, \zeta \frac{db}{d\xi_1}\frac{\partial \varphi_1}{\partial \zeta} + b\varphi_1 \frac{\partial \bar{U}_{Im}^2}{\partial \xi_1} + \bar{U}_{Im}^2\, \varphi_1 \frac{db}{d\xi_1} - \bar{U}_{Im}^2\, \varphi_1 \frac{db}{d\xi_1} \qquad (7.17)$$

Adding terms with similar derivatives and making using of earlier specified approximations, Eq. (7.17) reduces to:

$$\frac{\partial}{\partial \xi_1}(\bar{U}_I^2)\, b = (-2\, U_\infty\, \bar{U}_{1m} + \bar{U}_{1m}^2)\frac{db}{d\xi_1}\frac{\partial}{\partial \zeta}(\zeta \varphi^2) + \varphi^2 \frac{\partial(2\, U_\infty \bar{U}_{1m} b - \bar{U}_{1m}^2 b)}{\partial \xi_1}$$

$$\frac{\partial}{\partial \xi_1}(\bar{U}_I^2)\, b = [-2\, U_\infty\, \bar{U}_{1m}\frac{db}{d\xi_1} + \bar{U}_{1m}^2 \frac{db}{d\xi_1}]\frac{\partial}{\partial \zeta}(\zeta \varphi_1) + 2\, \bar{U}_{1m}\, b\, (1-\frac{\xi_2}{R})\varphi_1 \frac{\partial U_{P_o}}{\partial \xi_1}$$

$$+ 2\, U_\infty\, \varphi_1 \frac{\partial}{\partial \xi_1}(\bar{U}_{1m} b) - \varphi_1 \frac{\partial}{\partial \xi_1}(\bar{U}_{1m}^2 b)$$

Assuming that constant impulse requires $\bar{U}_{1m}\, b$ to be constant, $\partial U_{p_o}/\partial \xi_1 \approx 0$ for a zero pressure gradient case, implementing these approximations in the above expression, and integrating the resulting expression leads to:

$$\int \frac{\partial}{\partial \xi_1}(\bar{U}_I^2)\, b\, \partial \zeta = -2U_{p_o}\, \bar{U}_{1m}\frac{\partial b}{\partial \xi_1}\int (1-\frac{\zeta b}{R})\frac{\partial}{\partial \zeta}(\zeta \varphi_1)\, \partial \zeta +$$

$$\bar{U}_{1m}^2 \frac{\partial b}{\partial \xi_1}\int \frac{\partial}{\partial \zeta}(\zeta \varphi_1)\, \partial \zeta + c$$

Evaluation of integrals results in:

$$\int \frac{\partial}{\partial \xi_1}(\bar{U}_I^2)\, b\, \partial \zeta = -2U_{p_o}\bar{U}_{1m}\frac{db}{d\xi_1}[\zeta \varphi_1 - \frac{b\varphi_1}{R}(\frac{1}{2}+\zeta^2)] + \bar{U}_{1m}^2 \frac{db}{d\xi_1}\zeta \varphi_1 + c \qquad (7.18)$$

Final expression for the total impulse then is:

$$(1+\frac{\xi_2}{R})\, \bar{UV} = U_{p_o}\bar{U}_{1m}\frac{db}{d\xi_1}[-2\zeta \varphi_1 + \frac{b\varphi_1}{R}(1+2\zeta^2)] + \bar{U}_{1m}^2 \frac{db}{d\xi_1}\zeta \varphi_1 + c$$

Nondimensionalizing the above equation with the square of the maximum wake velocity

defect, $\bar{U}_{1m}^2$ gives:

$$\frac{\bar{U}\bar{V}}{\bar{U}_{1m}^2} = \frac{R}{R+\xi_2}\frac{U_{P_o}}{\bar{U}_{1m}}\frac{db}{d\xi_1}\left[-2\zeta\varphi_1 + \frac{b\varphi_1}{R}(1+2\zeta^2)\right] + \frac{R}{R+\xi_2}\frac{db}{d\xi_1}\zeta\varphi_1 + \frac{c}{\bar{U}_{1m}^2} \qquad (7.19)$$

## 7.5. Expression for Reynolds Shear Stress

Shear stress is the difference between total impulse and partial impulse. This is one of the wake characteristics that is of great importance, which is evident from the order of magnitude analysis done in Chapter 5. Also, of all turbulent fluctuation impulses, shear stress contributes most to the transfer of the mean momentum of the flow. Expression for nondimensional Reynolds shear stress can be written from $\frac{\overline{uv}}{\bar{U}_{1m}^2} = \frac{\bar{U}\bar{V}}{\bar{U}_{1m}^2} - \frac{\bar{U}\bar{V}}{\bar{U}_{1m}^2}$ as:

$$\frac{\overline{uv}}{\bar{U}_{1m}^2} = \frac{R}{R+\xi_2}\frac{U_{P_o}}{\bar{U}_{1m}}\frac{db}{d\xi_1}\left[-\zeta\varphi_1 + \frac{b\varphi_1}{R}(1+\zeta^2)\right] + \frac{R}{R+\xi_2}\frac{db}{d\xi_1}\zeta\varphi_1(1-\varphi_1) + \frac{c}{\bar{U}_{1m}^2}$$

(7.20)

The constant, which is a function of $\xi_1$, is evaluated from the experimental results at $\zeta =$ 0. For the case of straight channel, it is evident from the experimental results that the constant is zero, since the normalized shear stress is zero at the wake center. But for the case of a curved channel, the value of normalized shear stress is different from zero at the wake center, which could be due to the influence of curvature.

## 7.6. Expression for Mean Longitudinal Turbulent Fluctuation Impulse

Though the contribution from the longitudinal turbulent fluctuation impulse is negligibly small in comparison to the mean momentum in longitudinal direction, a method for predicting its distribution has been presented basing on Prandtl's hypothesis.

The value of longitudinal turbulent fluctuation impulse at the wake center has been used as a nondimensionalizing variable here in this study.

From Prandtl's theory: $\frac{\overline{u}^2}{\overline{u}_m^2} = f(\zeta)\ \varphi_1$

Assuming $f(\zeta)$ to be a polynomial of second degree and also considering the effect of curvature, the above equation can now be written as:

$$\psi = \frac{\overline{u}^2}{\overline{u}_m^2} = \frac{R}{R+\xi_2}\ (a_0+a_1\zeta+a_2\zeta^2)\ \varphi_1 \tag{7.21}$$

The three constants can be evaluated from the conditions described below. The condition $\psi_{\zeta=0} = 1$ gives rise to $a_0 = 1$. The second condition is $(\frac{\partial\psi}{\partial\zeta})_{\zeta=0} = 0$, which implies that $a_1 = \frac{b}{R}$. The constant, $a_2$, needs to be evaluated from experimental measurements. Thus, the final expression for the longitudinal turbulent fluctuations can be written as:

$$\frac{\overline{u}^2}{\overline{u}_m^2} = \frac{R}{R+\xi_2}\ (1+\frac{b}{R}\zeta+a_2\zeta^2)\ \varphi_1 \tag{7.22}$$

### 7.7. Special Case: Expressions of Wake Characteristics for Straight Channel

The straight channel wake flow has been treated by theory as a special case of curved channel wake flow for which the radius of curvature approaches infinity. Thus, making $R \rightarrow \infty$ in the above derived expressions for curved channels give rise to the wake characteristics for a straight channel. Since it is known from experimental measurements that shear stress is zero at the wake center with symmetric distribution about the wake center, the integration constant in shear stress expression becomes zero. The summary of the resulting expressions is given below:

Mean lateral velocity:

$$\frac{\bar{V}}{\bar{U}_{1m}} = -\frac{db}{d\xi_1}\,\zeta\varphi_1 \tag{7.23}$$

Partial impulse:

$$\frac{\bar{U}\bar{V}}{\bar{U}_{1m}^2} = -\frac{U_{P_0}}{\bar{U}_{1m}}\,\frac{db}{d\xi_1}\,\zeta\varphi_1 + \frac{db}{d\xi_1}\,\zeta\varphi_1^2 \tag{7.24}$$

Total impulse:

$$\frac{\bar{U}\bar{V}}{\bar{U}_{1m}^2} = -2\,\frac{U_{P_0}}{\bar{U}_{1m}}\,\frac{db}{d\xi_1}\zeta\varphi_1 + \frac{db}{d\xi_1}\,\zeta\varphi_1 \tag{7.25}$$

Shear stress:

$$\frac{\overline{uv}}{\bar{U}_{1m}^2} = -\frac{U_{P_0}}{\bar{U}_{1m}}\,\frac{db}{d\xi_1}\,\zeta\varphi_1 + \frac{db}{d\xi_1}\,\zeta\varphi_1\,(1-\varphi_1) \tag{7.26}$$

Longitudinal turbulent fluctuation impulse:

$$\frac{\bar{u}^2}{\bar{u}_m^2} = (1 + a_2\zeta^2)\,\varphi_1 \tag{7.27}$$

# 8. WAKE CHARACTERISTICS WITH PRESSURE GRADIENT

The wake flow under the influence of streamline curvature and pressure gradients is of considerable interest from a turbomachinery viewpoint since it simulates the real situation in turbomachinery rotor cascade. No matter whether the pressure gradient is positive or negative, the expressions developed for wake characteristics remain the same except that the power laws dictating the growth of the wake width, decay of maximum wake velocity defect and variation of potential flow velocity at wake center with the streamwise distance vary in the two cases. It is evident from experiments that growth of wake width is highest in a positive pressure gradient case, while the decay of maximum wake velocity defect is fastest in a negative pressure gradient case. The task of deriving expressions for wake characteristics with streamline curvature and longitudinal pressure gradient has been undertaken in this chapter.

## 8.1. Expression for Mean Lateral Velocity

As done in the case of zero streamwise pressure gradient, the continuity equation with given mean velocity distribution in streamwise direction has been used to derive expression for mean lateral velocity. Rewriting the continuity equation, i.e. Eq. (5.7) gives rise to:

$$(1+\frac{\xi_2}{R})\ \bar{V} = -\int\frac{\partial \bar{U}}{\partial \xi_1}\ d\xi_2 + c \tag{8.1}$$

Using the nondimensional parameters, from Chapter 6, and from the definition of mean longitudinal velocity, it follows from Eq. (8.1) that:

$$(1+\frac{\xi_2}{R})\ \bar{V} = -\int\frac{\partial U_\infty}{\partial \xi_1}\ d\xi_2 + \int\frac{\partial \bar{U}_1}{\partial \xi_1}\ d\xi_2 + c \tag{8.2}$$

Using the approximation $U_\infty = U_{p_o}\ (1-\frac{\xi_2}{R})$, already derived in Chapter 6, the above

equation modifies to:

$$(1+\frac{\xi_2}{R})\ \bar{V} = -\int\frac{\partial U_{P_o}}{\partial \xi_1}\ (1-\frac{\xi_2}{R})\ b\ \partial\zeta + \int\frac{\partial \bar{U}_{1m}}{\partial \xi_1}\ \varphi_1\ b\ \partial\zeta + \int\bar{U}_{1m}\ \frac{\partial \varphi_1}{\partial \xi_1}\ b\ \partial\zeta + c$$

Adding and subtracting the term, $\int\bar{U}_{1m}\ \frac{\partial b}{\partial \xi_1}\ \varphi_1\ \partial\zeta$, and expanding $\frac{\partial \varphi_1}{\partial \xi_1}$ by chain rule,

the above equation modifies to:

$$(1+\frac{\xi_2}{R})\bar{V} = -\int\frac{\partial U_{P_o}}{\partial \xi_1}\ (1-\frac{\zeta b}{R})\ b\ \partial\zeta + \int\varphi_1\frac{\partial}{\partial \xi_1}(\bar{U}_{1m}\ b)\ \partial\zeta - \int\bar{U}_{1m}\ \frac{\partial b}{\partial \xi_1}\ \frac{\partial}{\partial\zeta}(\zeta\varphi_1)\ \partial\zeta + c$$

Evaluating the integrals leads to:

$$\bar{V} = -(\frac{R}{R+\xi_2})\ \frac{dU_{P_o}}{d\xi_1}\ b\ \zeta\ (1-\frac{b}{2\ R}\zeta) + (\frac{R}{R+\xi_2})\ \bar{U}_{1m}\ \frac{db}{d\xi_1}\ \frac{\sqrt{\pi}}{2}\ erf(\zeta)$$
$$+ \frac{R}{R+\xi_2}\ b\ \frac{d\bar{U}_{1m}}{d\xi_1}\ \frac{\sqrt{\pi}}{2}\ erf(\zeta) - \frac{R}{R+\xi_2}\ \bar{U}_{1m}\ \frac{db}{d\xi_1}\ \zeta\varphi_1 + c$$

From the condition that $\bar{V}$ is zero at $\zeta = 0$, the constant of integration evaluates to be equal to zero. Nondimensionalizing with maximum wake velocity defect, $\bar{U}_{1m}$, the final expression for mean lateral velocity can be written as:

$$\frac{\bar{V}}{\bar{U}_{1m}} = -(\frac{R}{R+\xi_2})\ \frac{b}{\bar{U}_{1m}}\ \frac{\partial U_{P_o}}{\partial \xi_1}\ \zeta\ (1-\frac{b}{2\ R}\zeta) + (\frac{R}{R+\xi_2})\ \frac{db}{d\xi_1}[-\zeta\varphi_1+\frac{\sqrt{\pi}}{2}\ erf(\zeta)]$$
$$+ (\frac{R}{R+\xi_2})\ \frac{b}{\bar{U}_{1m}}\ \frac{\partial \bar{U}_{1m}}{\partial \xi_1}\ \frac{\sqrt{\pi}}{2}\ erf(\zeta) \qquad (8.3)$$

Unlike the zero pressure gradient case, the present expression for mean lateral velocity has additional terms involving the longitudinal dependency of maximum wake velocity defect and potential flow velocity variations at the wake center which are not negligible in the case of flow under the influence of streamwise pressure gradient.

### 8.2. Expression for Partial Impulse

Since partial impulse is the product of the mean velocities in longitudinal and lateral directions, the expression for it is written by using the expression for $\bar{V}$, Eq. (8.3) derived from the continuity equation, and from the definition of $\bar{U}$ as:

$$\bar{U}\bar{V} = (U_\infty - \bar{U}_{1m}\varphi_1)\frac{R}{R+\xi_2}\left[-\frac{\partial U_{P_o}}{\partial \xi_1} b\,\zeta\,(1-\frac{b}{2R}\zeta) - \bar{U}_{1m}\frac{db}{d\xi_1}\zeta\varphi_1\right.$$

$$\left. + \bar{U}_{1m}\frac{db}{d\xi_1}\frac{\sqrt{\pi}}{2}\,erf(\zeta) + b\frac{\partial \bar{U}_{1m}}{\partial \xi_1}\frac{\sqrt{\pi}}{2}\,erf(\zeta)\right] \tag{8.4}$$

With the approximation $U_\infty = U_{P_o}(1-\frac{\xi_2}{R})$ and nondimensionalizing Eq. (8.4) with $\bar{U}_{1m}^2$ leads to the final expression for partial impulse as:

$$\frac{\bar{U}\bar{V}}{\bar{U}_{1m}^2} = -(\frac{R}{R+\xi_2})\frac{U_{P_o}}{\bar{U}_{1m}^2}\frac{\partial U_{P_o}}{\partial \xi_1} b\,\zeta\,(1-\frac{3}{2}\frac{b}{R}\zeta+\frac{b^2\zeta^2}{2R^2}) + (\frac{R}{R+\xi_2})\frac{db}{d\xi_1}[\zeta\varphi_1^2 - \frac{\sqrt{\pi}}{2}\,erf(\zeta)\varphi_1]$$

$$-(\frac{R}{R+\xi_2})\frac{U_{P_o}}{\bar{U}_{1m}}\frac{db}{d\xi_1}[\zeta\varphi_1 - \frac{b}{R}\zeta^2\varphi_1 - \frac{\sqrt{\pi}}{2}\,erf(\zeta)(1-\frac{b}{R}\zeta)] + (\frac{R}{R+\xi_2})\frac{b}{\bar{U}_{1m}}\frac{\partial U_{P_o}}{\partial \xi_1}(1-\frac{b}{2R}\zeta)\,\zeta\varphi_1$$

$$+ (\frac{R}{R+\xi_2})\frac{U_{P_o}}{\bar{U}_{1m}^2} b\frac{\partial \bar{U}_{1m}}{\partial \xi_1}\frac{\sqrt{\pi}}{2}\,erf(\zeta)\,(1-\frac{b}{R}\zeta) - (\frac{R}{R+\xi_2})\frac{b}{\bar{U}_{1m}}\frac{\partial \bar{U}_{1m}}{\partial \xi_1}\frac{\sqrt{\pi}}{2}\,erf(\zeta)\,\varphi_1$$

(8.5)

### 8.3. Expression for Total Impulse

The derivation for total impulse has been carried out by using the equation of motion in $\xi_1$ direction with the usual approximations, as stated in earlier chapters:

$$(\frac{R}{R+\xi_2})\,(\bar{U}^2+\bar{u}^2)_{,1} + (\bar{U}\bar{V})_{,2} + 2\frac{\bar{U}\bar{V}}{R+\xi_2} = -(\frac{R}{R+\xi_2})\frac{1}{\rho}\frac{\partial \bar{p}}{\partial \xi_1} \tag{8.6}$$

Considering the potential flow outside the wake and applying Bernoulli's equation in that region, enables one to arrive at a relation between the pressure gradient term and potential flow velocity as follows:

$$\frac{1}{\rho}\frac{\partial \bar{p}}{\partial \xi_1} = -U_\infty \frac{\partial U_\infty}{\partial \xi_1} \tag{8.7}$$

Assuming that the longitudinal turbulent fluctuation impulse is negligible in comparison with the mean velocity of the flow and with the usual definitions, i.e.

$\bar{U} = U_\infty - \bar{U}_1$

$\bar{U}^2 = U_\infty^2 - \bar{U}_I^2$ where $\bar{U}_I^2 = 2\, U_\infty\, \bar{U}_1 - \bar{U}_1^2$

Eq. (8.7) can be simplified as:

$$U_\infty \frac{\partial U_\infty}{\partial \xi_1} - \frac{\partial}{\partial \xi_1}(\bar{U}_I^2) = -\frac{\partial}{\partial \xi_2}[(1+\frac{\xi_2}{R})\bar{UV}] - \frac{\bar{UV}}{R}$$

Assuming that $\frac{\bar{UV}}{R} \ll \frac{\partial}{\partial \xi_2}[(1+\frac{\xi_2}{R})\bar{UV}]$, and integrating the resulting equation leads to:

$$\bar{UV} = -(\frac{R}{R+\xi_2}) \int U_\infty \frac{\partial U_\infty}{\partial \xi_1}\, d\xi_2 + (\frac{R}{R+\xi_2}) \int \frac{\partial}{\partial \xi_1}(\bar{U}_I^2)\, d\xi_2 + c \tag{8.8}$$

Now, each term on the right hand side of above equation has been treated separately. Evaluation of first term leads to:

$$\int U_\infty \frac{\partial U_\infty}{\partial \xi_1}\, d\xi_2 = U_{P_0} \frac{\partial U_{P_0}}{\partial \xi_1} \int (1 - 2\frac{\xi_2}{R} + \frac{\xi_2^2}{R^2})\, d\xi_2 = U_{P_0} \frac{\partial U_{P_0}}{\partial \xi_1}\, \xi_2\, (1 - \frac{\xi_2}{R} + \frac{\xi_2^2}{3\,R^2}) \tag{8.9}$$

Now, considering the second term, let:

$\bar{U}_I^2 = \bar{U}_{Im}^2\, \varphi_1$ where $\bar{U}_{Im}^2 = 2\, U_\infty\, \bar{U}_{1m} - \bar{U}_{1m}^2$ and $\varphi^2 \approx \varphi_1$

The approximate equality of nondimensional wake velocity and momentum defect functions has already been verified, as shown in Fig. 6(b) where the comparison is done for a positive pressure gradient case. The equality of $\varphi^2$ and $\varphi_1$ is also valid for negative pressure gradient case. Making use of the fact modifies second term of Eq. (8.8) to:

$$\int \frac{\partial}{\partial \xi_1}(\bar{U}_I^2)\, b\, d\zeta = \int b\varphi_1 \frac{\partial \bar{U}_{Im}^2}{\partial \xi_1}\, d\zeta + \int \bar{U}_{Im}^2\, b\, \frac{\partial \varphi_1}{\partial \xi_1}\, d\zeta$$

Adding and subtracting a term and some rearrangement gives rise to:

$$\int \frac{\partial}{\partial \xi_1}(\bar{U}_I^2)\, b\, d\zeta = -2\, U_{p_o} \bar{U}_{1m} \frac{\partial b}{\partial \xi_1} \int (1-\frac{\xi_2}{R}) \frac{\partial}{\partial \zeta}(\zeta \varphi_1)\, d\zeta + \bar{U}_{1m}^2 \frac{\partial b}{\partial \xi_1} \int \frac{\partial}{\partial \zeta}(\zeta \varphi_1)\, d\zeta$$

$$+ 2\, U_{p_o} \bar{U}_{1m} \frac{\partial b}{\partial \xi_1} \int (1-\frac{\xi_2}{R})\, \varphi_1\, d\zeta - \bar{U}_{1m}^2 \frac{\partial b}{\partial \xi_1} \int \varphi_1\, d\zeta - 2\, \bar{U}_{1m}\, b\, \frac{\partial \bar{U}_{1m}}{\partial \xi_1} \int \varphi_1\, d\zeta$$

$$+ 2\, U_{p_o} \frac{\partial \bar{U}_{1m}}{\partial \xi_1}\, b \int (1-\frac{b}{R}\zeta)\, \varphi_1\, d\zeta + 2\, \bar{U}_{1m} \frac{\partial U_{p_o}}{\partial \xi_1}\, b \int (1-\frac{b}{R}\zeta)\, \varphi_1\, d\zeta$$

Subsequent evaluation of the integrals, substitution into Eq. (8.8) and then nondimensionalizing with $\bar{U}_{1m}^2$ results in the final expression for total impulse as:

$$\frac{\bar{UV}}{\bar{U}_{1m}^2} = -(\frac{R}{R+\xi_2}) \frac{U_{p_o}}{\bar{U}_{1m}^2} \frac{dU_{p_o}}{d\xi_1}\, b\, \zeta\, [1-\frac{b}{R}\zeta+\frac{b^2}{3R^2}\zeta^2] + (\frac{R}{R+\xi_2}) \frac{db}{d\xi_1} [\zeta\varphi_1 - \frac{\sqrt{\pi}}{2}\, erf(\zeta)]$$

$$-(\frac{R}{R+\xi_2}) \frac{U_{p_o}}{\bar{U}_{1m}} \frac{db}{d\xi_1} [2\, \zeta\varphi_1 - \frac{b\varphi_1}{R}(2+2\zeta^2) - 2\frac{\sqrt{\pi}}{2}\, erf(\zeta)] + (\frac{R}{R+\xi_2}) \frac{b}{\bar{U}_{1m}} \frac{d\bar{U}_{1m}}{d\xi_1}\, 2\frac{\sqrt{\pi}}{2}\, erf(\zeta)$$

$$+ (\frac{R}{R+\xi_2}) [2\, \frac{\sqrt{\pi}}{2}\, erf(\zeta) + \frac{b}{R}\varphi_1] [\frac{U_{p_o}}{\bar{U}_{1m}^2} \frac{d\bar{U}_{1m}}{d\xi_1}\, b + \frac{b}{\bar{U}_{1m}} \frac{dU_{p0}}{d\xi_1}] + \frac{c}{\bar{U}_{1m}^2} \qquad (8.10)$$

### 8.4. Expression for Reynolds Shear Stress

As stated earlier in Chapter 7, shear stress is the difference of total impulse and partial impulse and therefore the expression for shear stress follows from the relation:

$$\frac{\overline{uv}}{\bar{U}_{1m}^2} = \frac{\bar{U}\bar{V}}{\bar{U}_{1m}^2} - \frac{\bar{U}\bar{V}}{\bar{U}_{1m}^2}$$

Making use of the Eqs. (8.5) and (8.10), the final form of Reynolds shear stress is:

$$\begin{aligned}
\frac{\overline{uv}}{\bar{U}_{1m}^2} = & -\left(\frac{R}{R+\xi_2}\right)\frac{U_{P_o}}{\bar{U}_{1m}^2}\frac{\partial U_{P_o}}{\partial \xi_1}\frac{b^2}{2R}\zeta^2\left[1-\frac{b}{3R}\zeta\right] \\
& - \left(\frac{R}{R+\xi_2}\right)\frac{b}{\bar{U}_{1m}}\frac{\partial \bar{U}_{1m}}{\partial \xi_1}\left[\frac{\sqrt{\pi}}{2}\,erf(\zeta)\,(2-\varphi_1)\right] \\
& - \left(\frac{R}{R+\xi_2}\right)\frac{U_{P_o}}{\bar{U}_{1m}}\frac{db}{d\xi_1}\left[\zeta\varphi_1 - \frac{b}{R}\varphi_1(2+\zeta^2) - \frac{\sqrt{\pi}}{2}\,erf(\zeta)\,(1+\frac{b}{R}\zeta)\right] \\
& + \left(\frac{R}{R+\xi_2}\right)\frac{db}{d\xi_1}\left[\zeta\varphi_1 - \frac{\sqrt{\pi}}{2}\,erf(\zeta)\right](1-\varphi_1) \\
& + \left(\frac{R}{R+\xi_2}\right)\frac{U_{P_o}}{\bar{U}_{1m}^2}\frac{\partial \bar{U}_{1m}}{\partial \xi_1}\,b\left[\frac{b}{R}\varphi_1+\frac{\sqrt{\pi}}{2}\,erf(\zeta)\,(1+\frac{b}{R}\zeta)\right] \\
& + \left(\frac{R}{R+\xi_2}\right)\frac{b}{\bar{U}_{1m}}\frac{\partial U_{P_o}}{\partial \xi_1}\left[2\frac{\sqrt{\pi}}{2}\,erf(\zeta)+\frac{b}{R}\varphi_1(1+\frac{\zeta^2}{2})-\zeta\varphi_1\right] + \frac{c}{\bar{U}_{1m}^2}
\end{aligned} \tag{8.11}$$

The constant of integration is a function of $\xi_1$ and should be evaluated from experimental results, from the value corresponding to $\zeta = 0$. Unlike a straight channel wake flow case, in curved channels, shear stress is not zero at the wake center because of the effect of curvature. This fact is implemented into theory by evaluating the constant of integration in above expression from experimental results at wake center.

# 9. DISCUSSION OF RESULTS

General validation of the theory has been accomplished by a comparison of theory with experimental measurements made available from the Turbomachinery Performance Laboratory (refer to Fig. 7 for the layout of the test facility) at Texas A&M University, as well as from the literature. In order to carry out the comparison of theory with experimental measurements, information regarding the wake width, maximum wake velocity defect, and the hypothetical potential flow velocity at the wake center as a function of streamwise distance, i.e. $f(\xi_1/d)$, is necessary. The value of shear stress at the wake center for different locations downstream of the wake generating body is also necessary to evaluate the constant of integration in the expression for Reynolds shear stress. Information regarding these parameters that was provided from experiments and that was actually implemented in theory, after curve fitting, is presented in Figs. 8 through 13. In all figures, the legend title is denoted with x/d followed by a numerical value corresponding to the streamwise location. Here it should be noted that 'x' in the legend title does not represent the cartesian coordinate, but it corresponds to curvilinear coordinate $\xi_1$. Thus x/d actually stands for $\xi_1/d$. In Fig. 14, the distribution of $(\bar{U}_{1m}b)/(U_{p_o}d)$ for different streamwise locations for all the three streamwise pressure gradients, zero (zpr), positive (ppr), and negative (npr), in the curved channel is presented.

The test facility at Texas A&M University has been developed, as described by Schobeiri (1987, 1992), to systematically investigate the influence of unsteady inlet flow, pressure gradient, and curvature on boundary layer development, wake development, and heat transfer. This test facility is capable of simulating periodic unsteady flow at the inlet of a curved section, where zero, positive and negative pressure gradients can be easily established by horizontally sliding the concave wall of the test section. The minimum and maximum obtainable inlet:exit area ratios of the test section are 1:0.7 and 1:1.3,

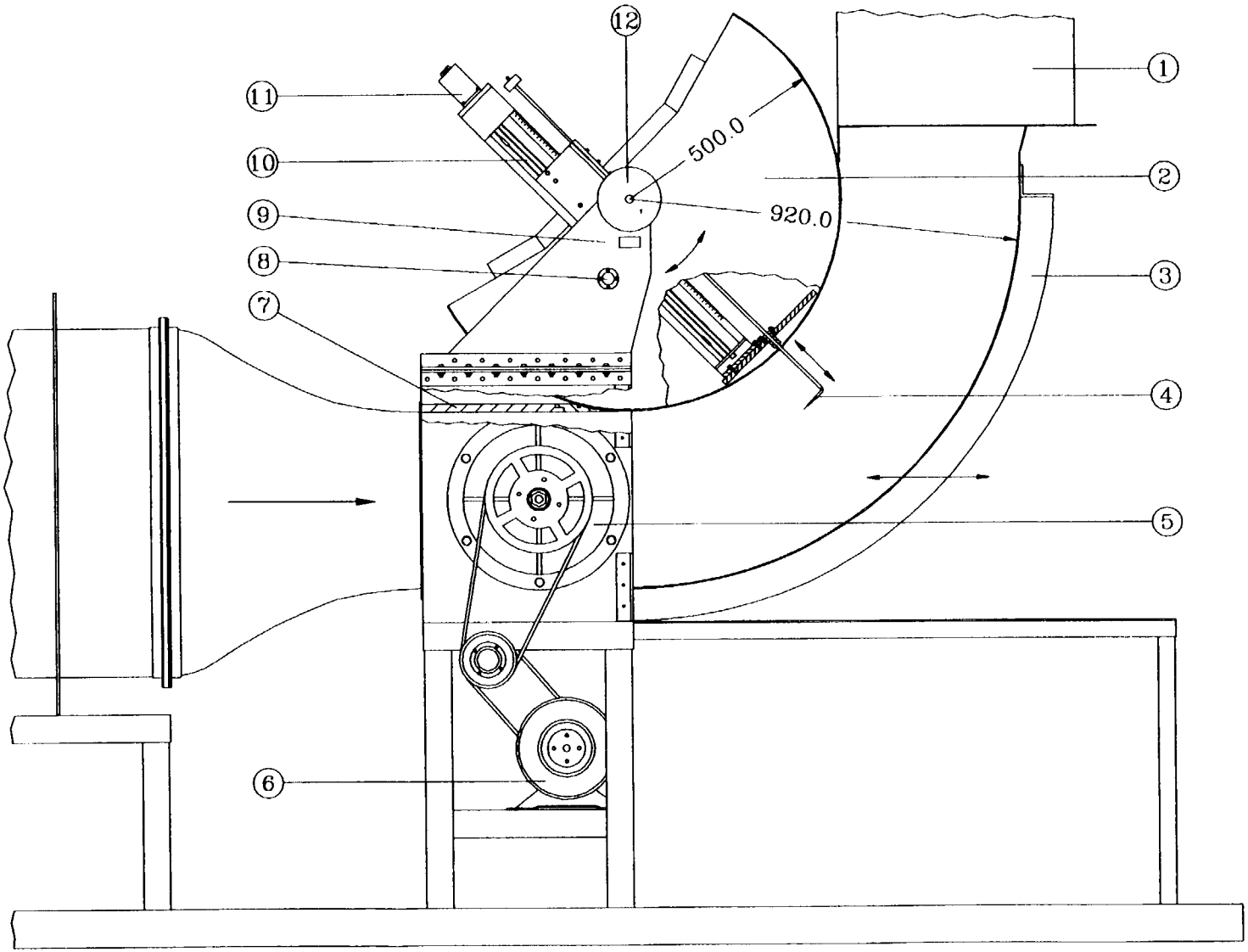


Fig. 7 Test section (1-exit duct, 2-convex wall, 3-concave wall, 4-probe, 5-wake generator, 6-motor, 7-top wall, 8-safety pin, 9-wall with vernier, 10-traversing system, 11-stepped motor, 12-locking wheel)

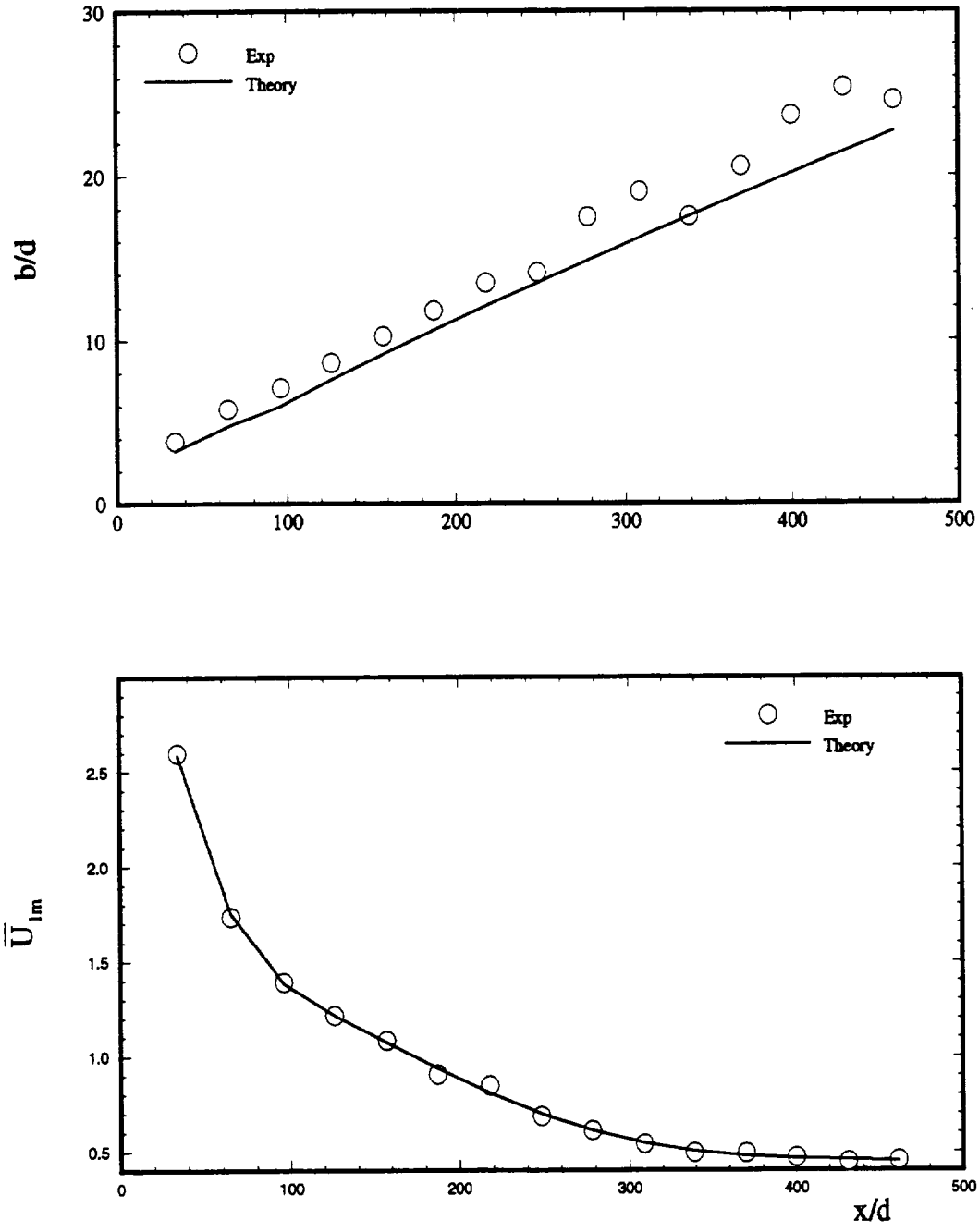


Fig. 8 Wake width and $U_{1m}$ for curved channel without pressure gradient

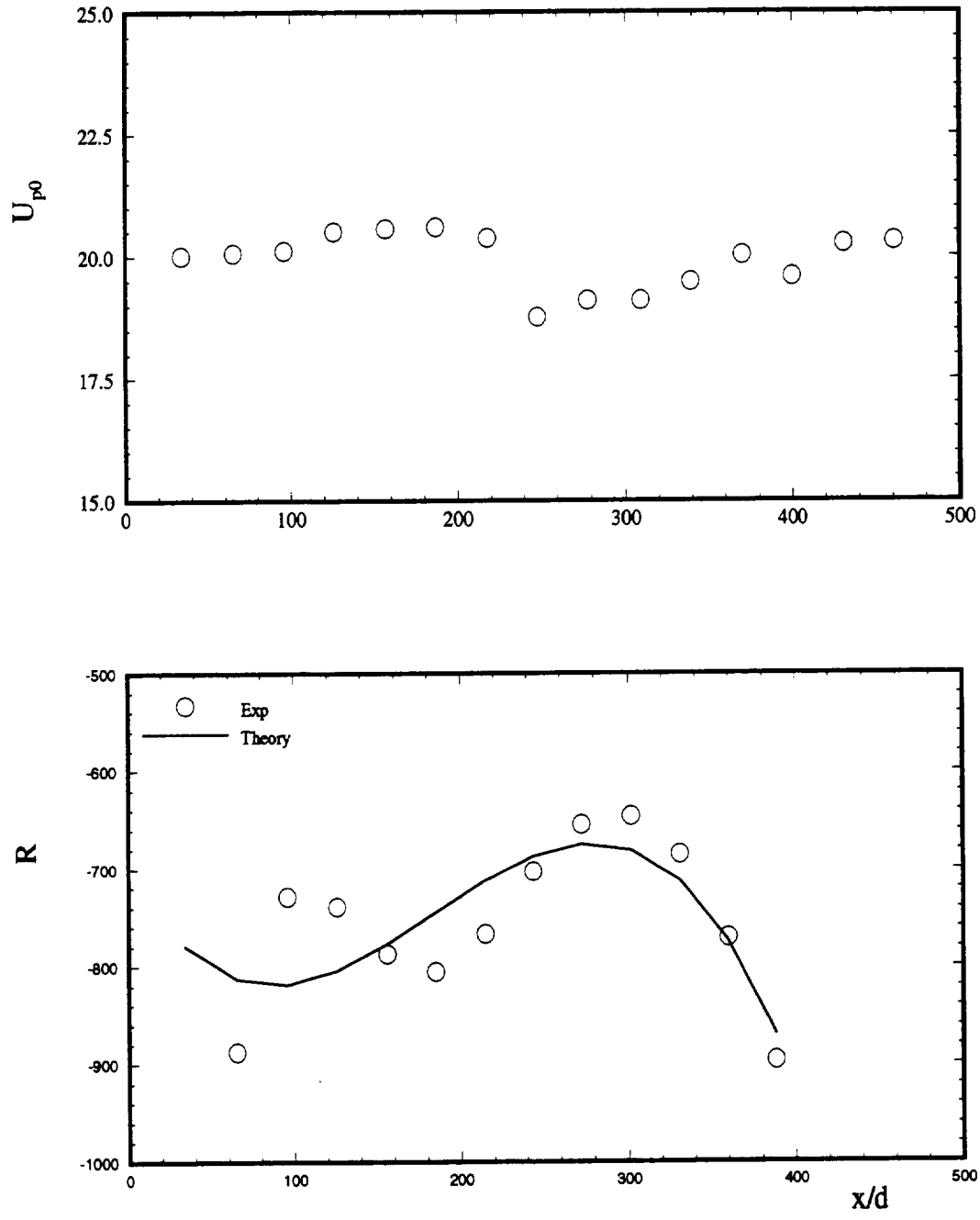


Fig. 9 $U_{p0}$ and Curvature for curved channel without pressure gradient

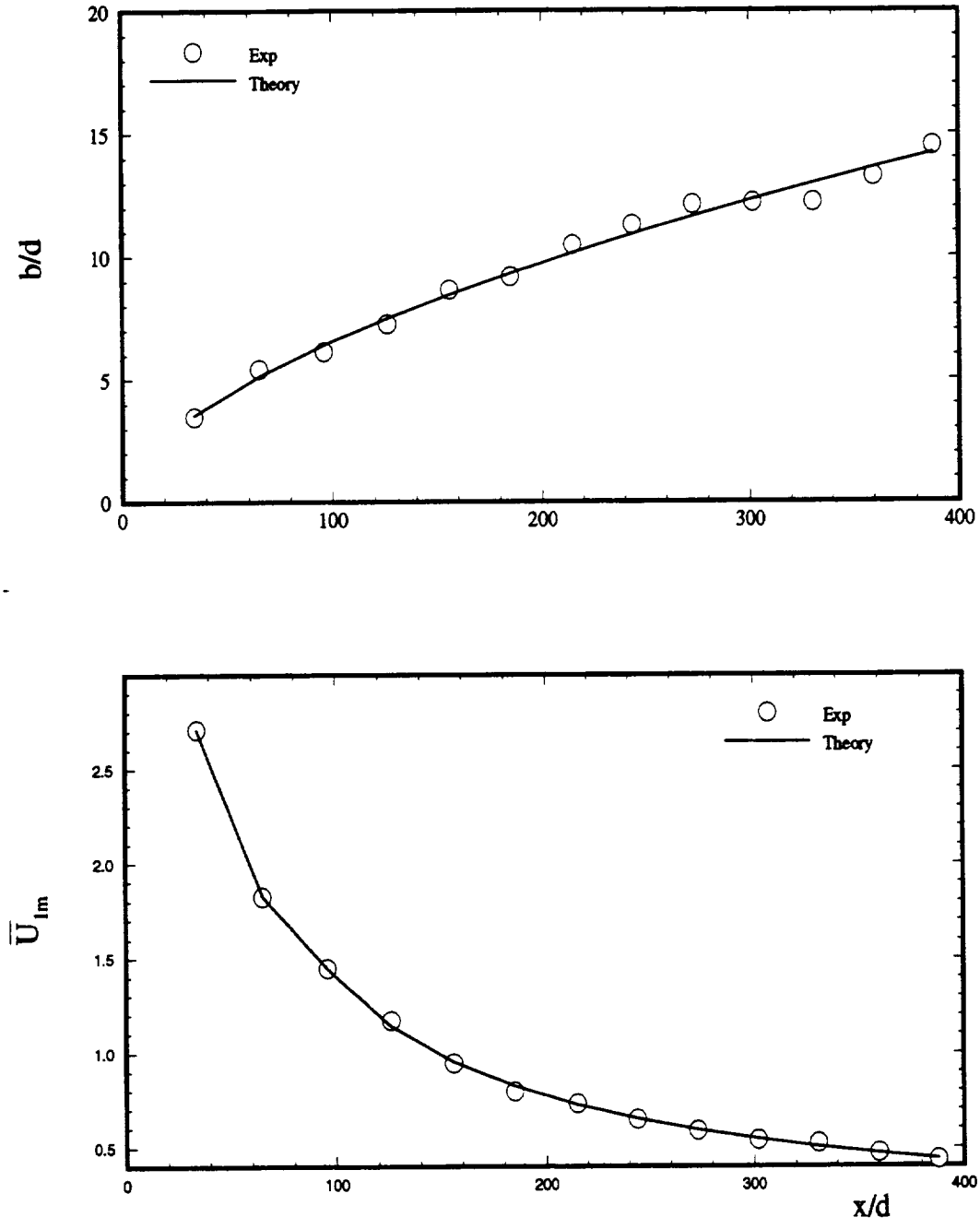


Fig. 10 Wake width and $U_{lm}$ for curved channel with negative pressure gradient

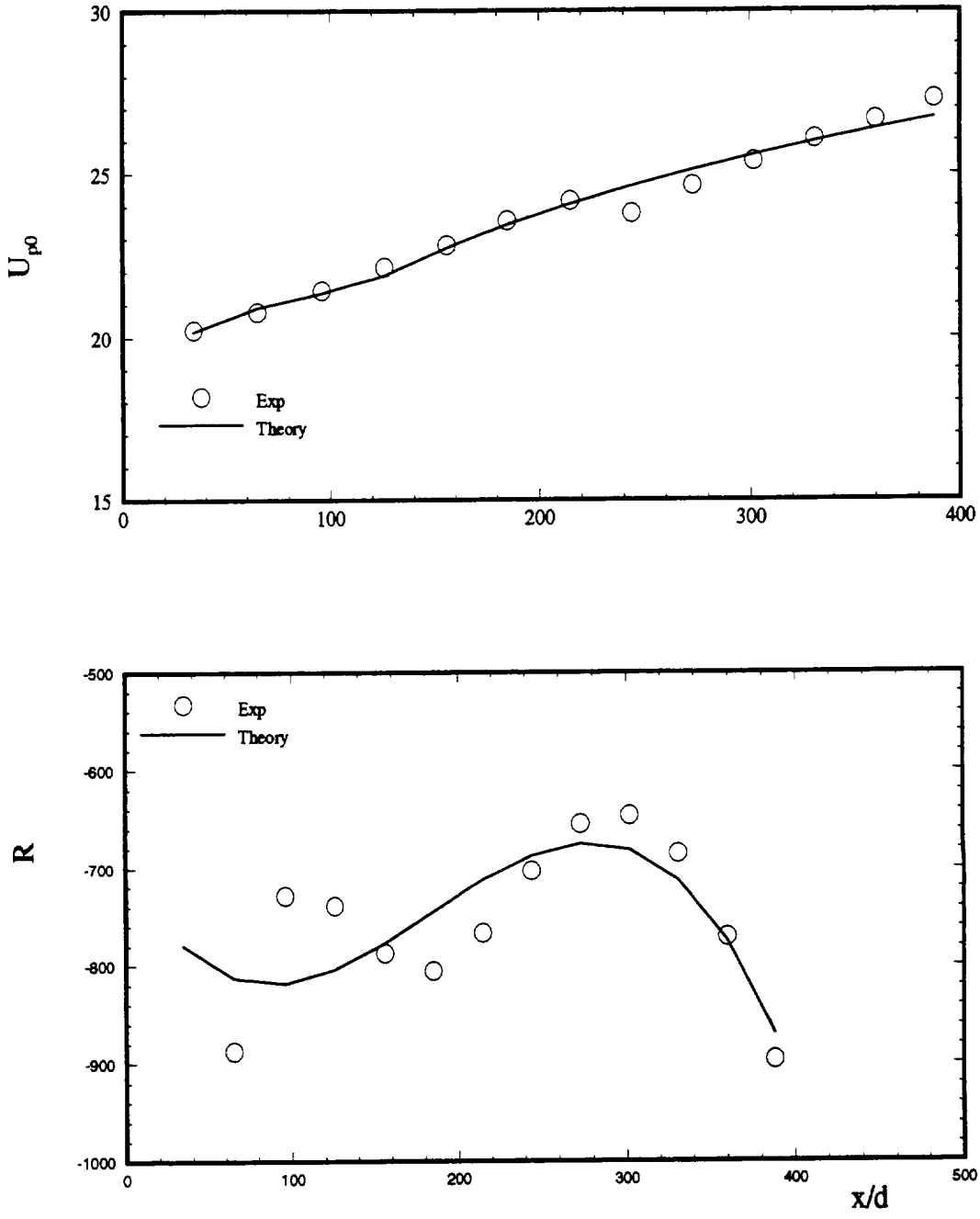


Fig. 11 $U_{p0}$ and Curvature for curved channel with negative pressure gradient

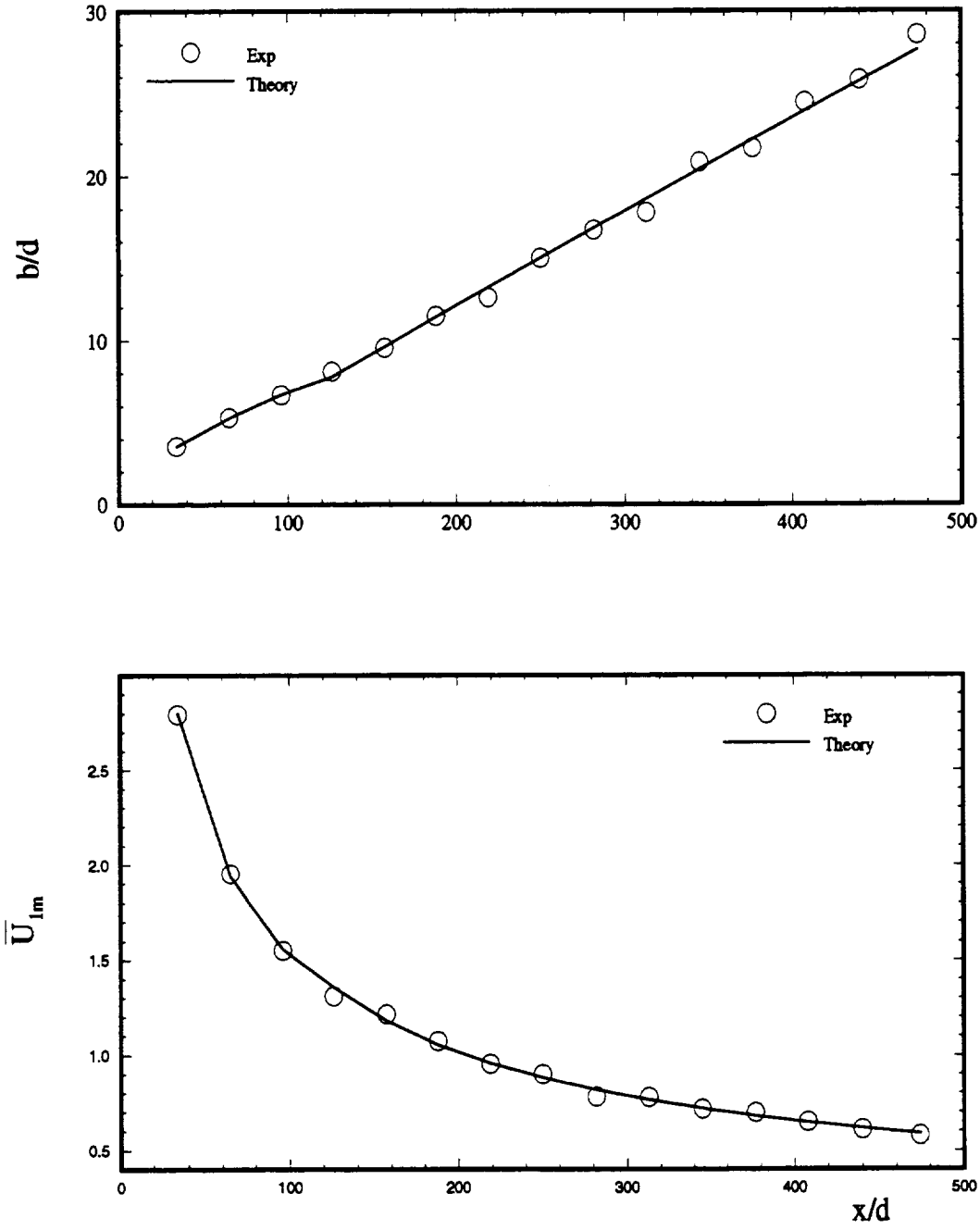


Fig. 12 Wake width and $U_{1m}$ for curved channel with positive pressure gradient

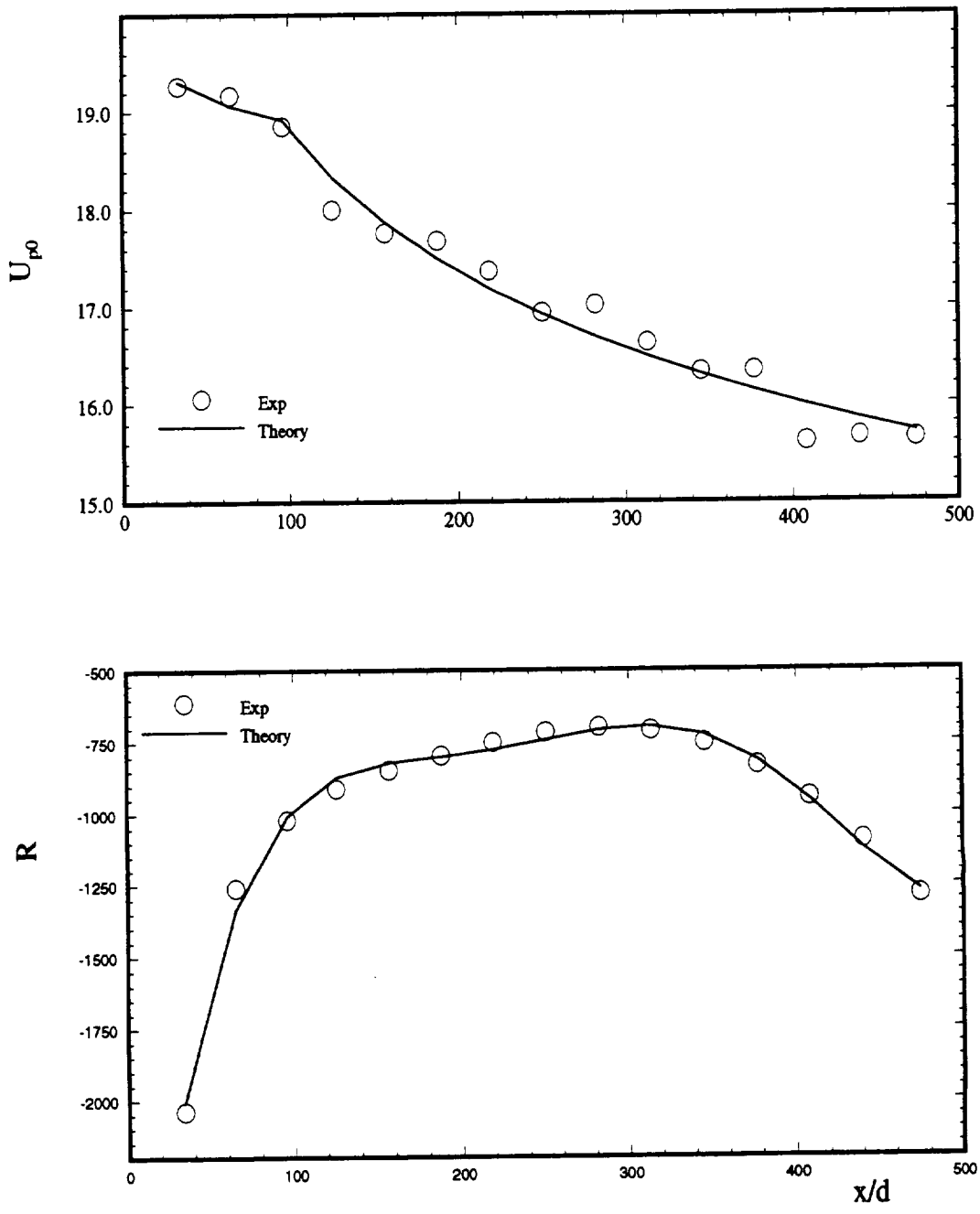


Fig. 13 $U_{p0}$ and Curvature for curved channel with positive pressure gradient

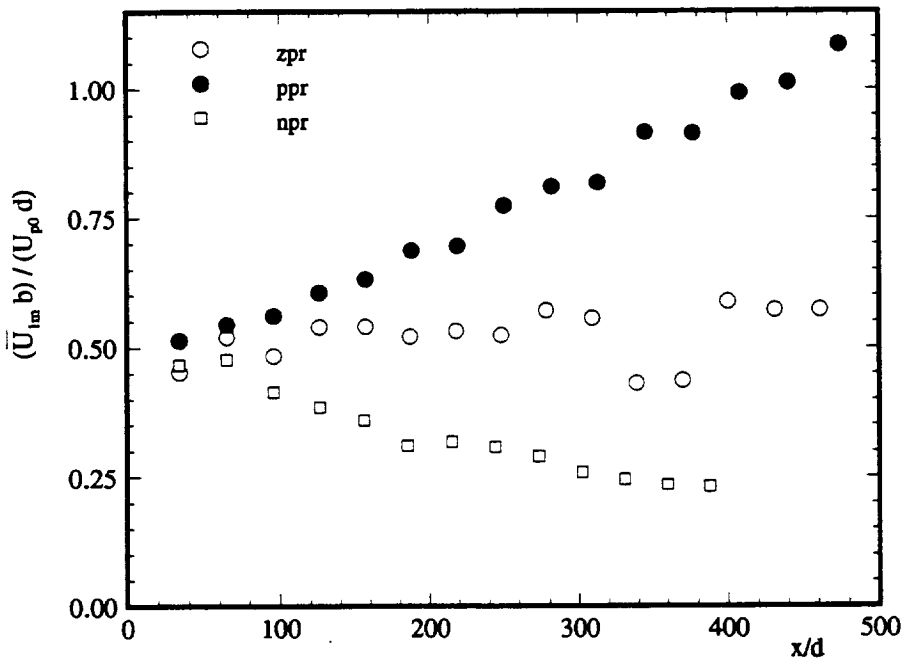


Fig. 14 $(U_{lm}b)/(U_{p0}d)$ distribution for zero, positive and negative longitudinal pressure gradients in curved channel for different streamwise locations

respectively. For the special case of straight wake under no streamwise pressure gradient, theory has been compared with experimental measurements carried out by Eifler (1975).

### 9.1. Zero Pressure Gradient, Straight Channel

Eifler (1975) carried out an experimental study of cylinder wake characteristics for a wide range of downstream locations, and also for different diameters of cylinders in a straight channel. Figures 15-21 show the comparison between theory and experiment for different wake characteristics.

Figures 15-17 demonstrate excellent agreement between theory and experiment for nondimensional wake velocity defect function, $\varphi_1 = e^{-\zeta^2}$, for all locations downstream of wake generating body and for all cylinder diameters. A comparison of Reynolds shear stress is shown in Figs. 18 and 19. Theory is in excellent agreement with experimental measurements, with the peak stress being predicted quite well. Figures 20 and 21 show the development of nondimensional longitudinal turbulent fluctuation impulse for different streamwise locations, and also for different diameters of wake generating body. The constant $a_2$ in Eq. (7.27) is calculated to be 2.668. Except for a slight overprediction of peaks in Fig. 20(a), the theory holds good for remainder of the two cases. The deviation evident in Fig. 20(a) could be a result of calculating one of the constants in Eq. (7.27) from experimental data at a specific streamwise location.

From an overall perspective, theory provides excellent predictions for the special case of straight channel wake flow with no streamwise pressure gradient.

### 9.2. Zero Pressure Gradient, Curved Channel

Comparison of theory and experiment for a curved channel in the absence of streamwise pressure gradient has been summarized in Figs. 22-31. As seen in the straight channel case, the nondimensional wake velocity defect function perfectly matches the experimental measurements (Figs. 22 and 23). Mean longitudinal velocity profiles

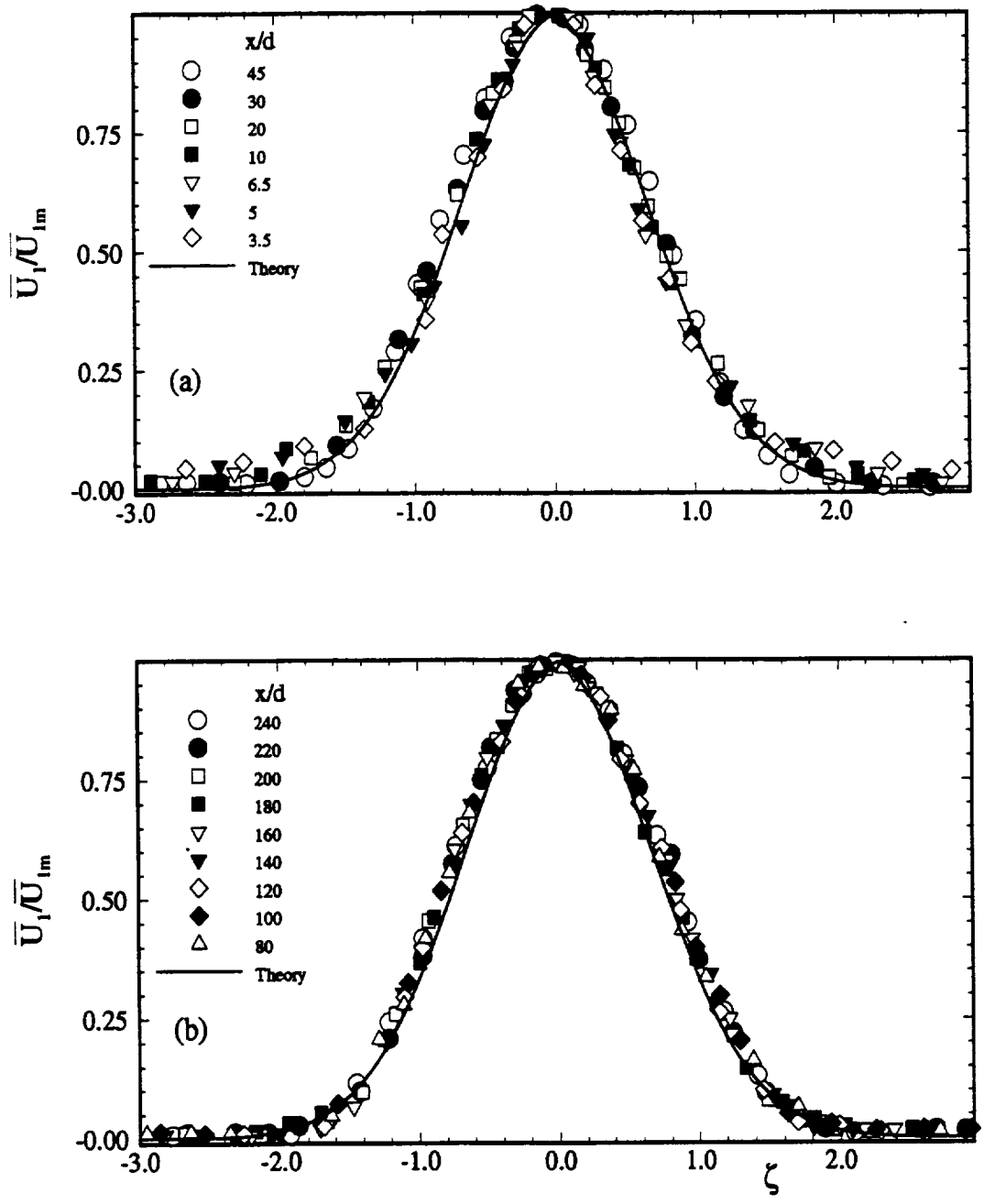


Fig. 15 Mean defect velocity distribution in straight channel for zero pressure gradient, theory compared with experimental data from Eifler (1975), d = 10mm

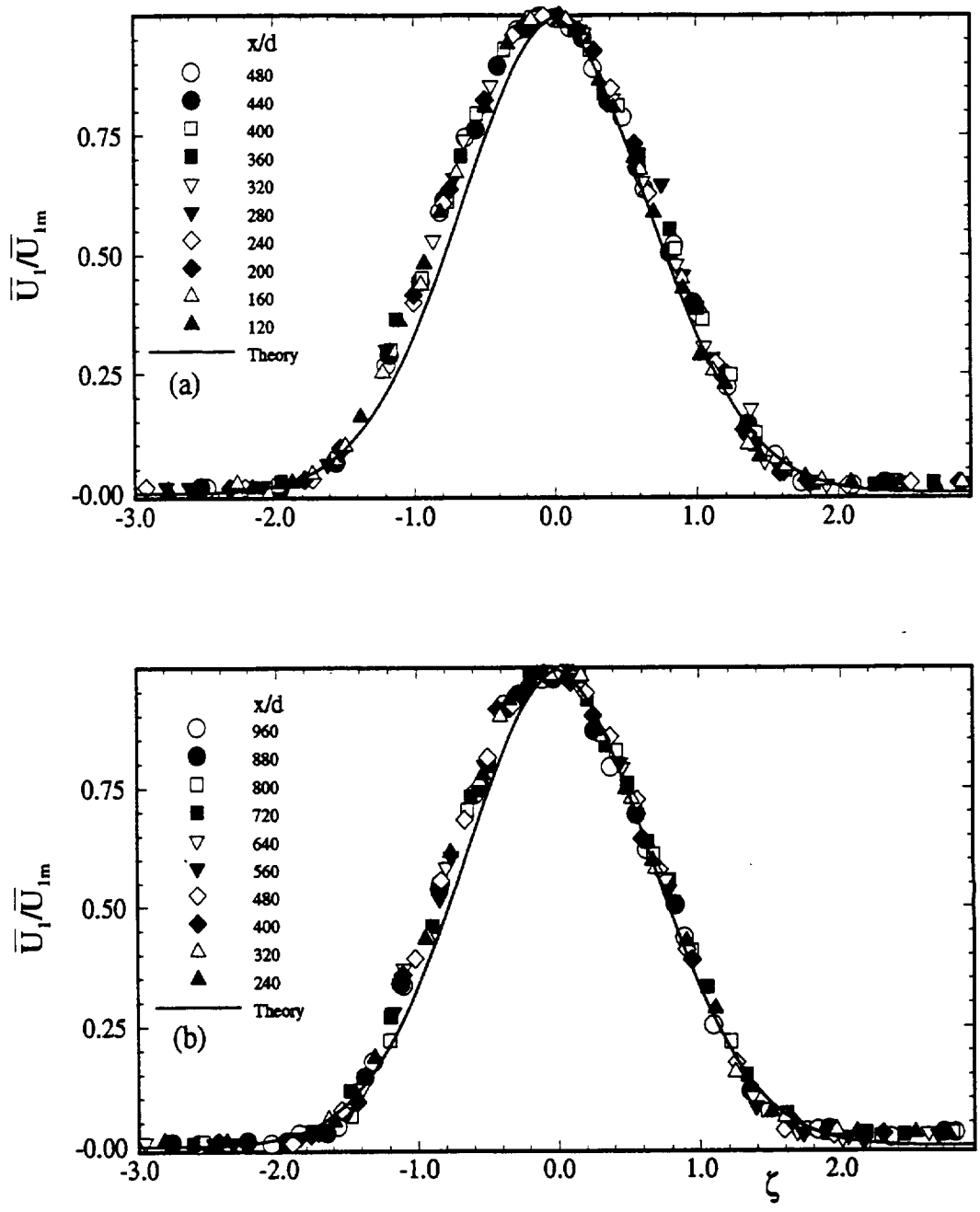


Fig. 16 Mean defect velocity distribution in straight channel for zero pressure gradient, theory compared with experimental data from Eifler (1975), d = 2mm

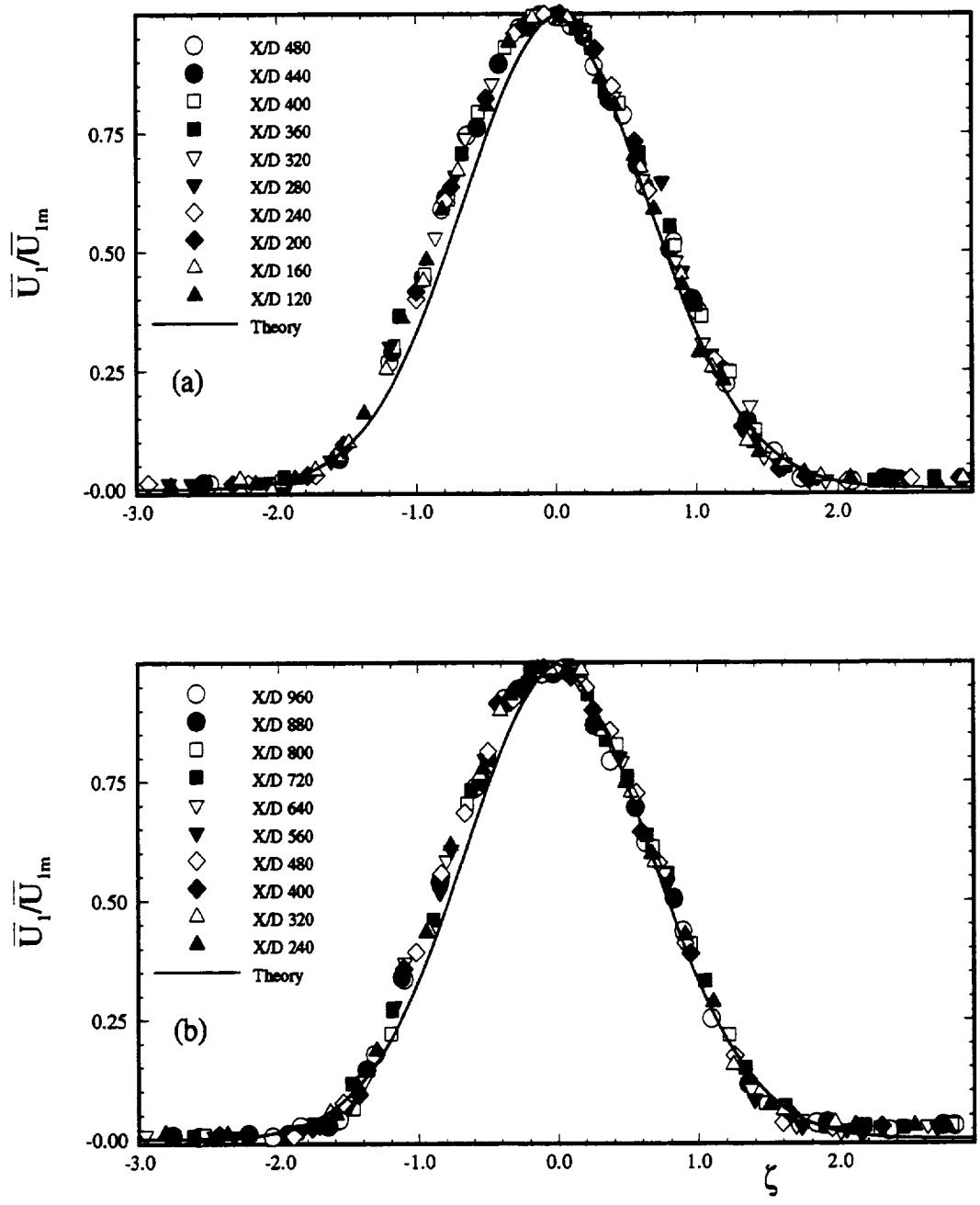


Fig. 17 Mean defect velocity distribution in straight channel for zero pressure gradient, theory compared with experimental data from Eifler (1975), (a) d = 1mm, (b) d = 0.5mm

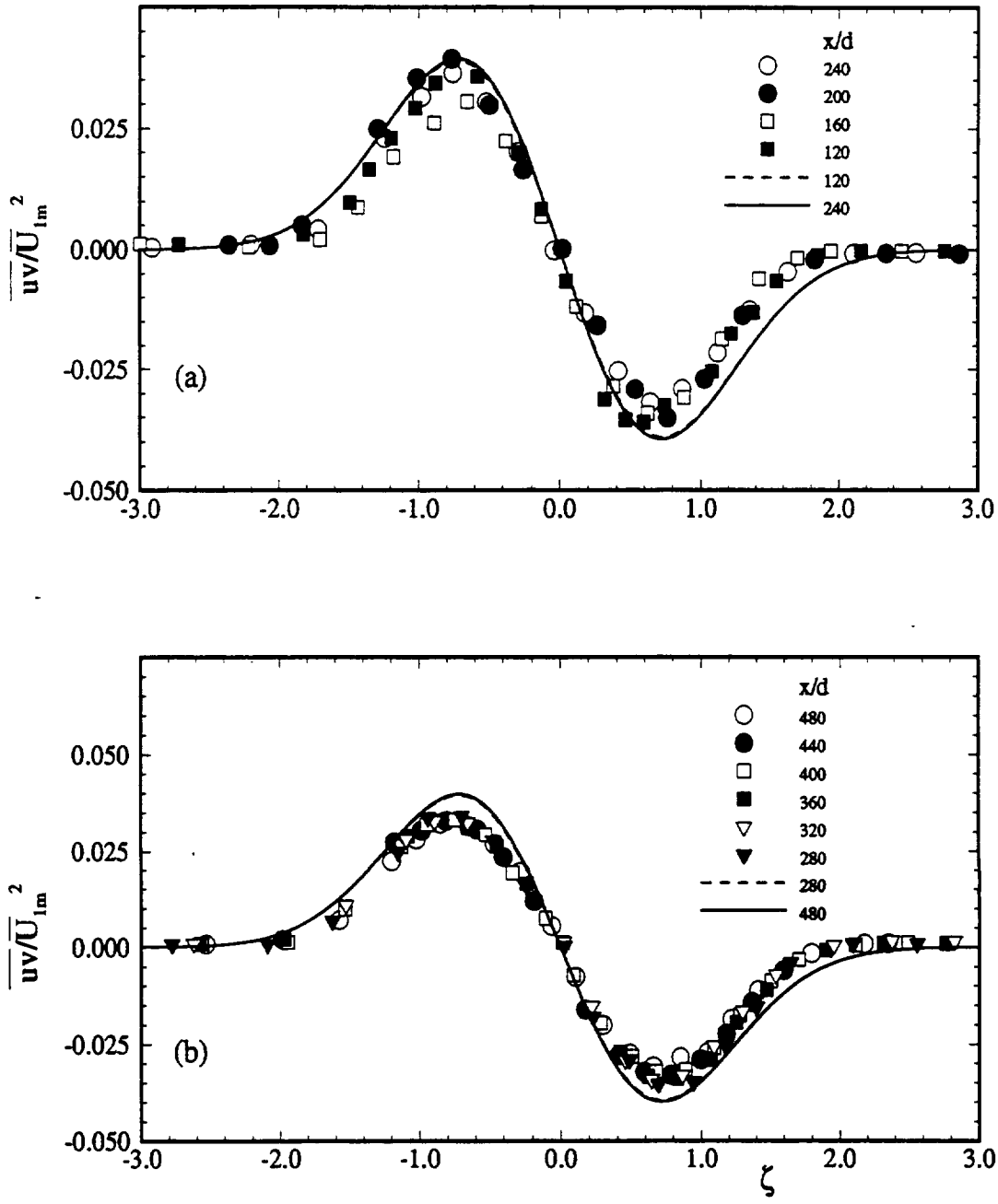


Fig. 18 Reynolds shear stress distribution in straight channel for zero pressure gradient, theory compared with experimental data from Eifler (1975), d = 1mm

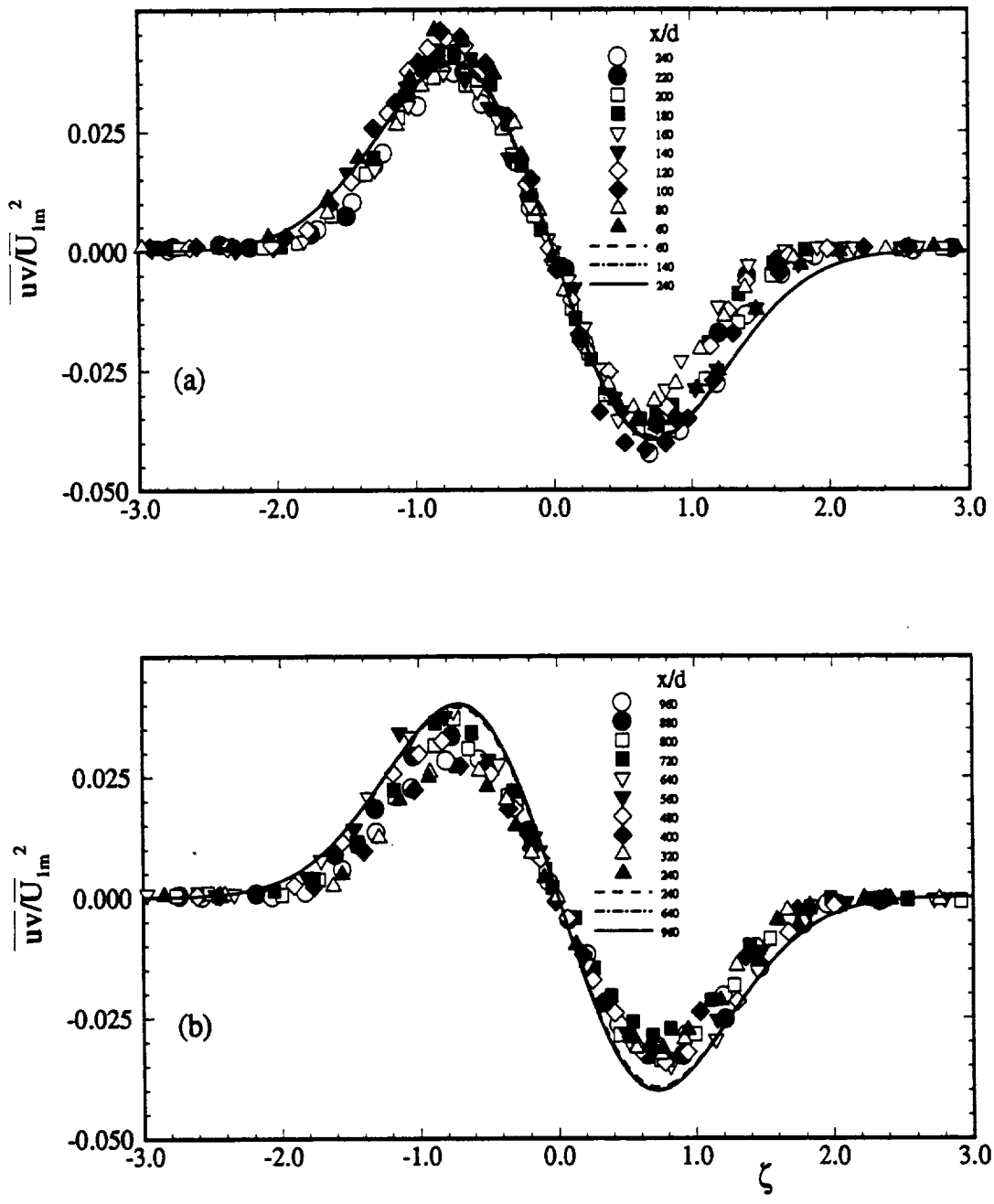


Fig. 19 Reynolds shear stress distribution in straight channel for zero pressure gradient, theory compared with experimental data from Eifler (1975), (a) d = 2mm, (b) d = 0.5mm

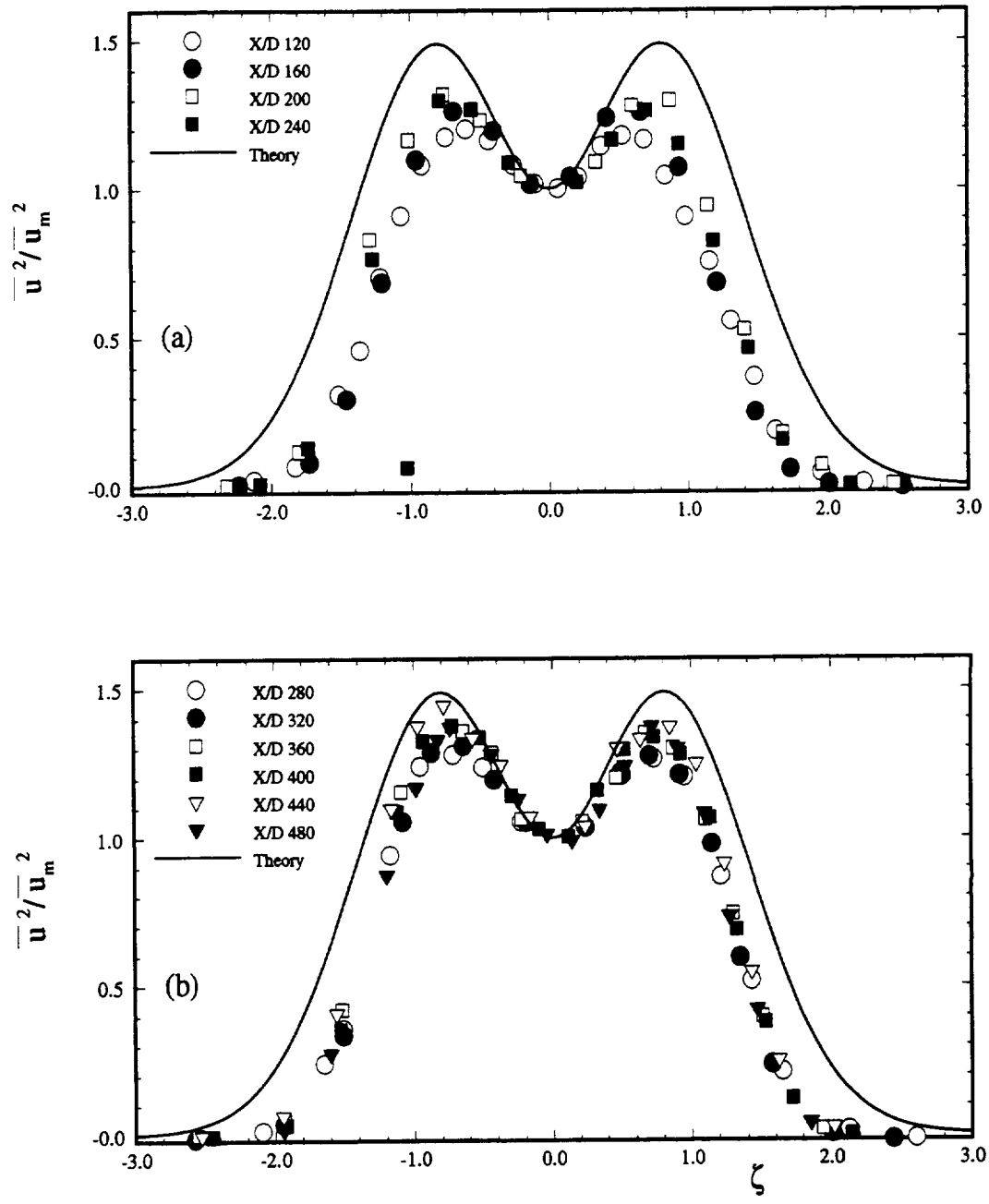


Fig. 20 Mean longitudinal turbulent fluctuations in straight channel for zero pressure gradient, theory compared with experimental data from Eifler (1975), d = 1mm

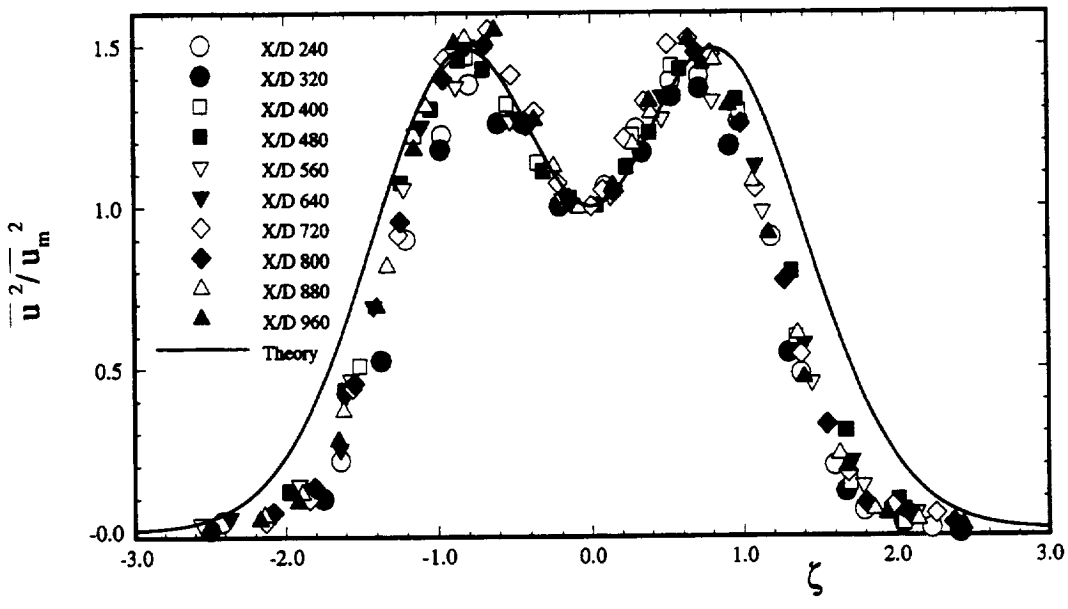


Fig. 21 Mean longitudinal turbulent fluctuations in straight channel for zero pressure gradient, theory compared with experimental data from Eifler (1975), d = 0.5mm

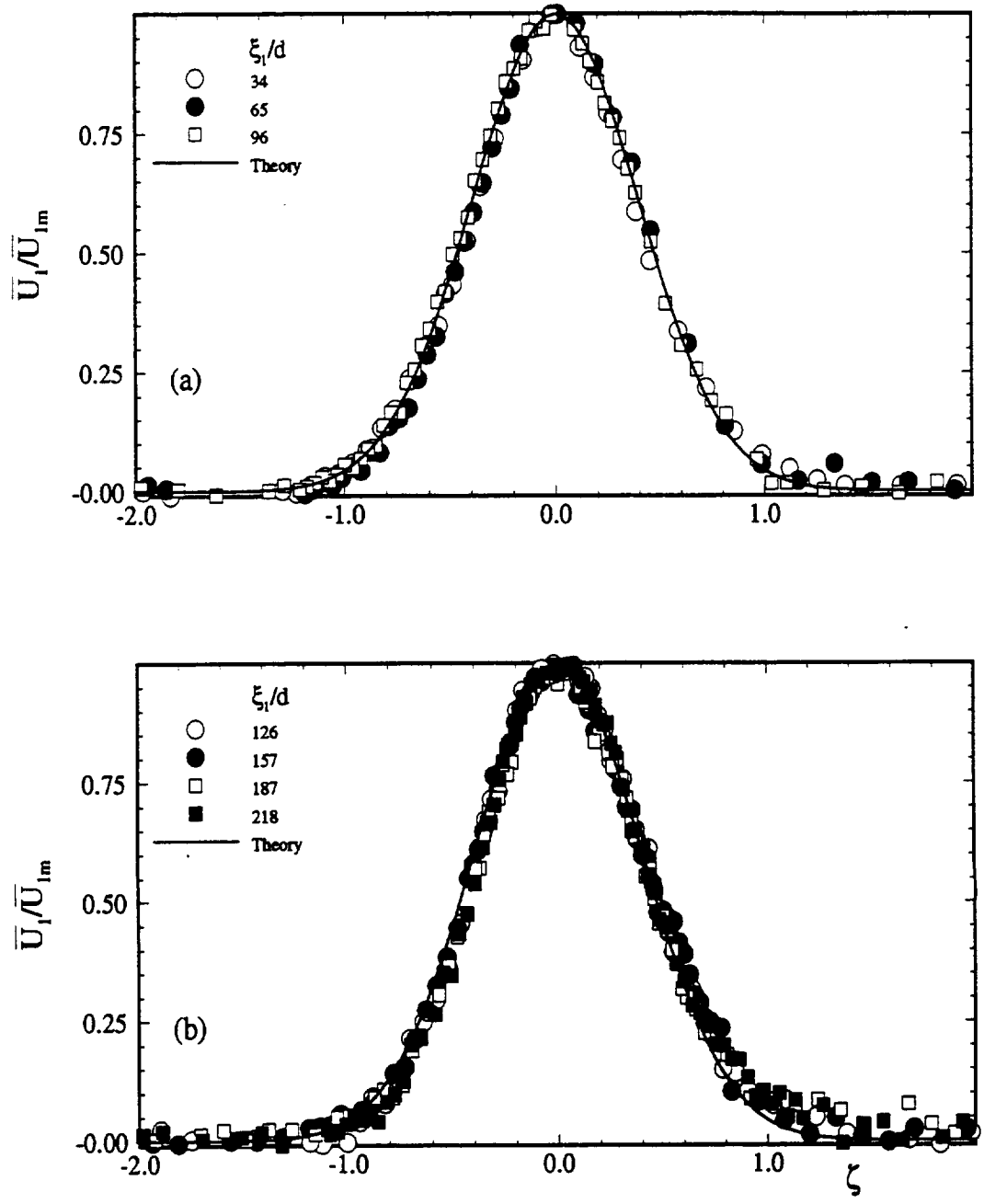


Fig. 22 Mean defect velocity distribution in curved channel for zero pressure gradient, comparison of theory (lines) and experiment (symbols), (x/d:34-218)

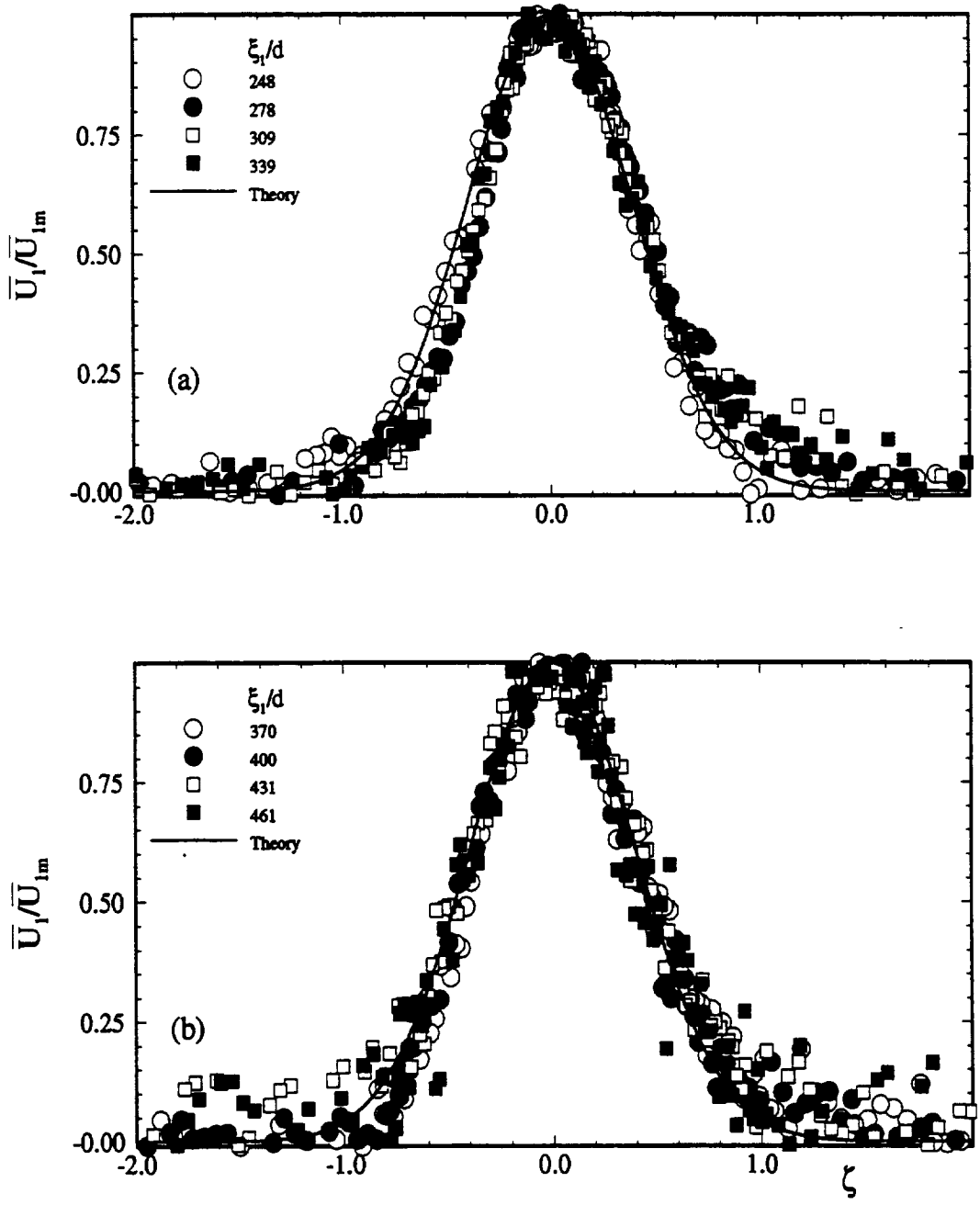


Fig. 23 Mean defect velocity distribution in curved channel for zero pressure gradient, comparison of theory (lines) and experiment (symbols), (x/d:248-461)

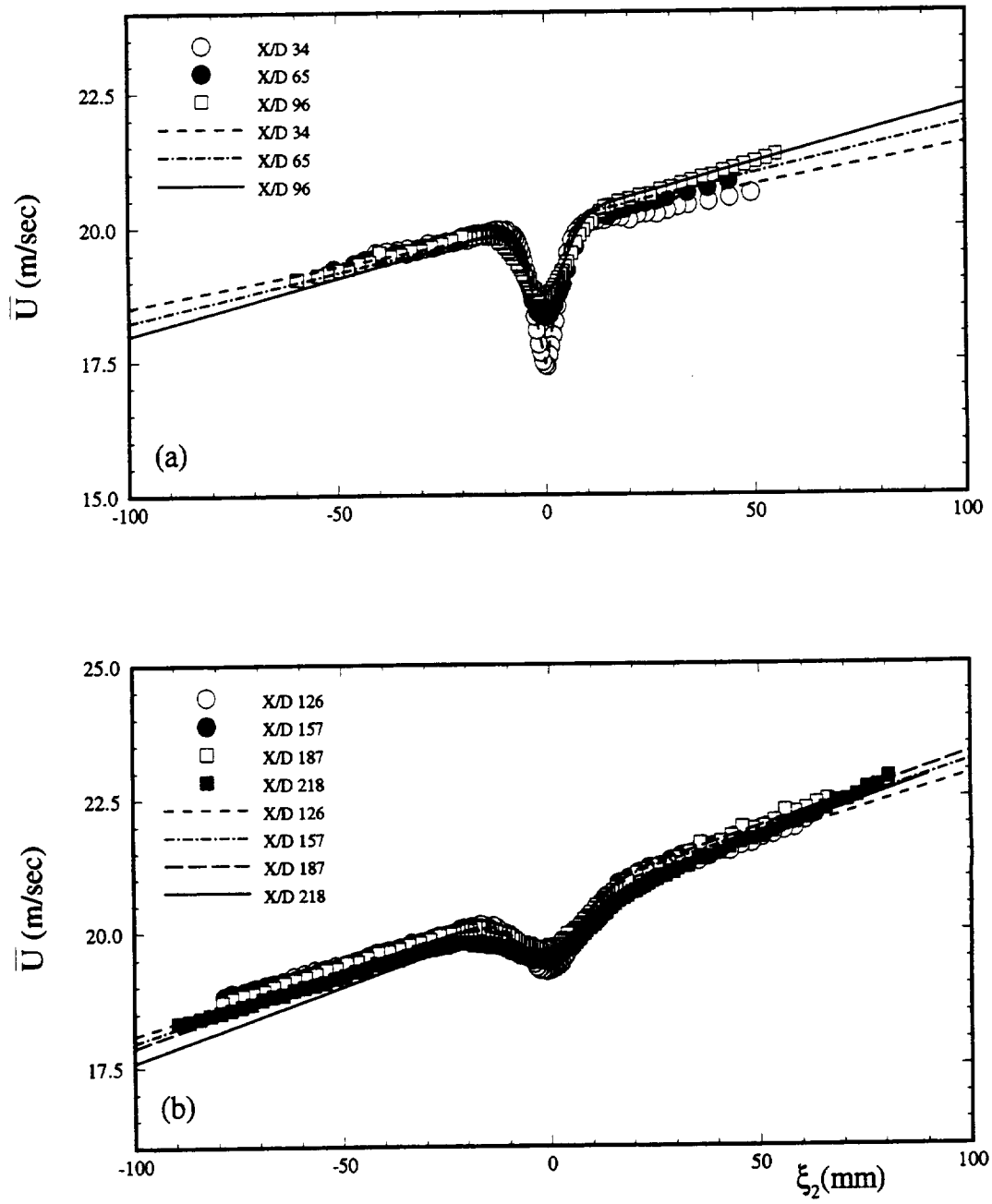


Fig. 24 Mean longitudinal velocity distribution in curved channel for zero pressure gradient, comparison of theory (lines) and experiment (symbols), (x/d:34-218)

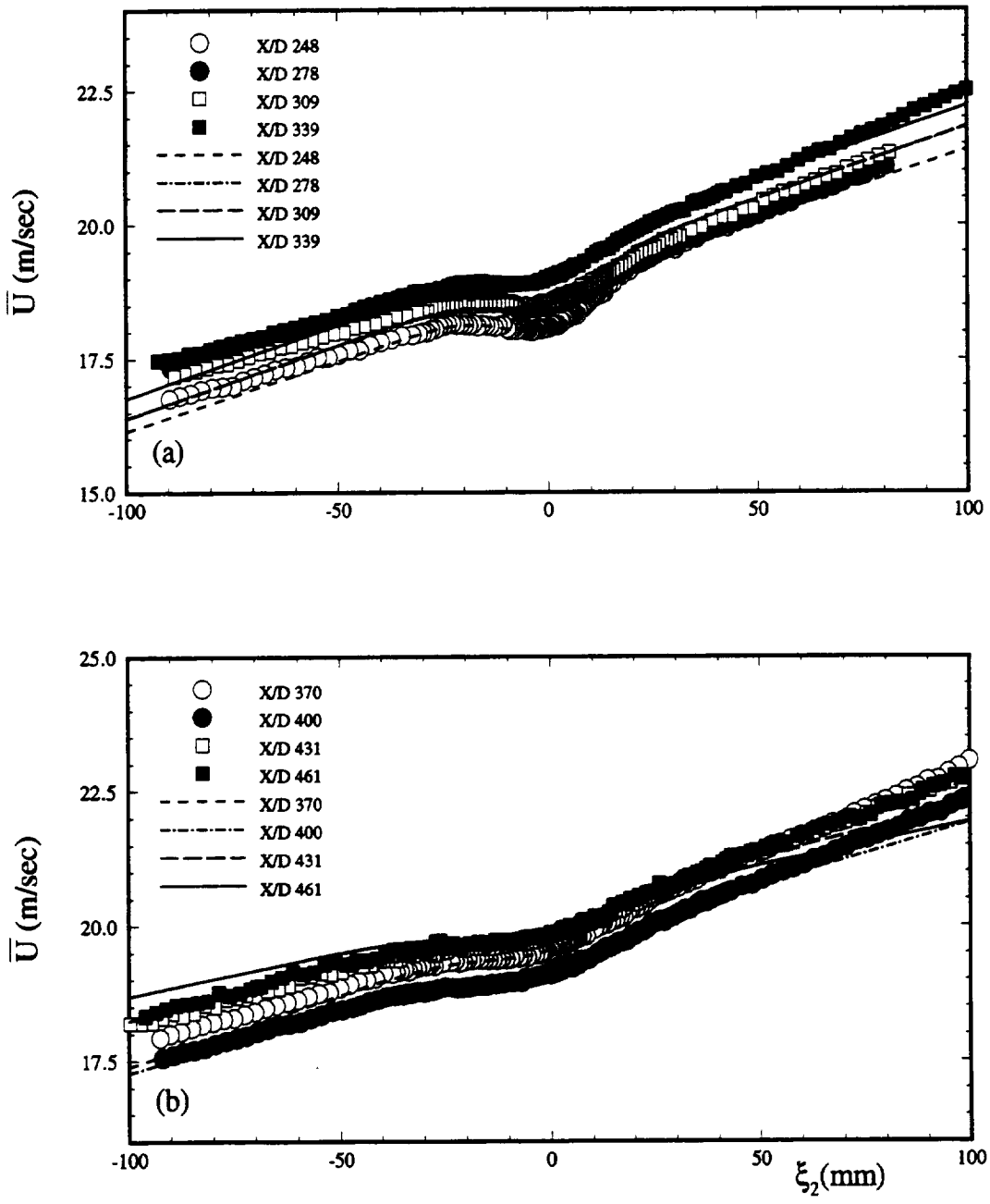


Fig. 25 Mean longitudinal velocity distribution in curved channel for zero pressure gradient, comparison of theory (lines) and experiment (symbols), (x/d:248-461)

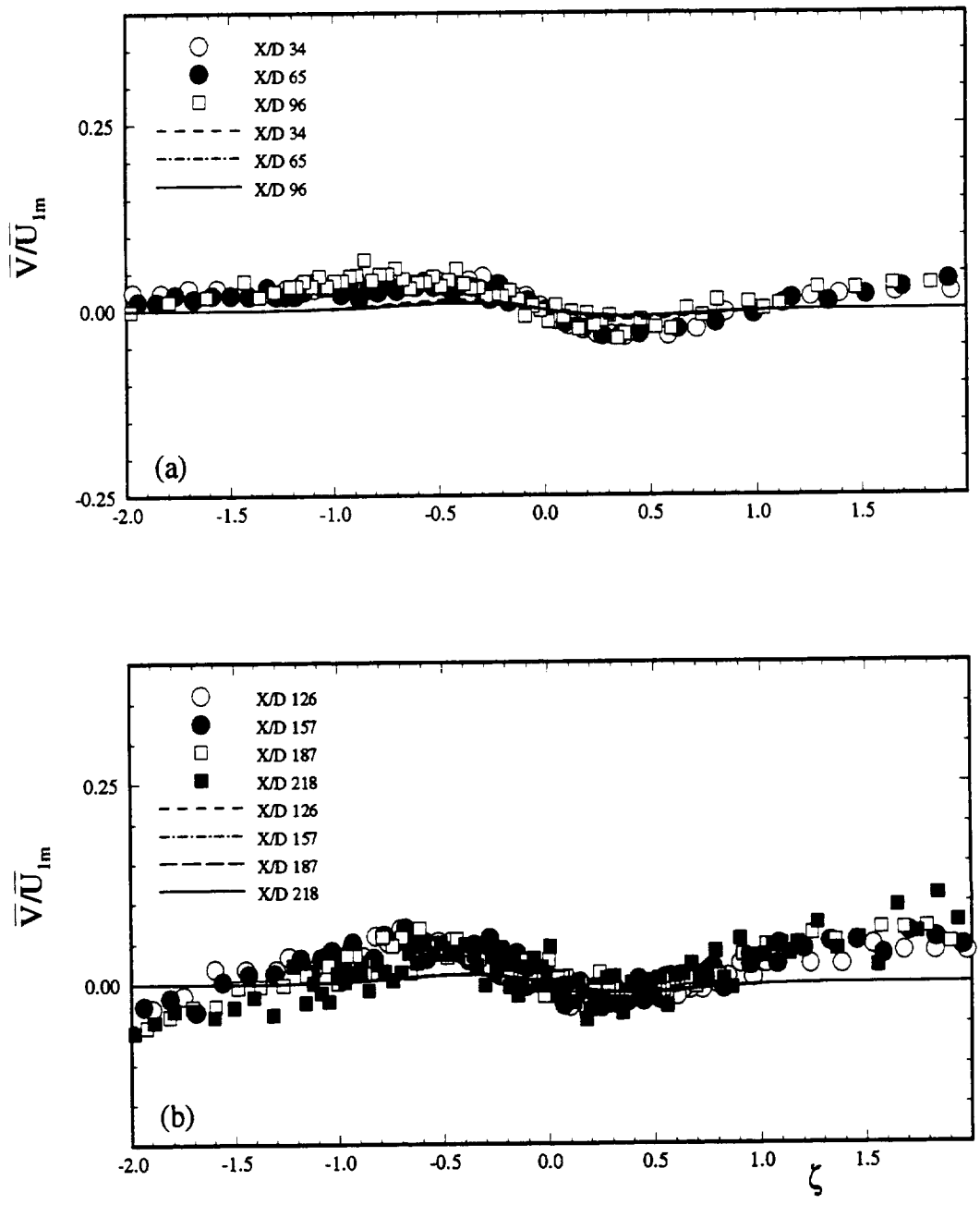


Fig. 26 Mean lateral velocity distribution in curved channel for zero pressure gradient, comparison of theory (lines) and experiment (symbols), (x/d:34-218)

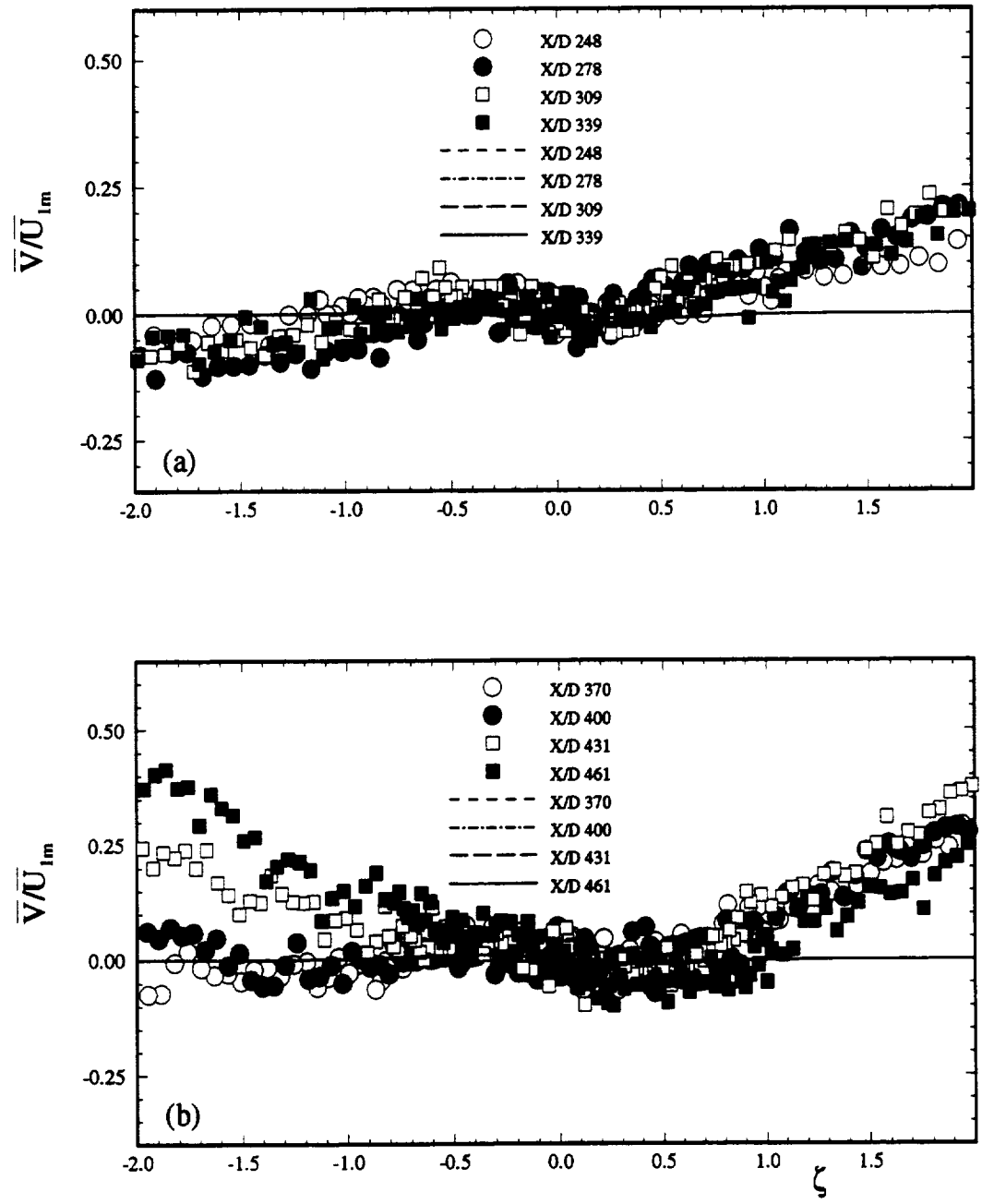


Fig. 27 Mean lateral velocity distribution in curved channel for zero pressure gradient, comparison of theory (lines) and experiment (symbols), (x/d:248-461)

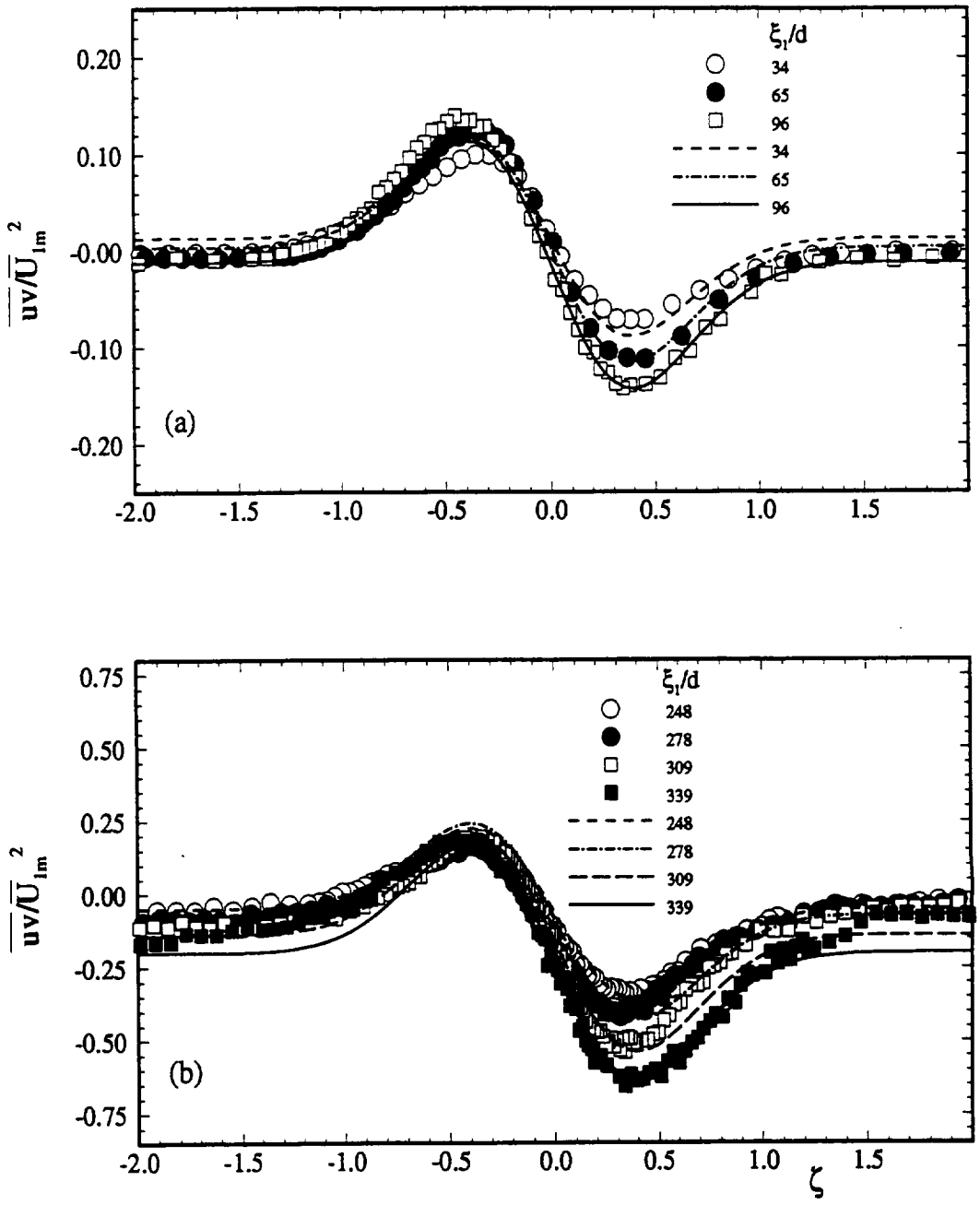


Fig. 28 Reynolds shear stress distribution in curved channel for zero pressure gradient, comparison of theory (lines) and experiment (symbols), (x/d:34-218)

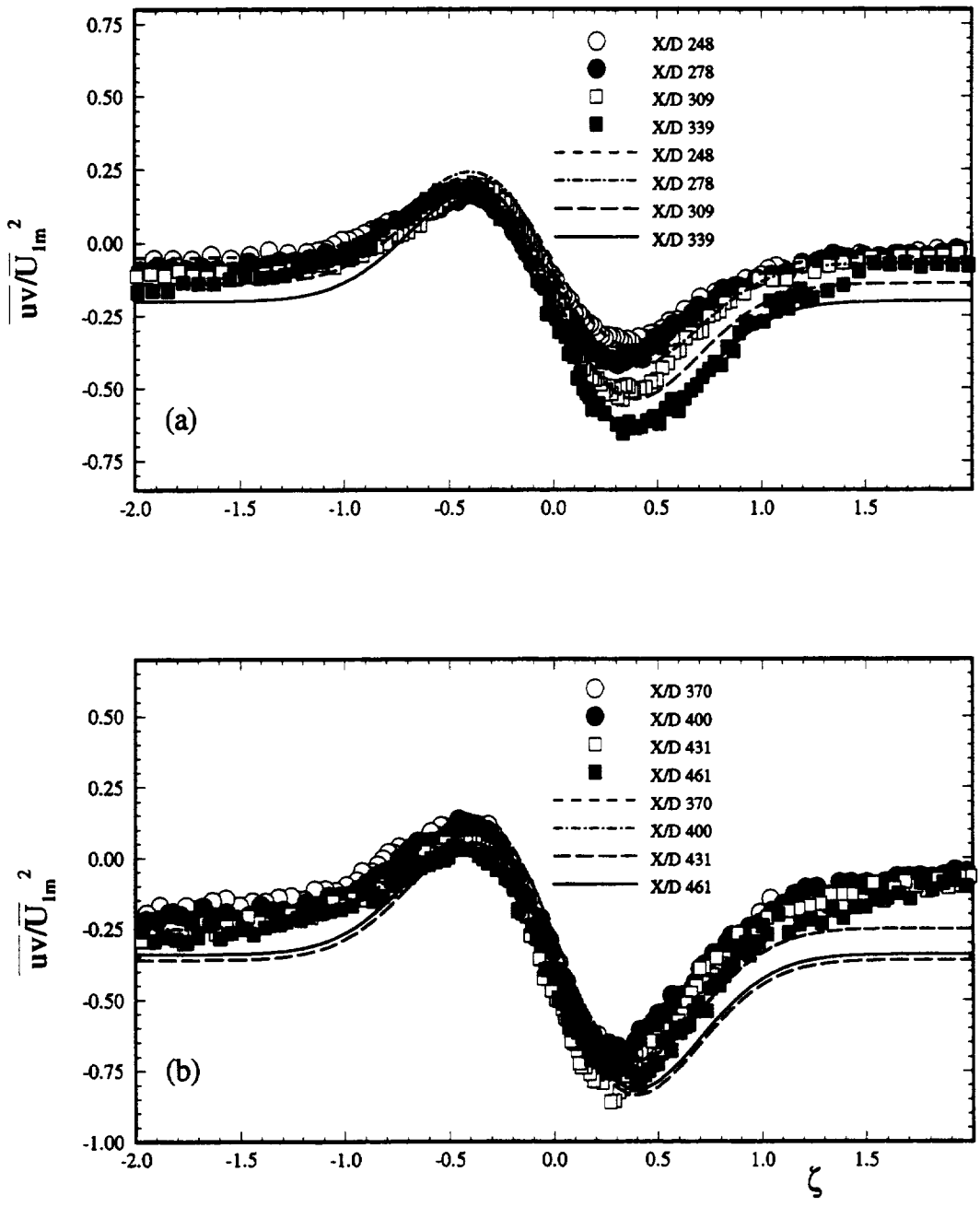


Fig. 29 Reynolds shear stress distribution in curved channel for zero pressure gradient, comparison of theory (lines) and experiment (symbols), (x/d:248-461)

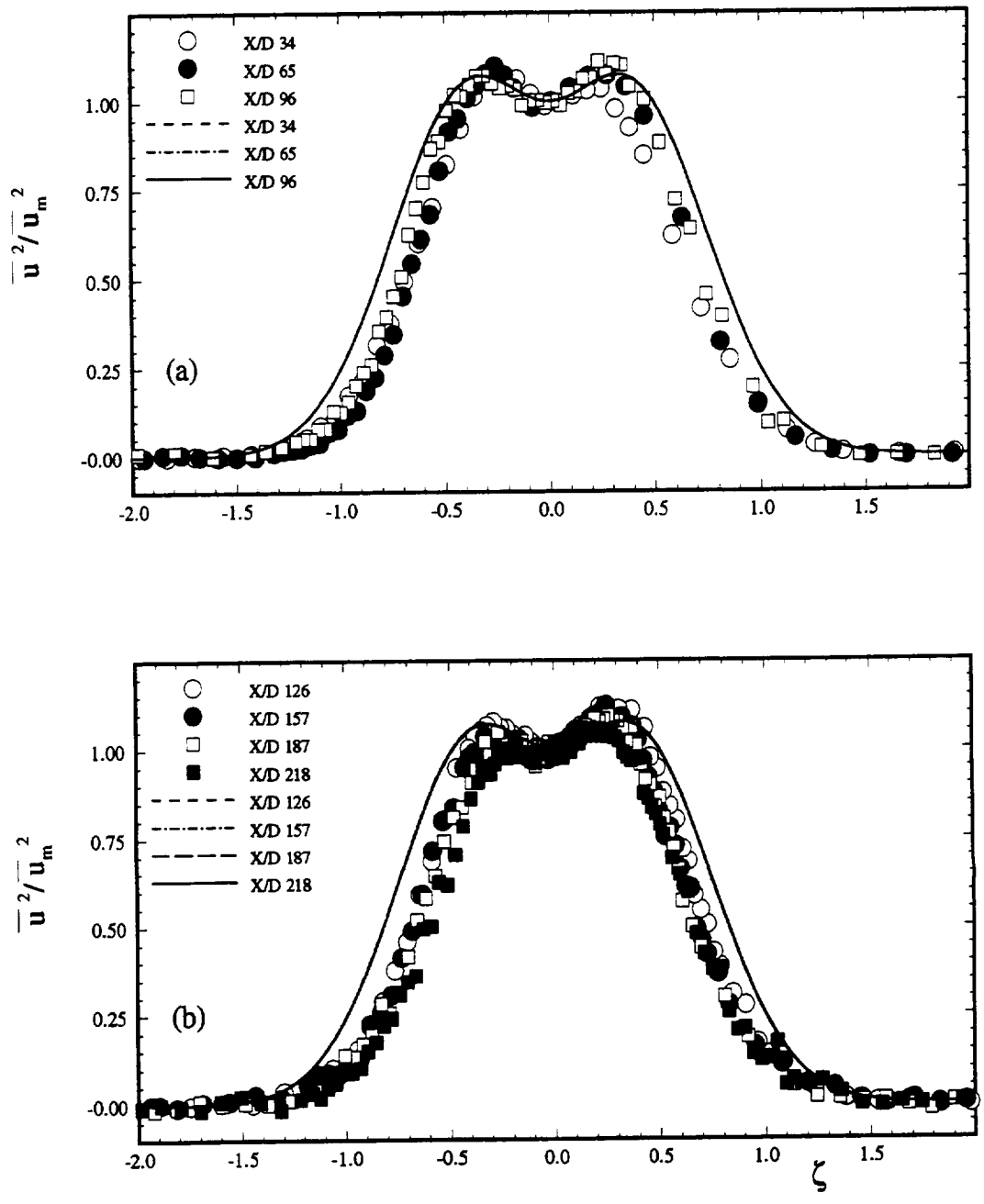


Fig. 30 Mean longitudinal turbulent fluctuations in curved channel for zero pressure gradient, comparison of theory (lines) and experiment (symbols), (x/d:34-218)

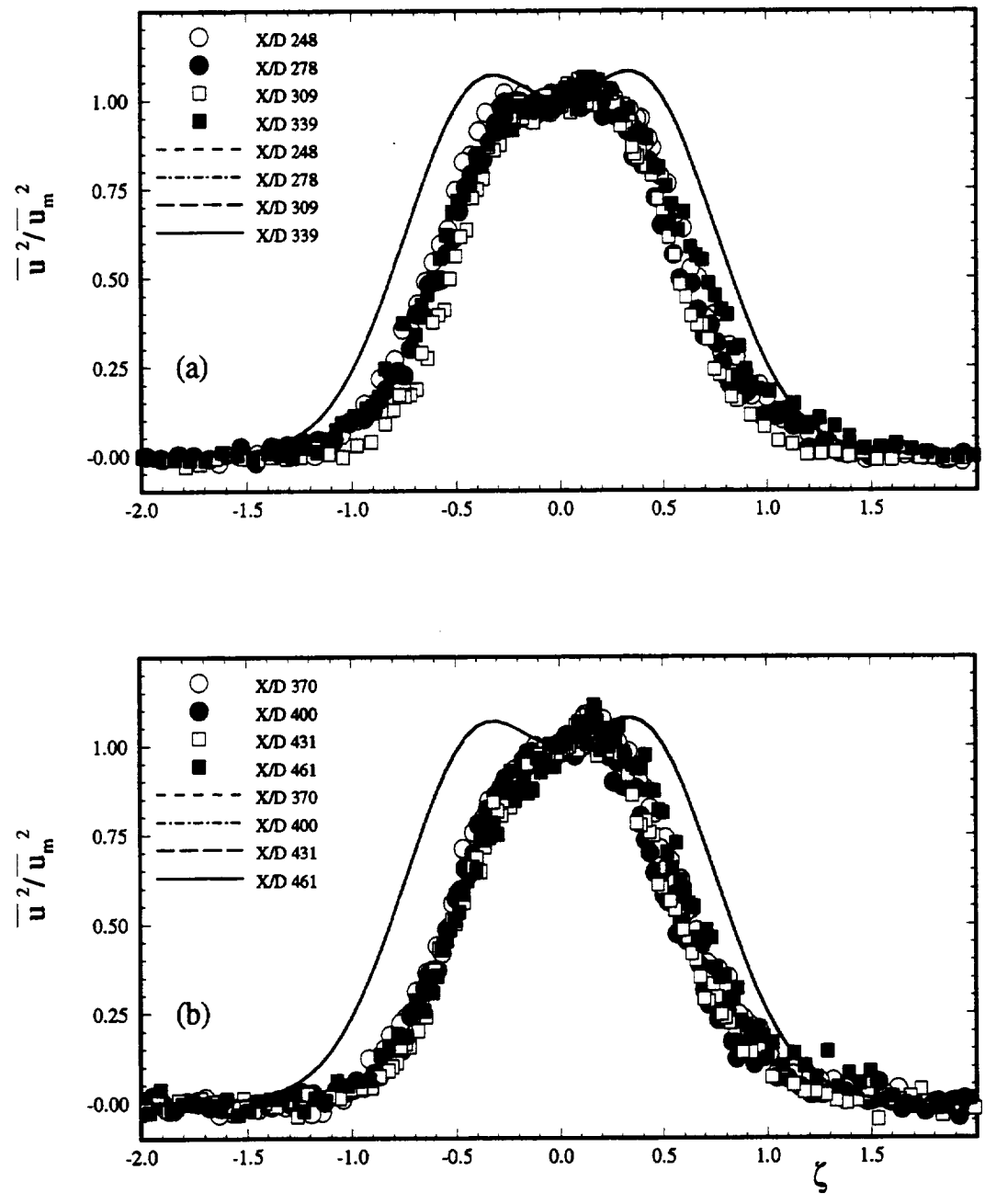


Fig. 31 Mean longitudinal turbulent fluctuations in curved channel for zero pressure gradient, comparison of theory (lines) and experiment (symbols), (x/d:248-461)

(Figs. 24 and 25) show reasonable agreement between theory and measurements, except for a slight deviation at the edges for higher x/d. The theory slightly under-predicted the mean lateral velocity (Figs. 26 and 27) distribution, which could be a result of the assumption that there is absolutely no streamwise pressure gradient inside the channel. In fact, experimental investigations show a mild favorable pressure gradient in the channel, so in that case, this deviation is justifiable. Comparison of Reynolds shear stress distribution for different locations downstream of the wake generating body is shown in Figs. 28 and 29. The values of the constant of integration in the expression have been evaluated from experiments and are presented in Table 1 (Appendix). As discussed earlier, this constant is a function of the longitudinal coordinate $\xi_1$. Except for a slight deviation at the edges, the peaks have been predicted quiet well, demonstrating asymmetry in shear stress distributions for all streamwise locations. Dimensionless longitudinal turbulent fluctuation impulse is presented in Figs. 30 and 31. This wake characteristic has been presented just to illustrate how it fits into a semi-theoretical framework. The value calculated for constant $a_2$ in Eq. (7.22) is 1.5. Thus, there is good agreement between theory and measurement up to an x/d of 218. The deviation beyond this location, as explained earlier in the straight channel case, could be a result of evaluating one of the constants in Eq. (7.22) from experimental values at a specific streamwise location.

### 9.3. Negative Pressure Gradient, Curved Channel

A summary of the comparison of theoretical predictions and experimental measurements for the case of flow under the influence of curvature and negative pressure gradient is shown in Figs. 32-43. Even in this case, the validation of the dimensionless wake velocity defect function, $\varphi_1 = e^{-\zeta^2}$ is evident, with excellent matching of results (Figs. 32 and 33). The mean longitudinal velocity profiles (Figs. 34 and 35) show perfect agreement up to a location of x/d = 215. Beyond this location, there is some deviation

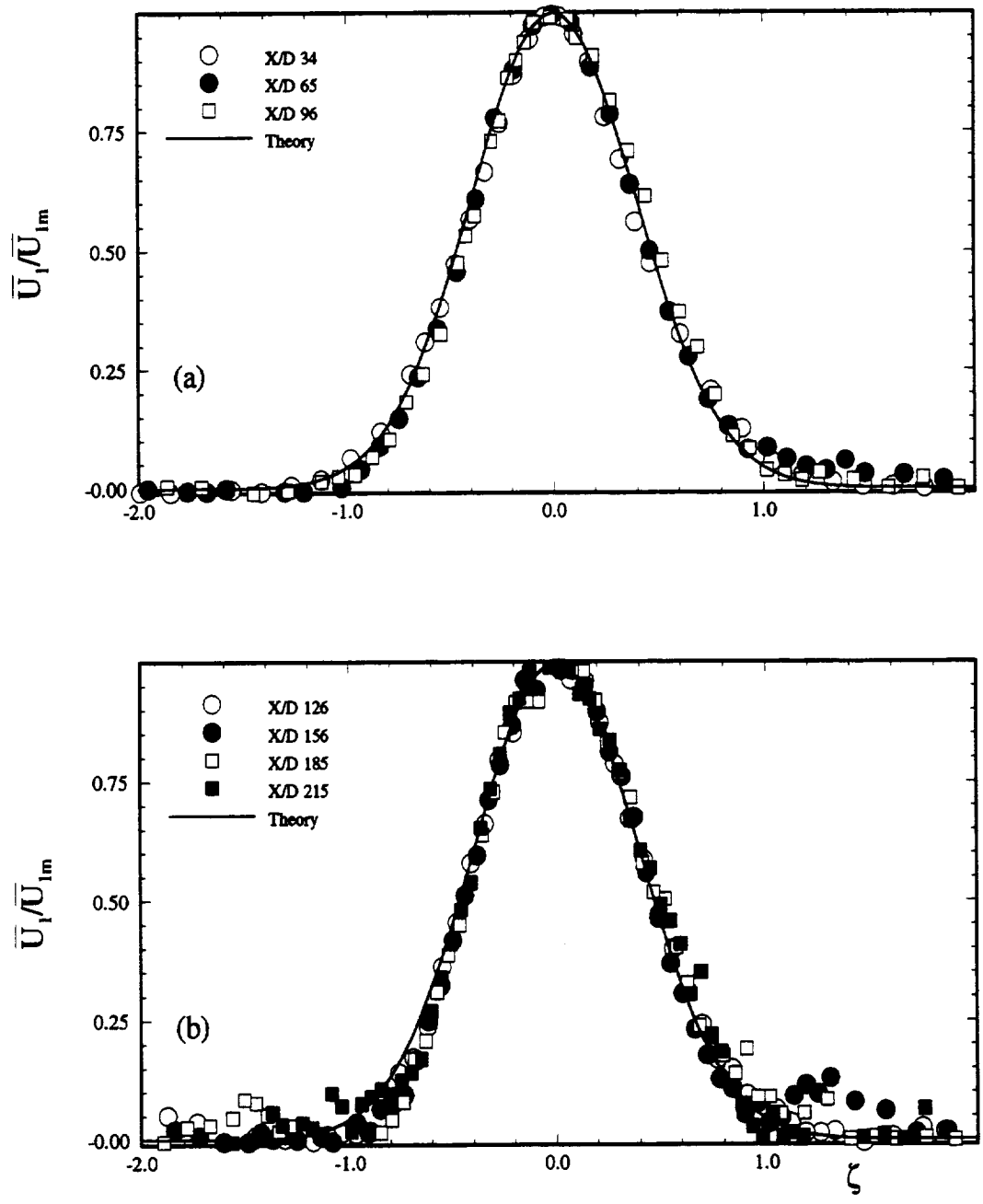


Fig. 32 Mean defect velocity distribution in curved channel for negative pressure gradient, comparison of theory (lines) and experiment (symbols), (x/d:34-215)

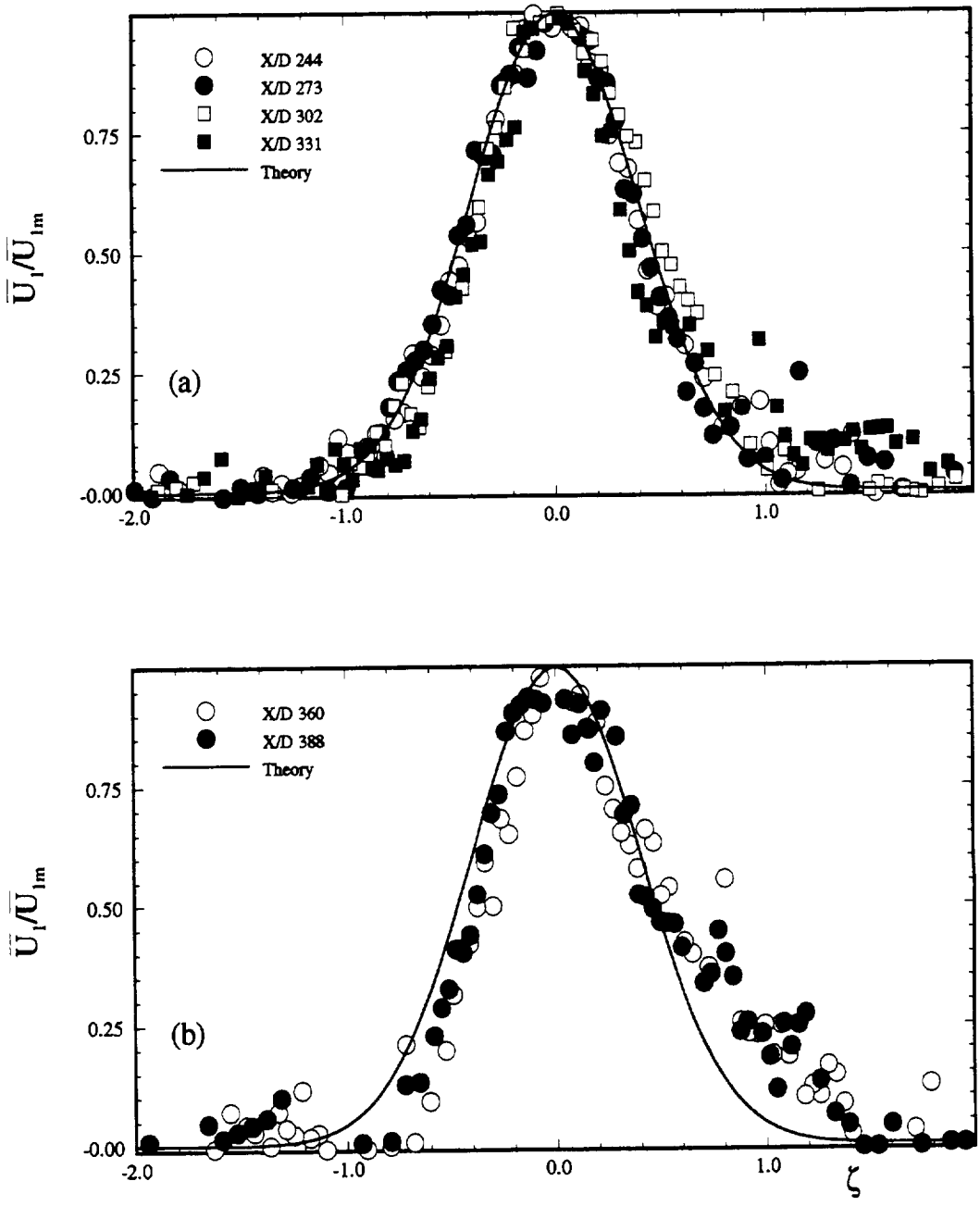


Fig. 33 Mean defect velocity distribution in curved channel for negative pressure gradient, comparison of theory (lines) and experiment (symbols), (x/d:244-388)

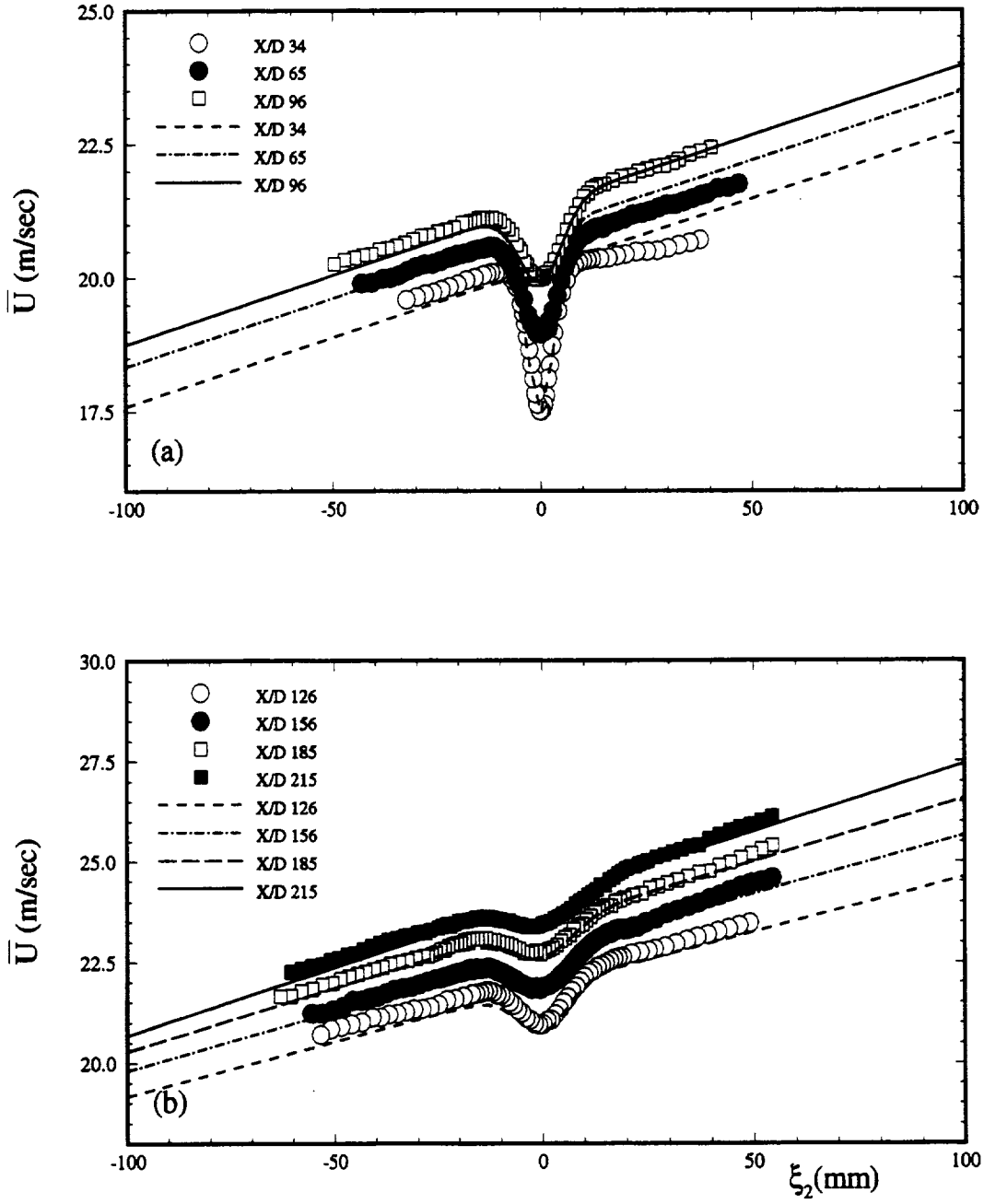


Fig. 34 Mean longitudinal velocity distribution in curved channel for negative pressure gradient, comparison of theory (lines) and experiment (symbols), (x/d:34-215)

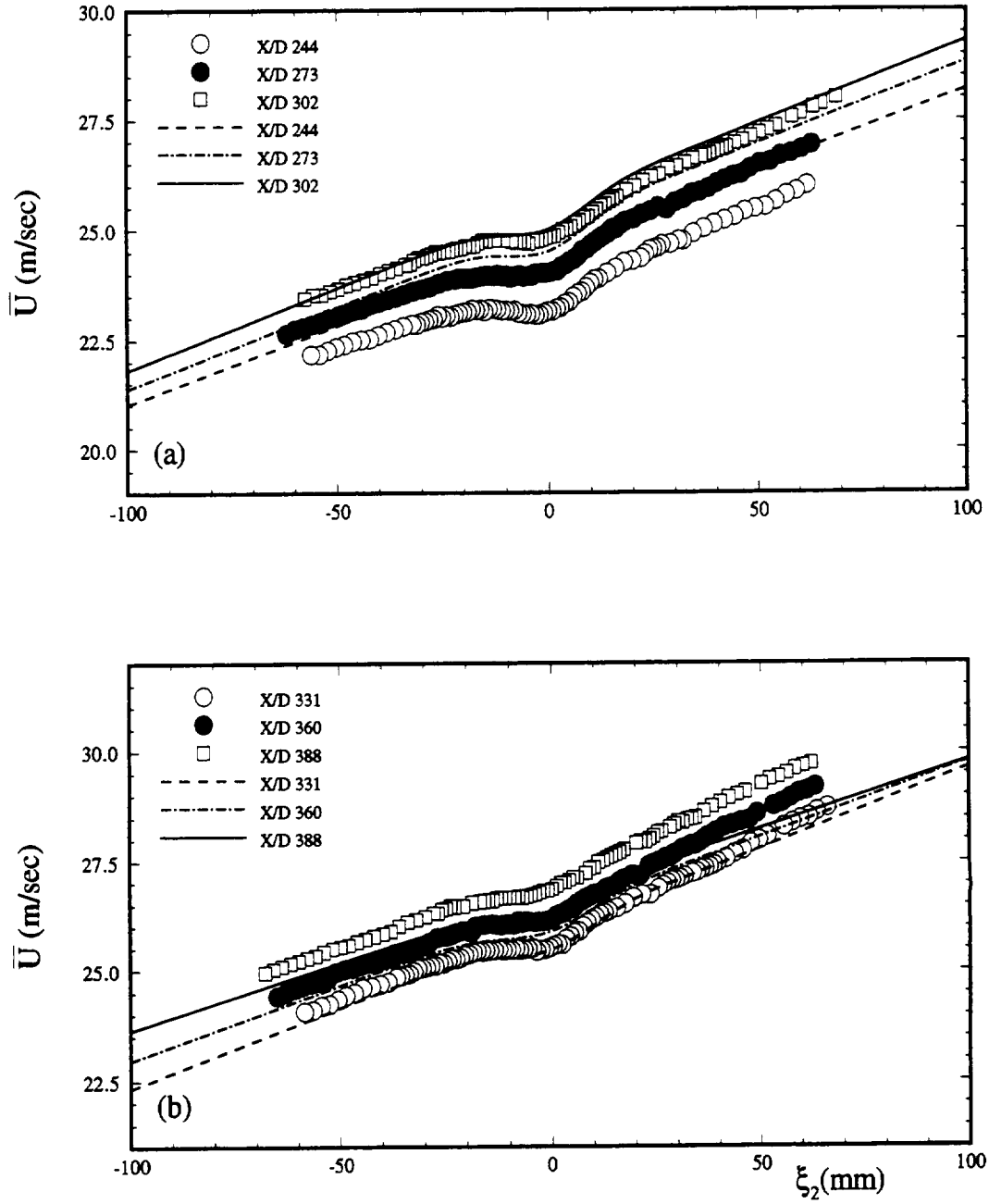


Fig. 35 Mean longitudinal velocity distribution in curved channel for negative pressure gradient, comparison of theory (lines) and experiment (symbols), (x/d:244-388)

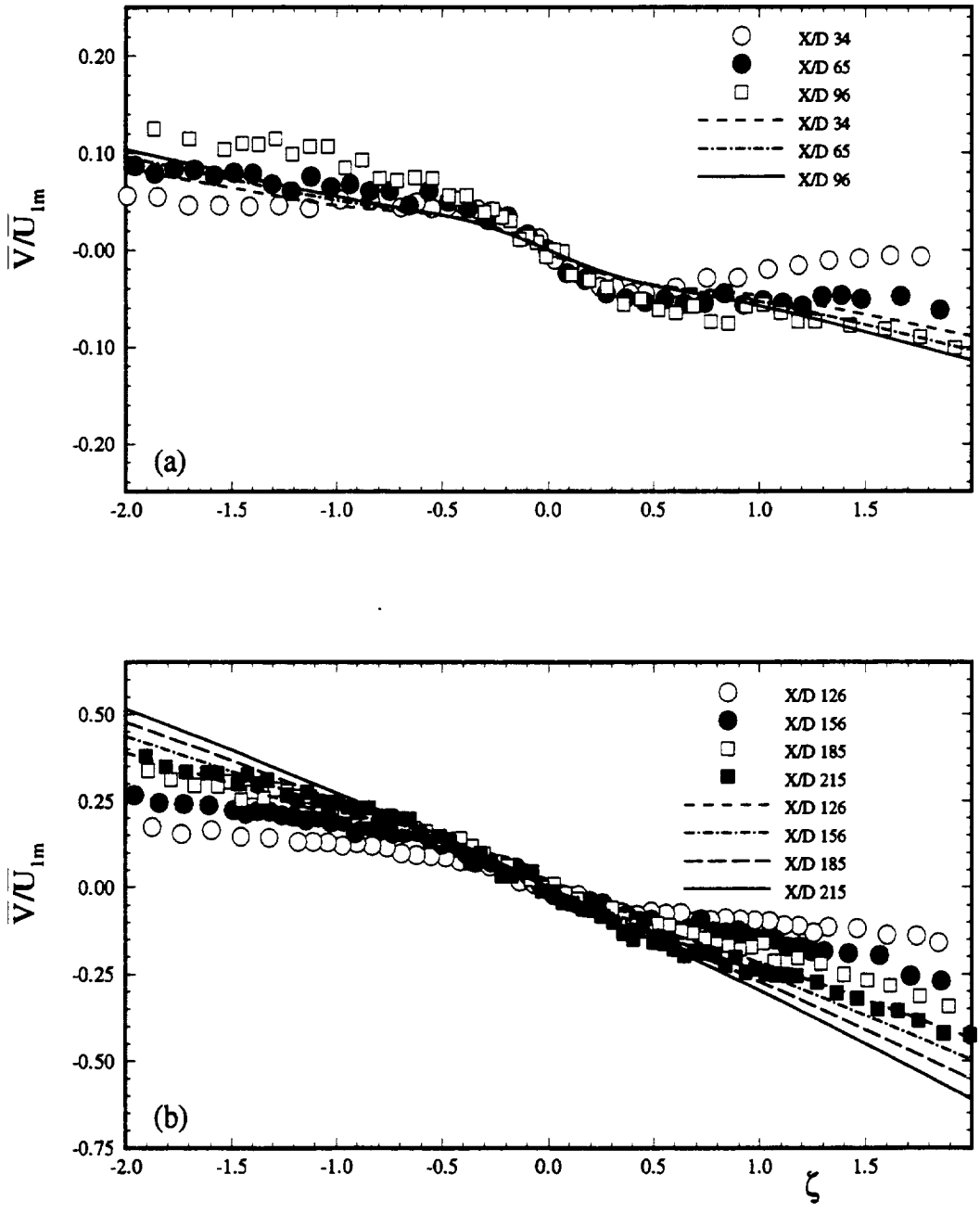


Fig. 36 Mean lateral velocity distribution in curved channel for negative pressure gradient, comparison of theory (lines) and experiment (symbols), (x/d:34-215)

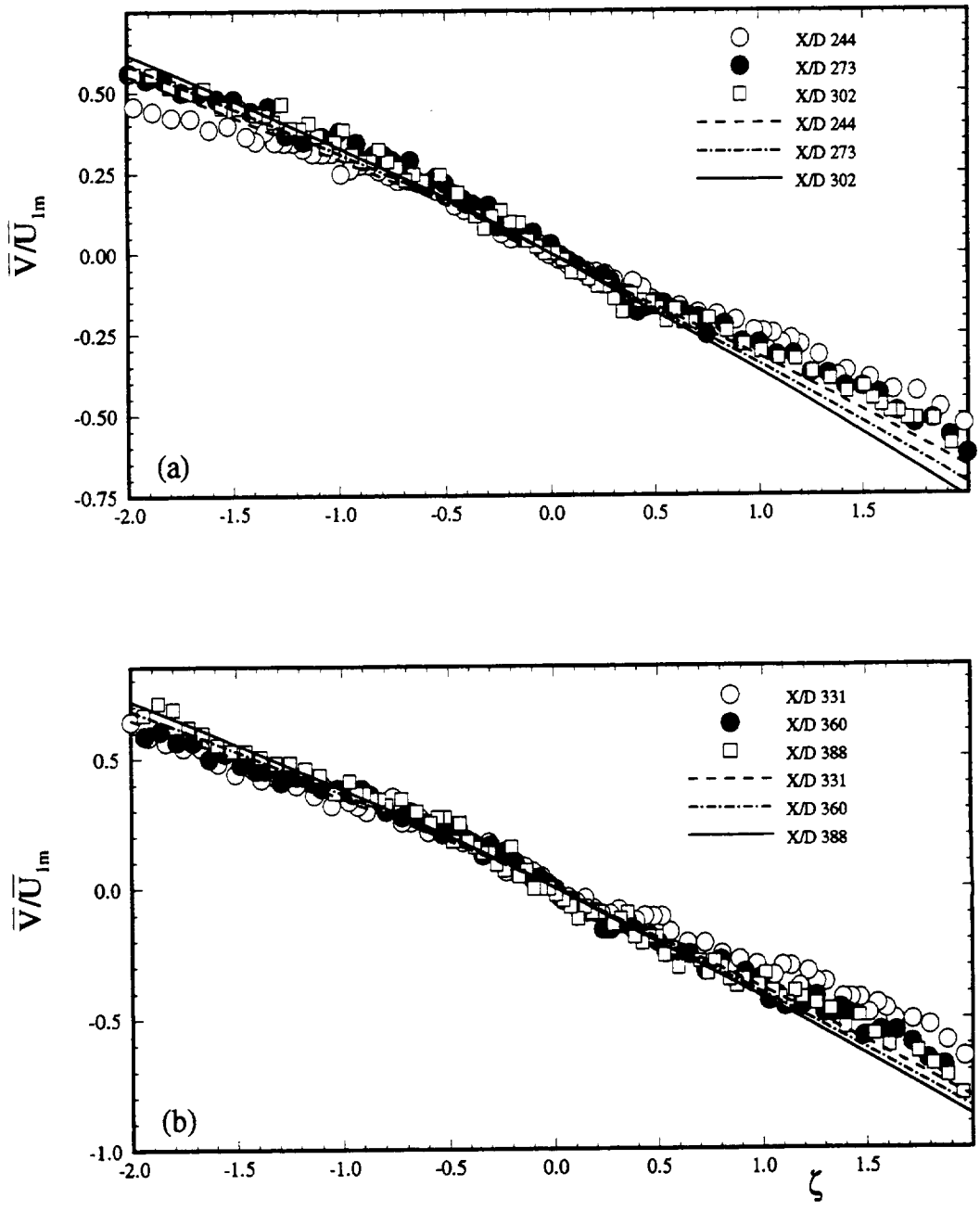


Fig. 37 Mean lateral velocity distribution in curved channel for negative pressure gradient, comparison of theory (lines) and experiment (symbols), (x/d:244-388)

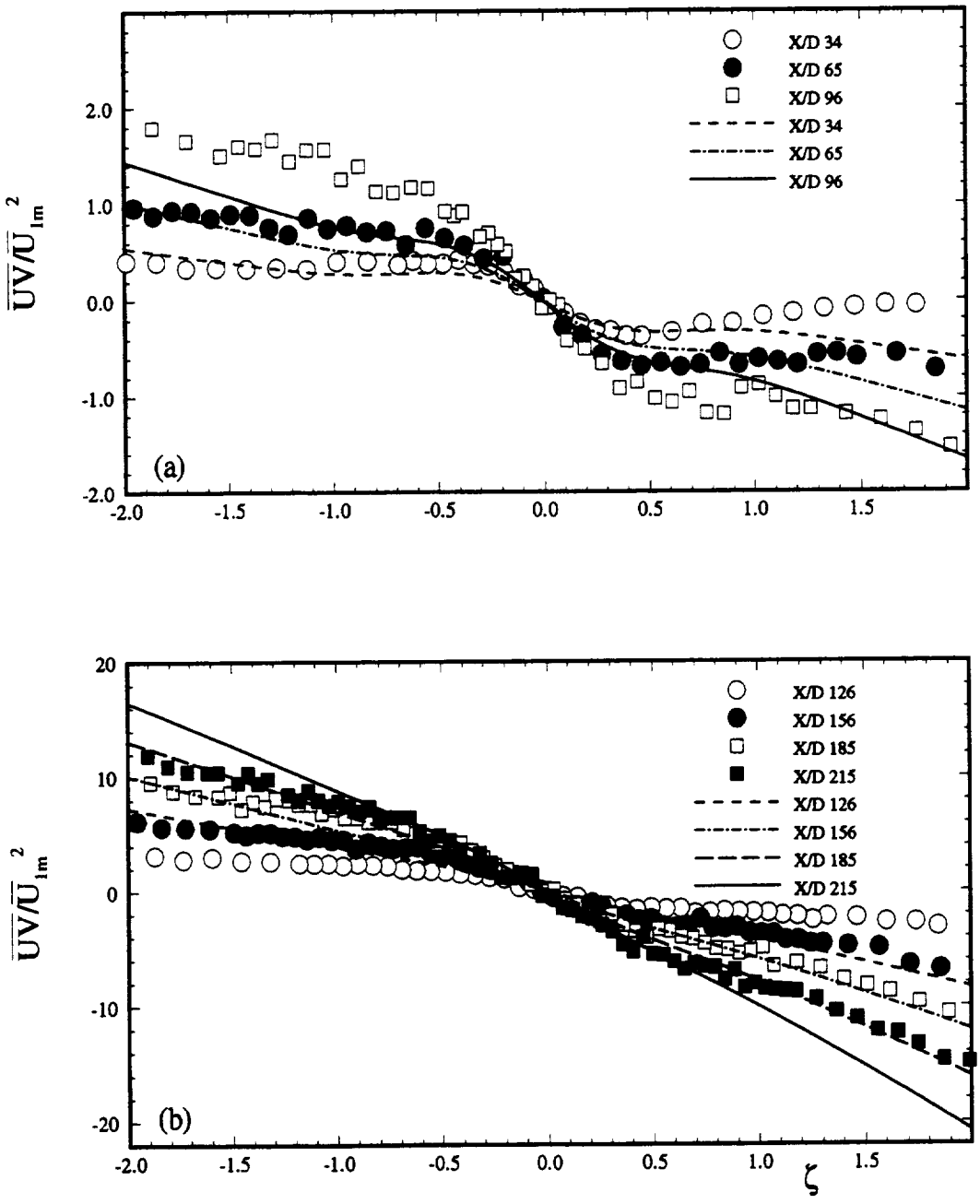


Fig. 38 Total impulse distribution in curved channel for negative pressure gradient, comparison of theory (lines) and experiment (symbols), (x/d:34-215)

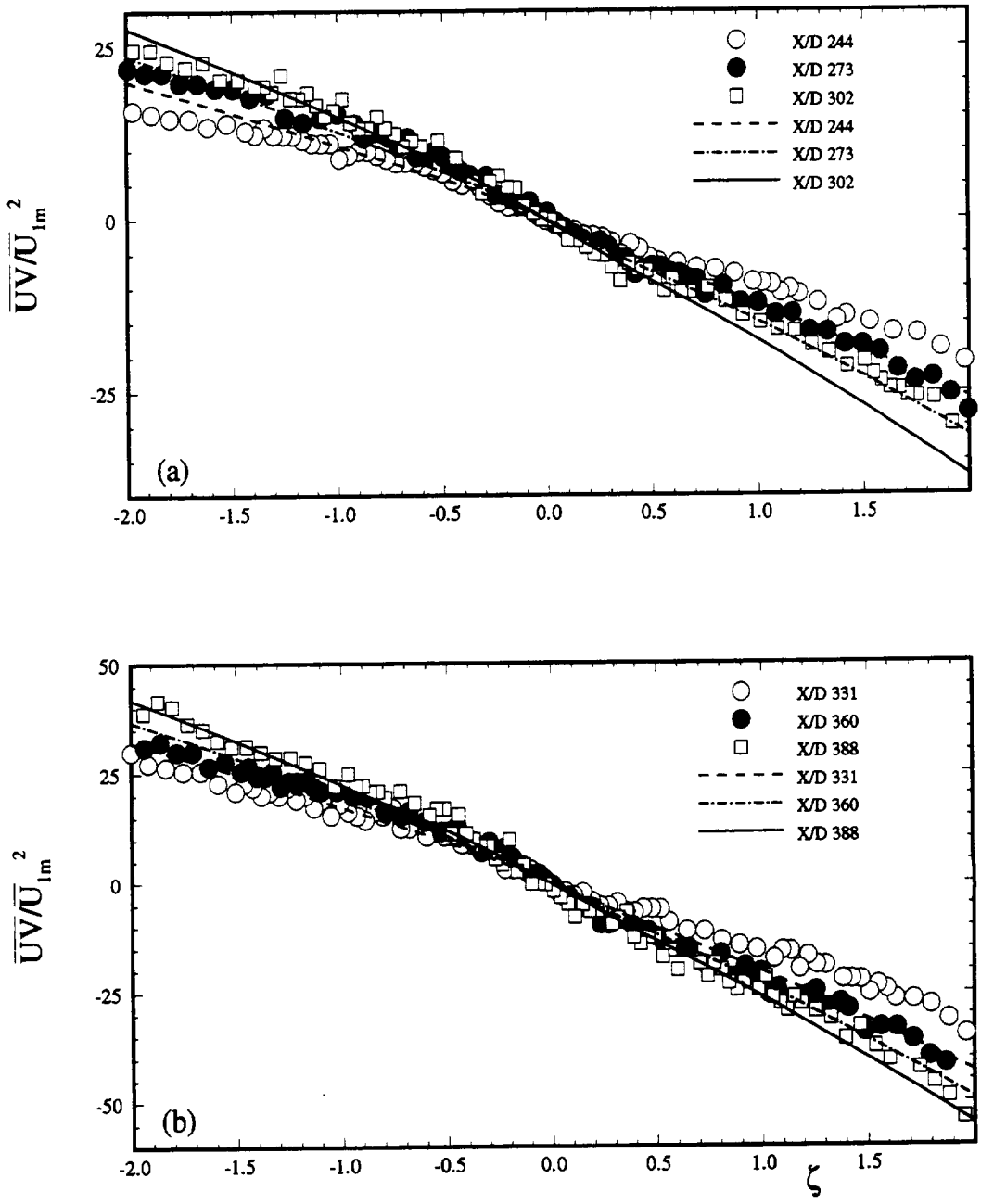


Fig. 39 Total impulse distribution in curved channel for negative pressure gradient, comparison of theory (lines) and experiment (symbols), (x/d:244-388)

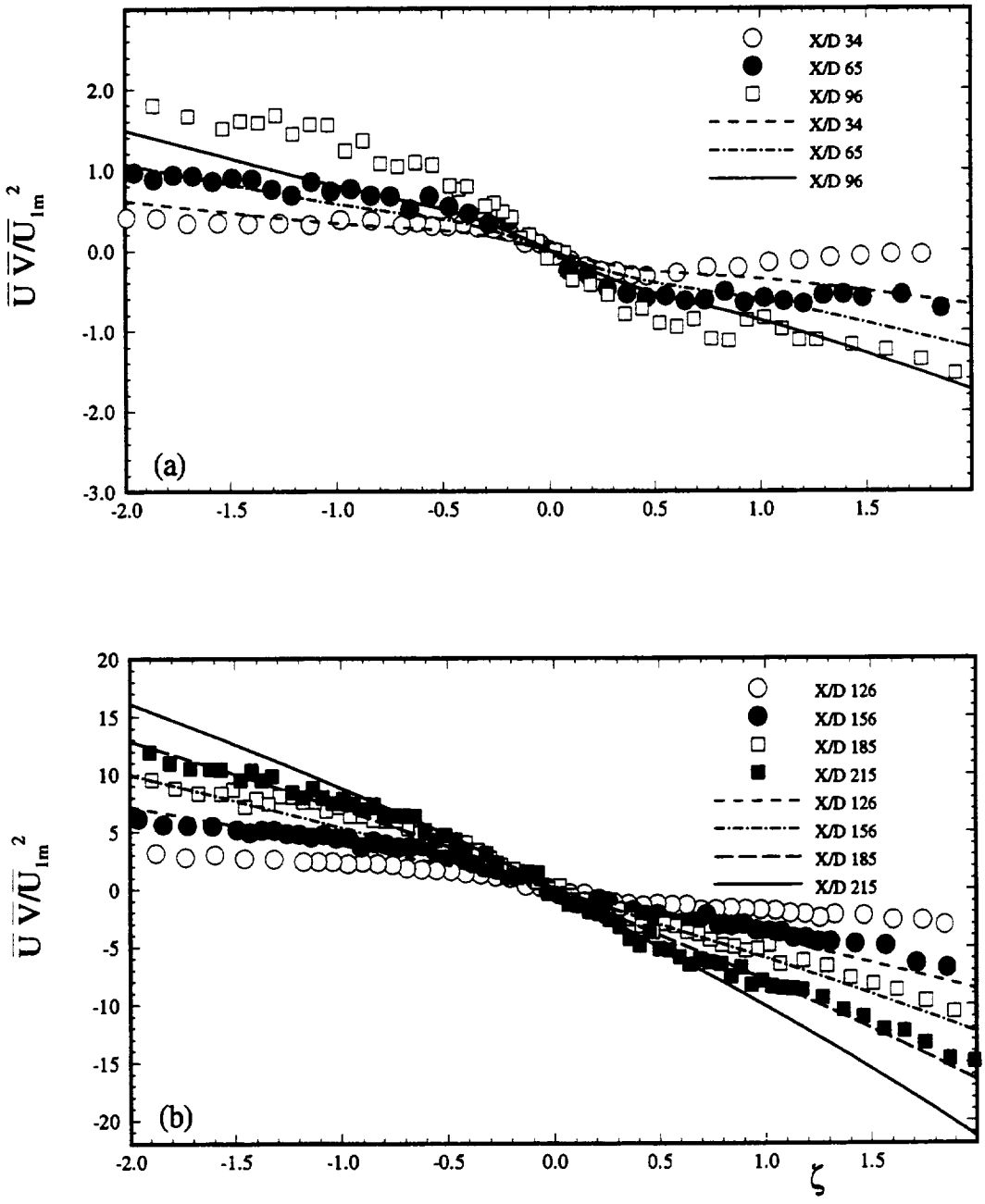


Fig. 40 Partial impulse distribution in curved channel for negative pressure gradient, comparison of theory (lines) and experiment (symbols), (x/d:34-215)

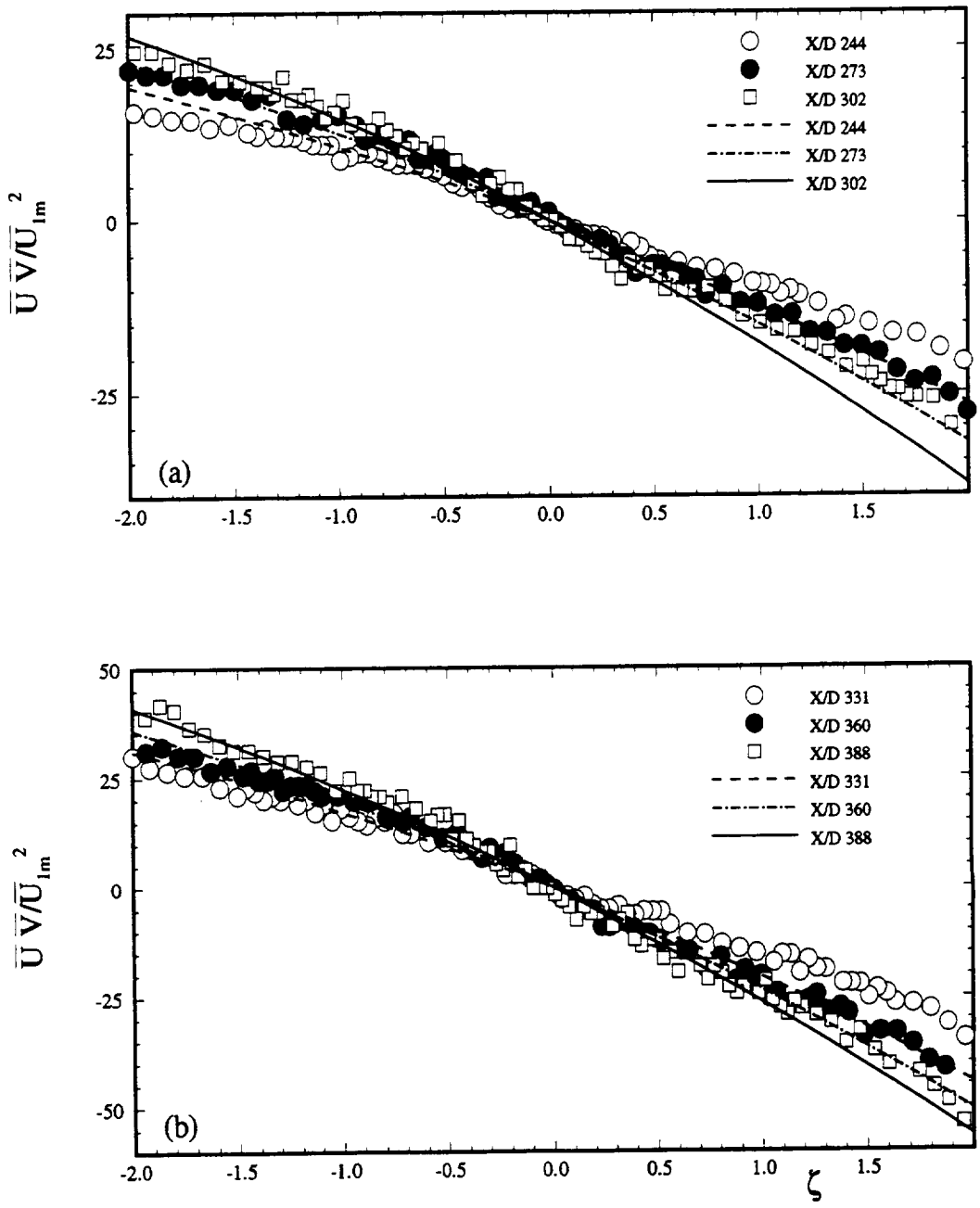


Fig. 41 Partial impulse distribution in curved channel for negative pressure gradient, comparison of theory (lines) and experiment (symbols), (x/d:244-388)

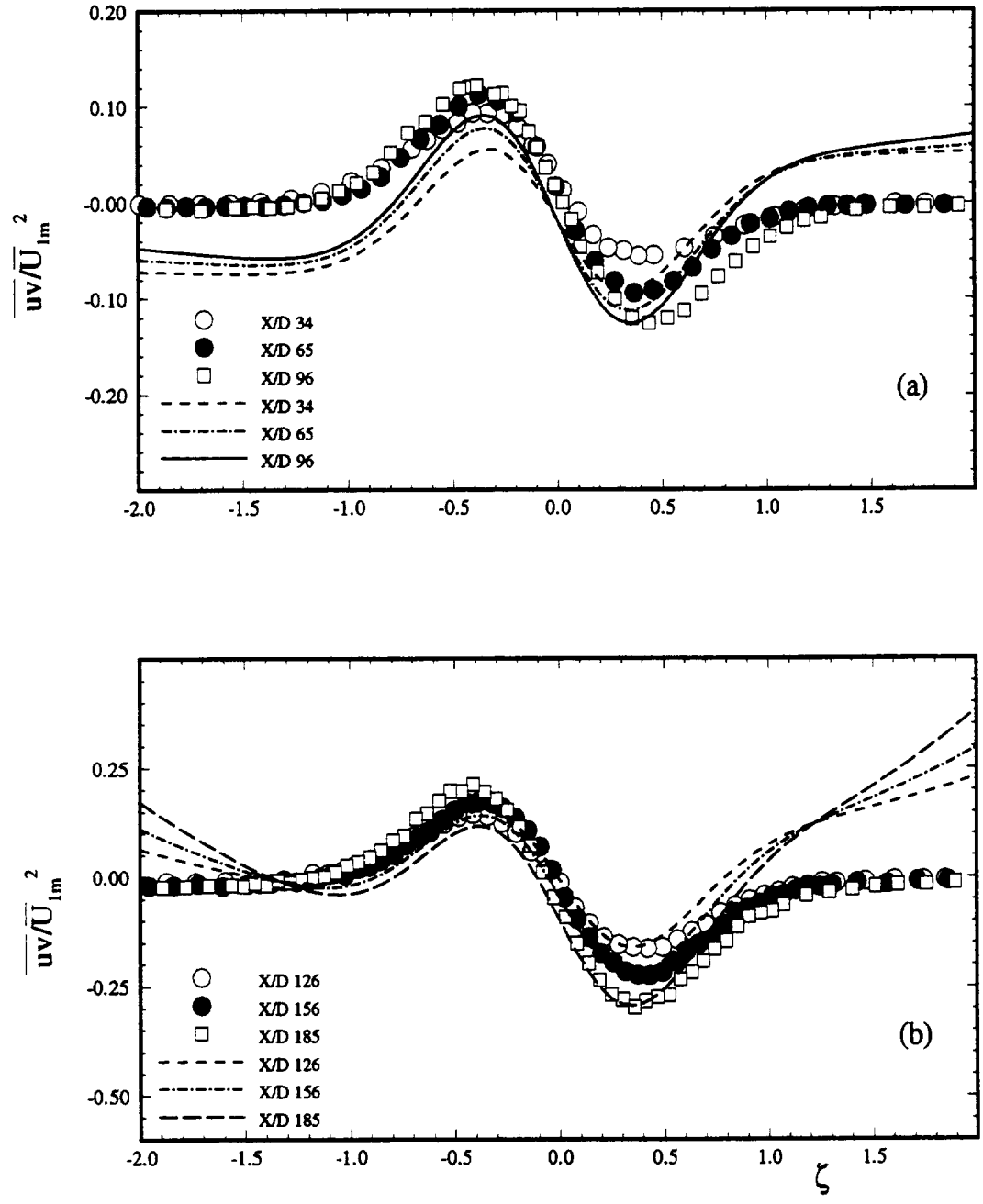


Fig. 42 Reynolds shear stress distribution in curved channel for negative pressure gradient, comparison of theory (lines) and experiment (symbols), (x/d:34-185)

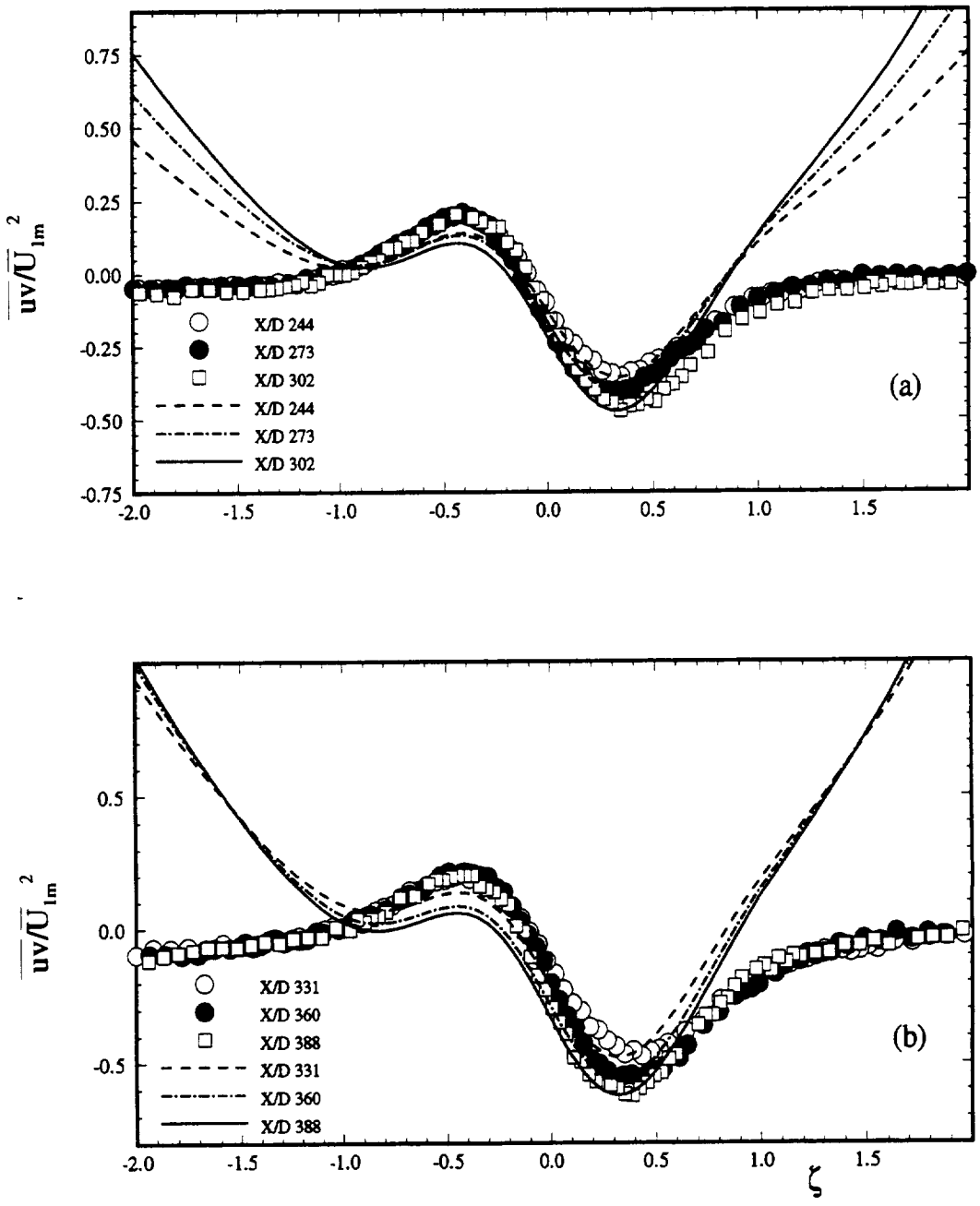


Fig. 43 Reynolds shear stress distribution in curved channel for negative pressure gradient, comparison of theory (lines) and experiment (symbols), (x/d:244-388)

between the theory and experimental results for some x/d. This deviation is a reflection of the deviation in $U_{p0}$ provided from experiments (shown by symbols) and the actual $U_{p0}$ implemented into theory (shown by solid line) through a power fit (Fig. 11). The given $U_{p0}$ (shown by symbols) cannot be directly implemented because it is necessary to evaluate $\partial U_{p_0}/\partial \xi_1$ from the differentiation of the fit that has been put through given $U_{p0}$. Unlike the zero pressure gradient case, the mean lateral velocity profiles (Figs. 36 and 37) show reasonable agreement between theory and experiment. Except for a small deviation at the edges for lower x/d, the theory generally holds good. Figures 38 and 39 show the total impulse distribution, while Figs. 40 and 41 show the partial impulse distribution for different locations downstream of the wake generating body. It is obvious from Figs. 42 and 43 that the core of the wake region ($-0.75<\zeta<0.75$), with respect to Reynolds shear stress, is predicted quite well by the theory. But there is a considerable amount of deviation outside this region, i.e. near the edges. This deviation is a contribution from the highly over-predicted total impulse and the slightly over-predicted partial impulse, because shear stress is calculated from their difference. This over-prediction is due to the slope of the plotted characteristics, which is sensitive to the distribution of $\partial U_{p_0}/\partial \xi_1$, which in turn is representative of the pressure gradient present in the channel. Had the pressure distribution been measured rather than calculated from a power fit through given $U_{p0}$, much better agreement might have been obtained. The value of the constant in the shear stress expression has been evaluated from experiments and is presented in Table 2 (Appendix).

### 9.4. Positive Pressure Gradient, Curved Channel

The results of the comparison of theoretical and experimental values for positive pressure gradient in a curved channel for different wake characteristics is shown in Figs. 44-55. Excellent agreement was found between theory and experiment in the dimensionless wake velocity defect function distribution (Figs. 44 and 45). Reasonably

better match of the theory with the experiment is apparent in mean longitudinal velocity profiles (Figs. 46 and 47). Theory has been able to predict the mean lateral velocity (Figs. 48 and 49) quite well up to a location of x/d = 345, except for small deviations at the edges. A comparison of Reynolds shear stress distributions is presented in Figs. 54 and 55. The evaluated constant of integration in the shear stress expression is presented in Table 3 (Appendix). Reasonable agreement is evident up to an x/d of 157, beyond which the deviation at the edges becomes more and more apparent with increasing x/d. As discussed earlier in the case of negative pressure gradient, the core of the wake region is well predicted, while deviation at the edges coming from over-predicted total impulse and partial impulse distributions has been attributed to the lack of pressure distribution.

### 9.5. Mild Pressure Gradient, Mild Curvature

Discussion of the comparison of theory with the experimental measurements of Nakayama (1987), available from literature, is presented in this section. Nakayama studied the influence of mild curvature and mild pressure gradient on fully developed two-dimensional turbulent wakes deflected by an airfoil-like thin plate placed at small angles in the external flow. A wire of diameter 1.6 mm was used as a wake generator and the deflector plate was placed below the wake at two angles, ± 7 degrees. The flow when the angle of attack of the deflector is + 7 degrees was referred to as Flow A and that corresponding to - 7 degrees was Flow B. The free-stream velocity $U_\infty$ was held constant within 1% of 15 m/sec. Measurements of mean longitudinal, lateral velocities, wake velocity defect and Reynolds shear stress for Flow A were compared with theory. Information about $U_{p0}$ and $\bar{U}_{1m}$ necessary to implement the theory are calculated and presented in Table 4 (Appendix) and also shown in Fig. 56, based on the information provided in his paper.

The results of comparison for different wake characteristics are shown in Figs.

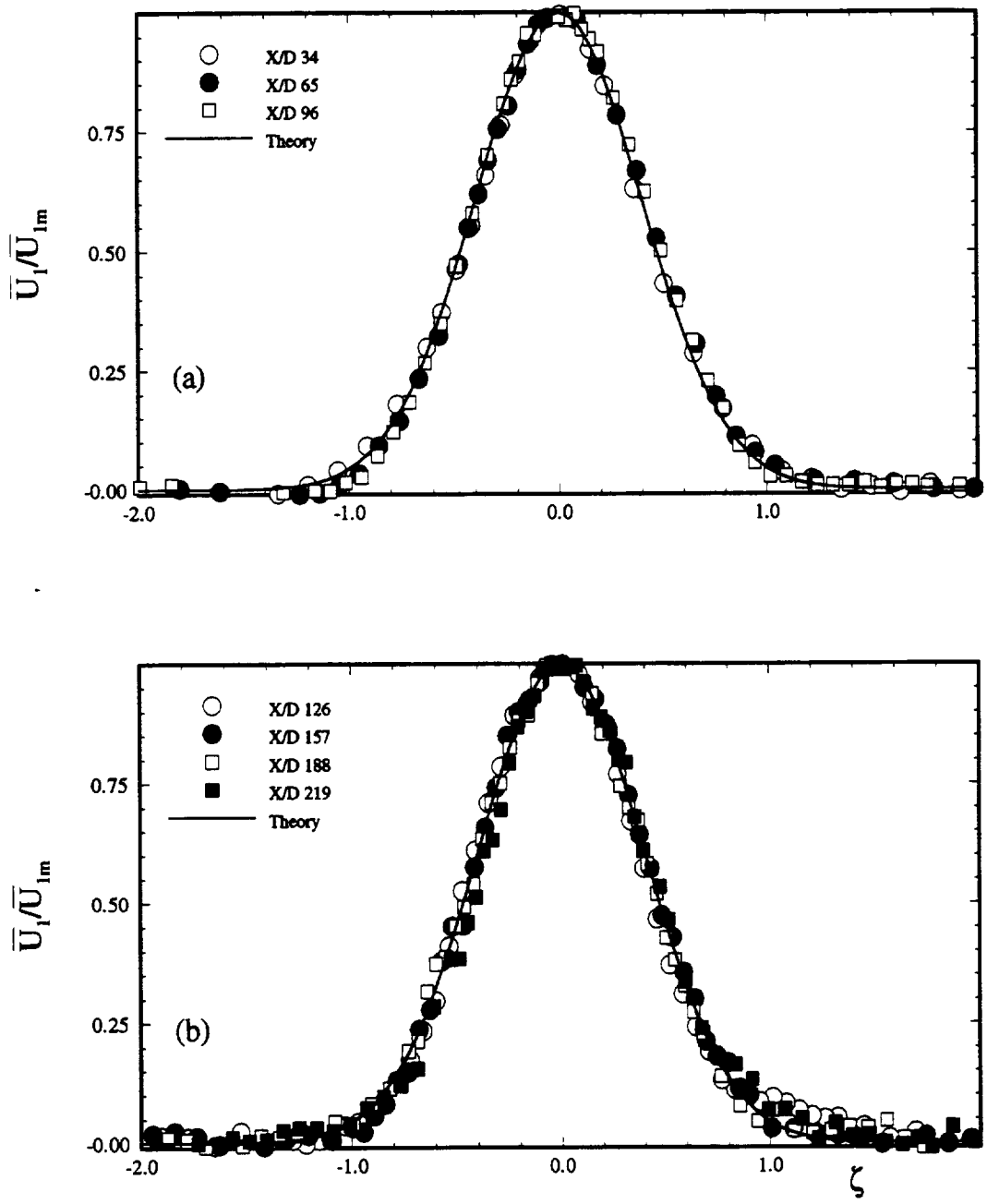


Fig. 44 Mean defect velocity distribution in curved channel for positive pressure gradient, comparison of theory (lines) and experiment (symbols), (x/d:34-219)

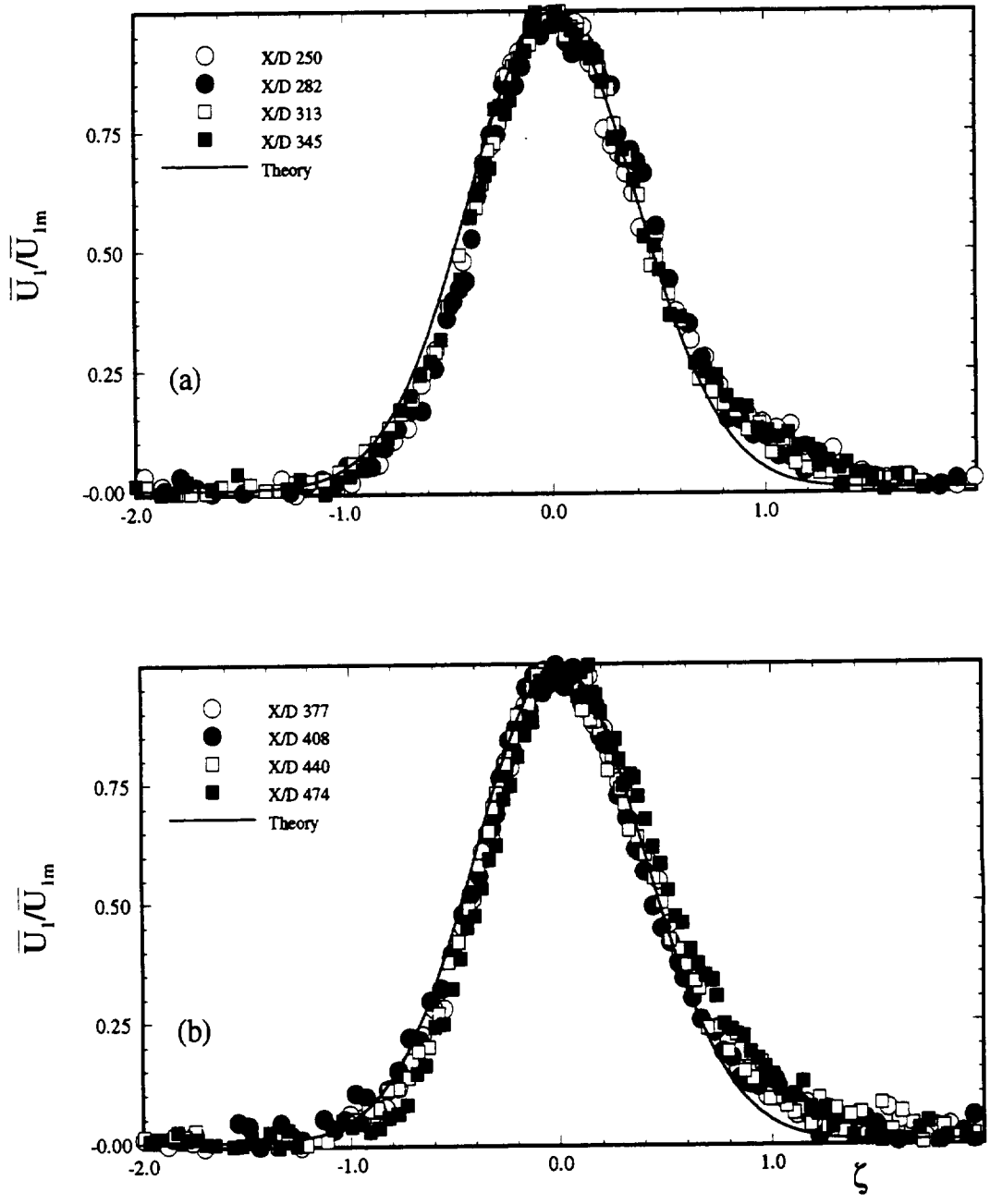


Fig. 45 Mean defect velocity distribution in curved channel for positive pressure gradient, comparison of theory (lines) and experiment (symbols), (x/d:250-474)

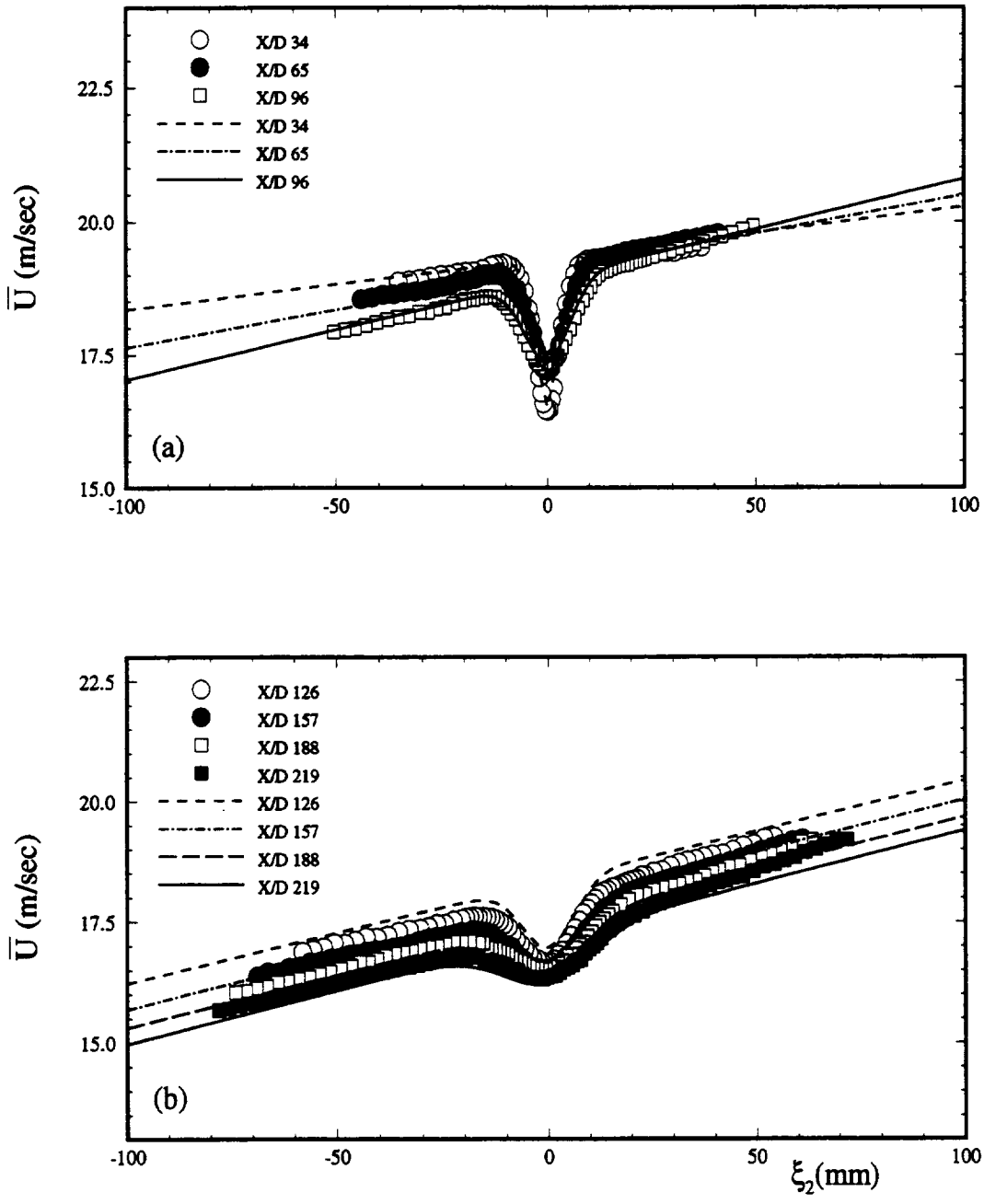


Fig. 46 Mean longitudinal velocity distribution in curved channel for positive pressure gradient, comparison of theory (lines) and experiment (symbols), (x/d:34-219)

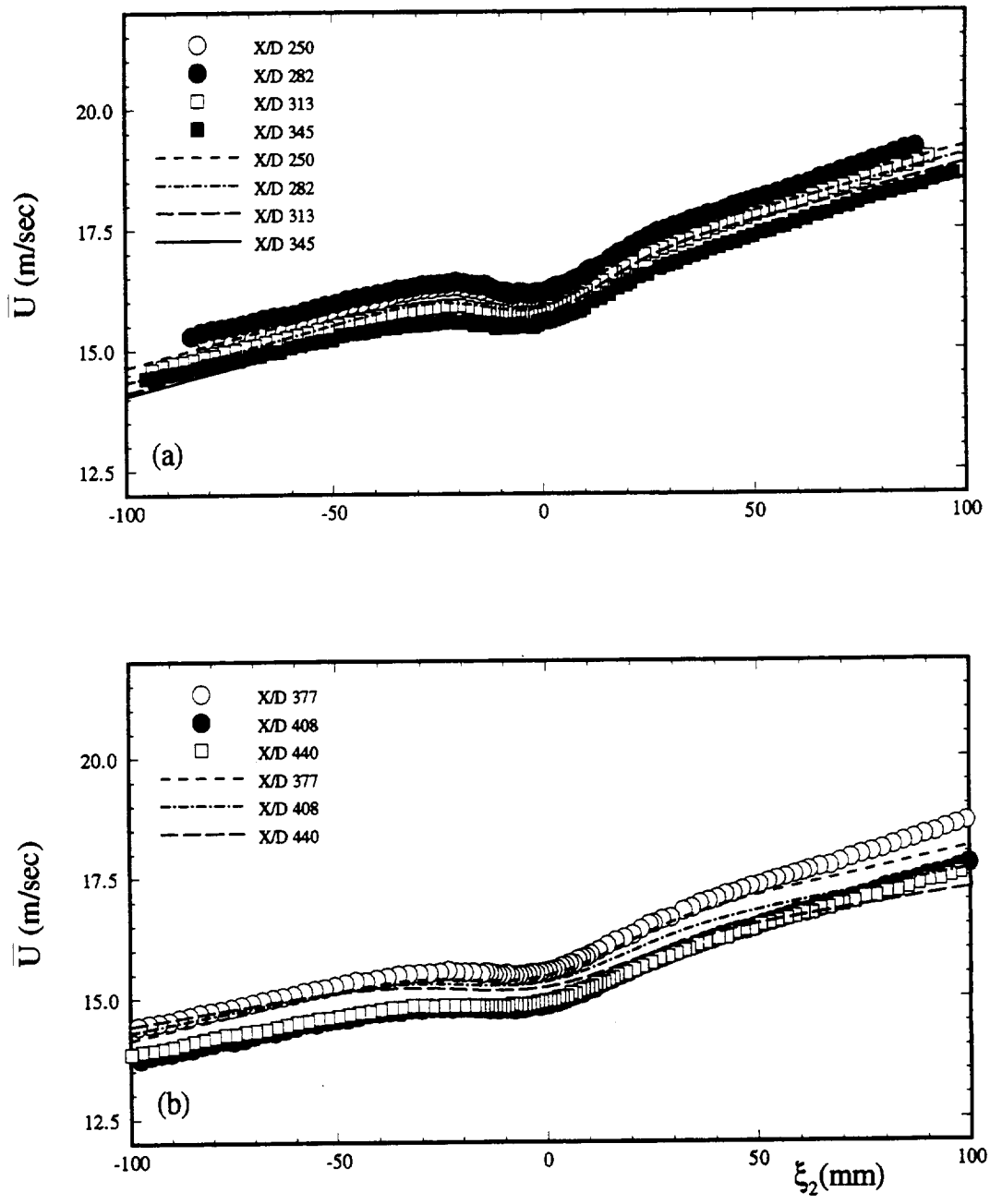


Fig. 47 Mean longitudinal velocity distribution in curved channel for positive pressure gradient, comparison of theory (lines) and experiment (symbols), (x/d:250-440)

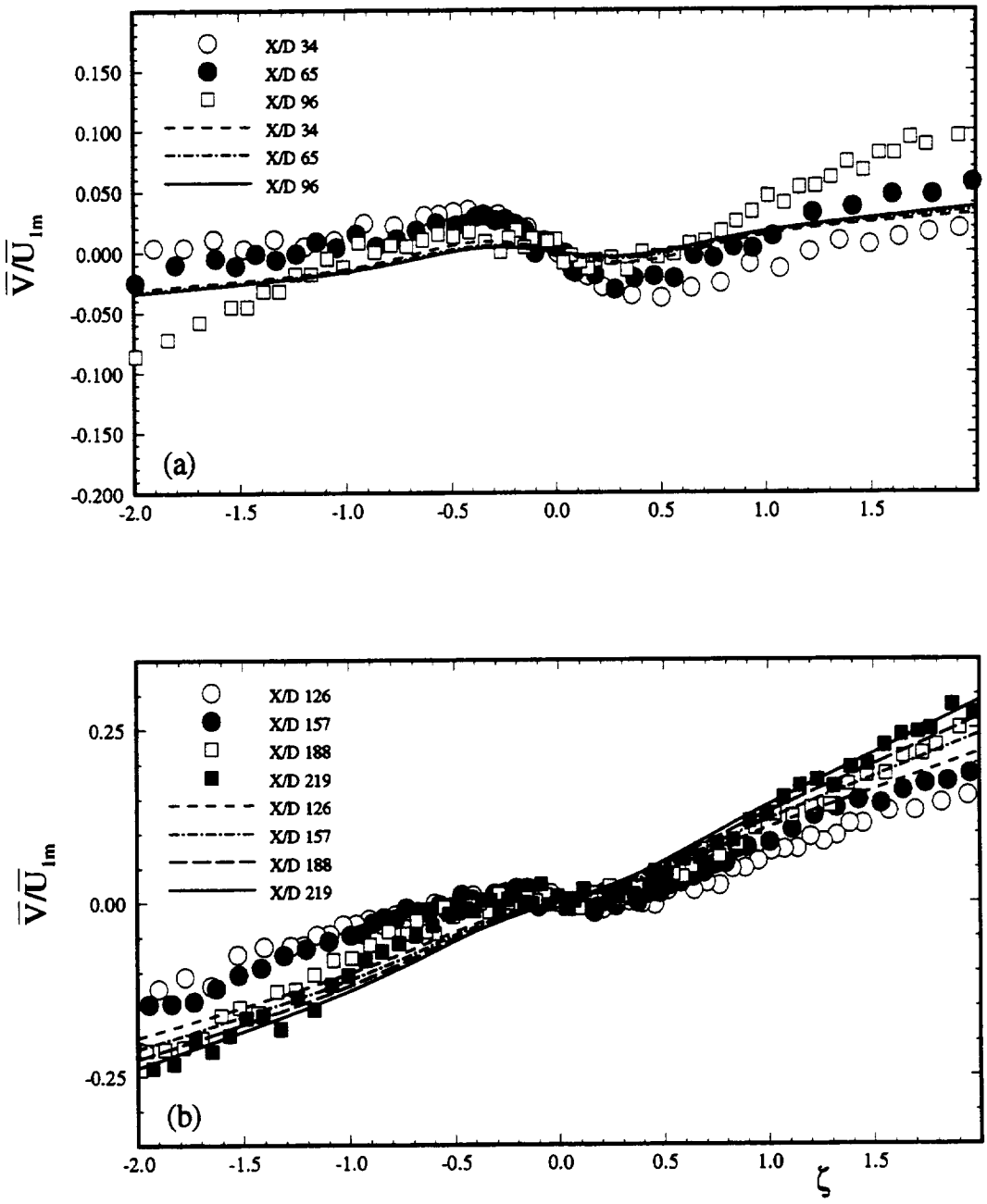


Fig. 48 Mean lateral velocity distribution in curved channel for positive pressure gradient, comparison of theory (lines) and experiment (symbols), (x/d:34-219)

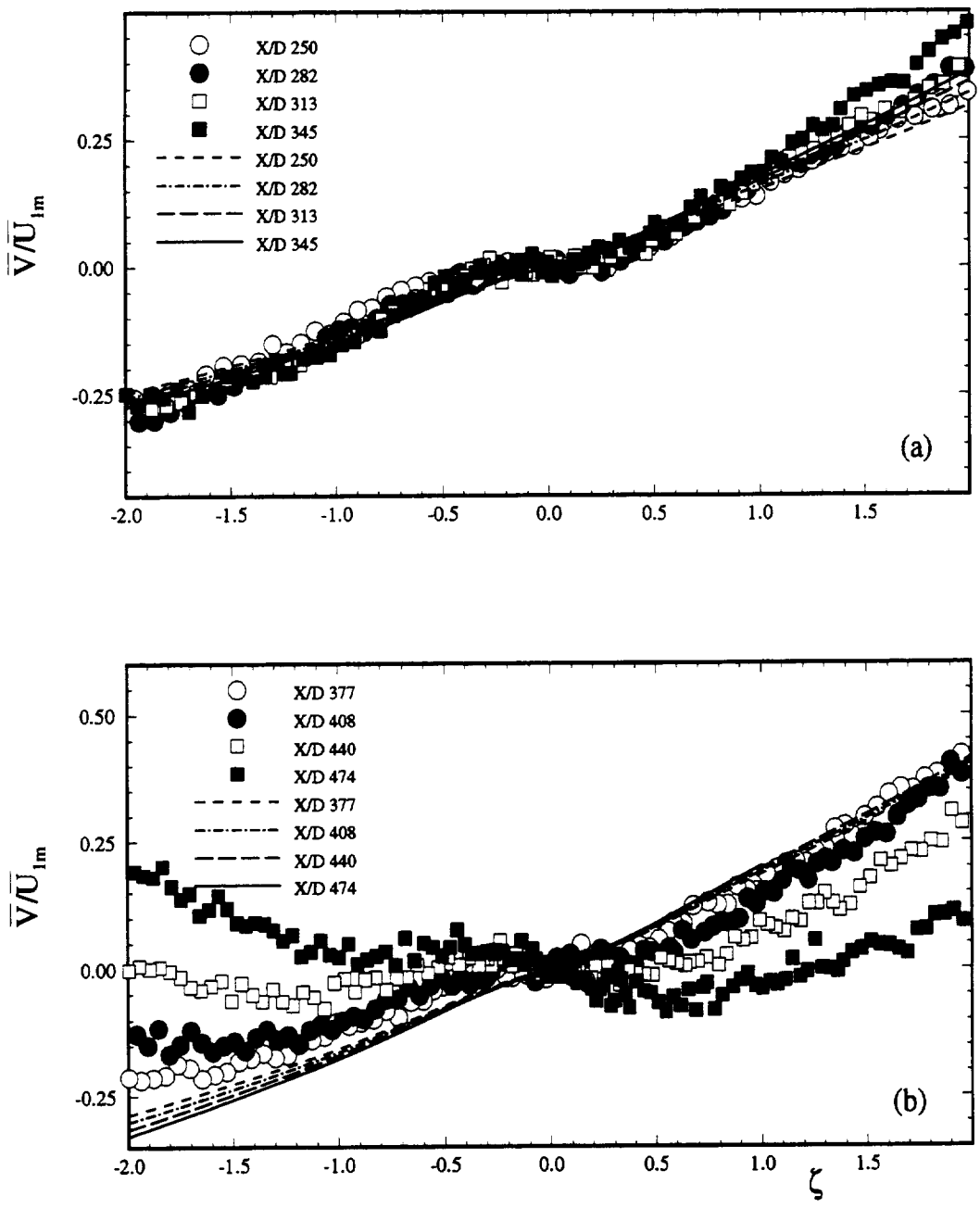


Fig. 49 Mean lateral velocity distribution in curved channel for positive pressure gradient, comparison of theory (lines) and experiment (symbols), (x/d:250-474)

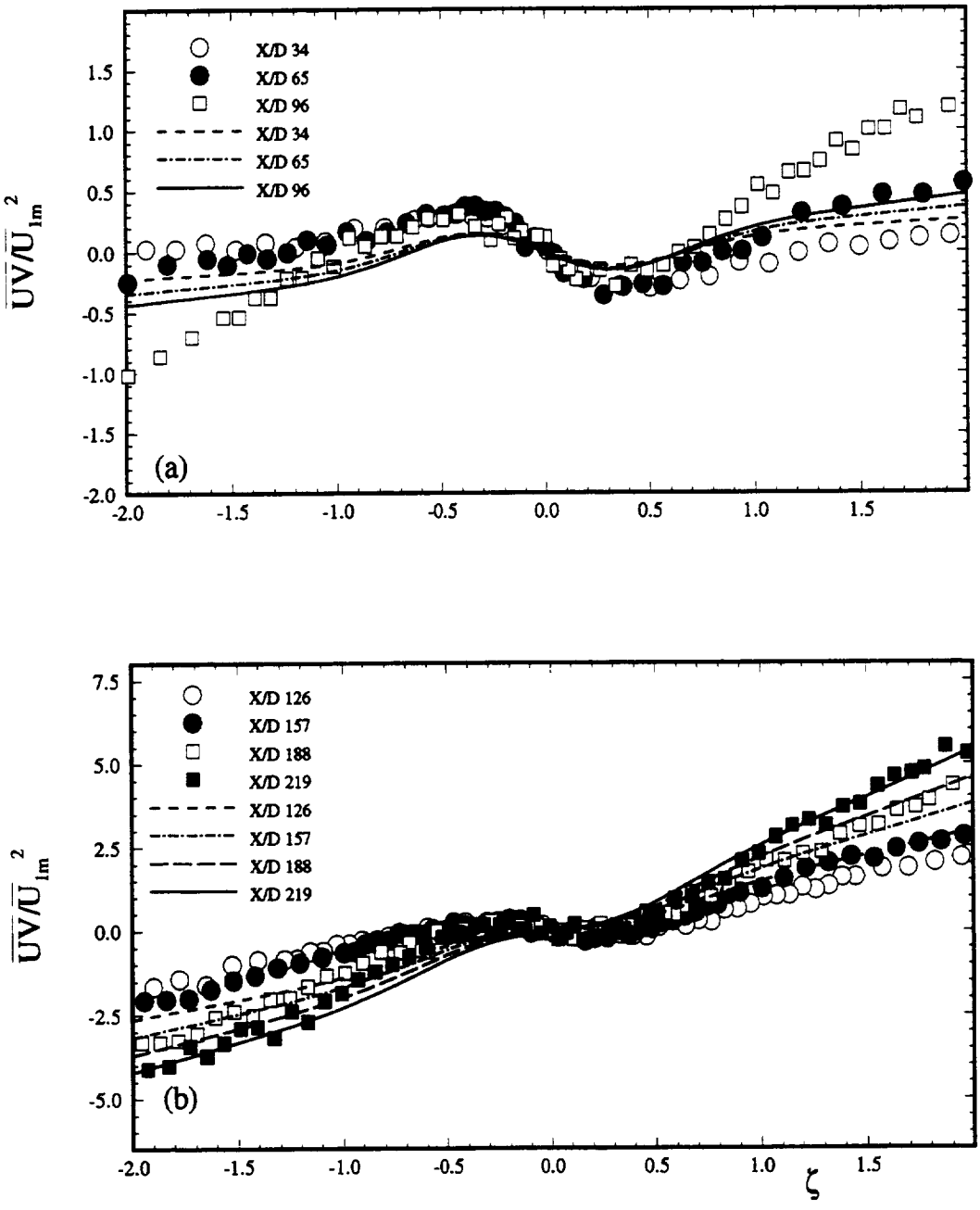


Fig. 50 Total impulse distribution in curved channel for positive pressure gradient, comparison of theory (lines) and experiment (symbols), (x/d:34-219)

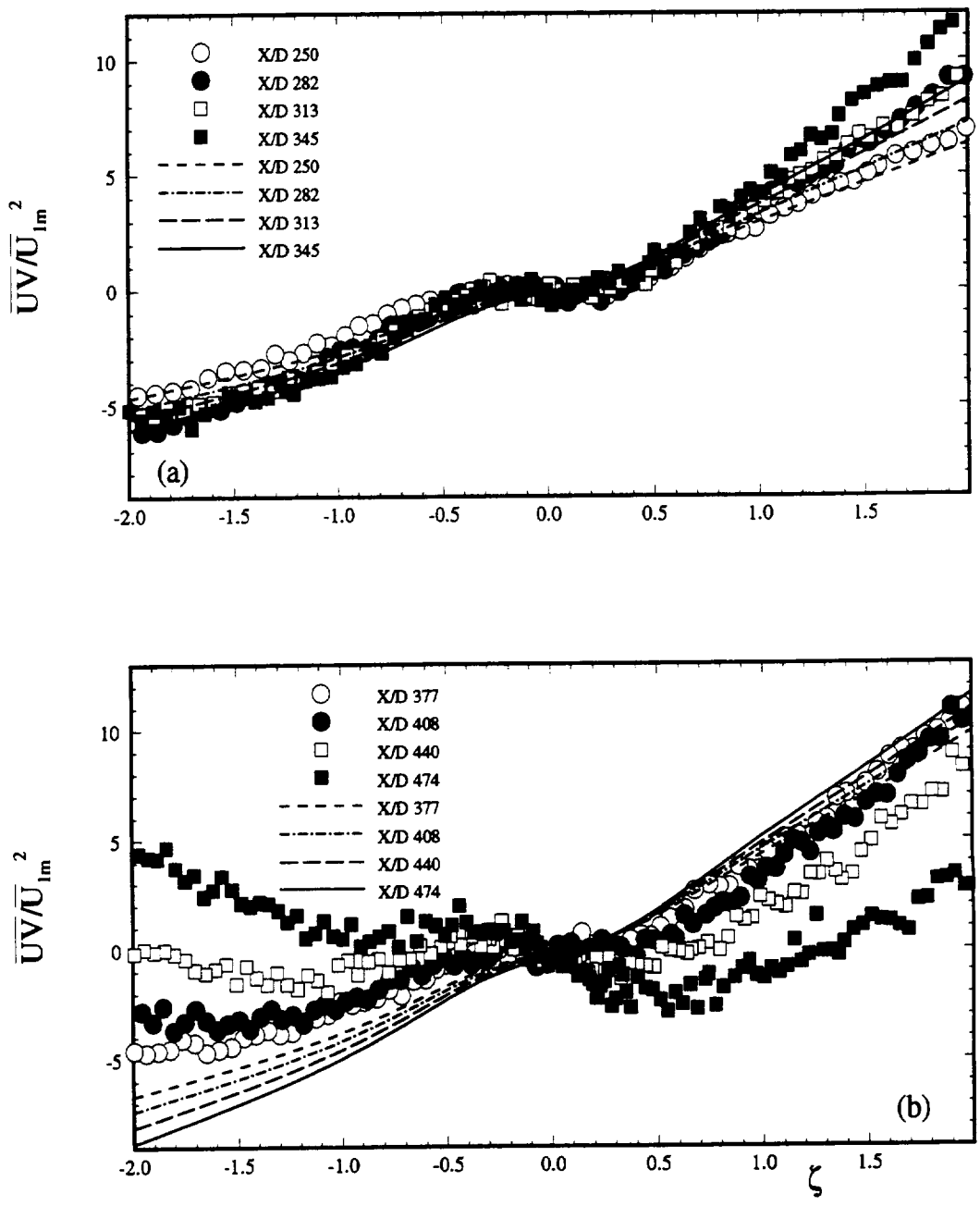


Fig. 51 Total impulse distribution in curved channel for positive pressure gradient, comparison of theory (lines) and experiment (symbols), (x/d:250-474)

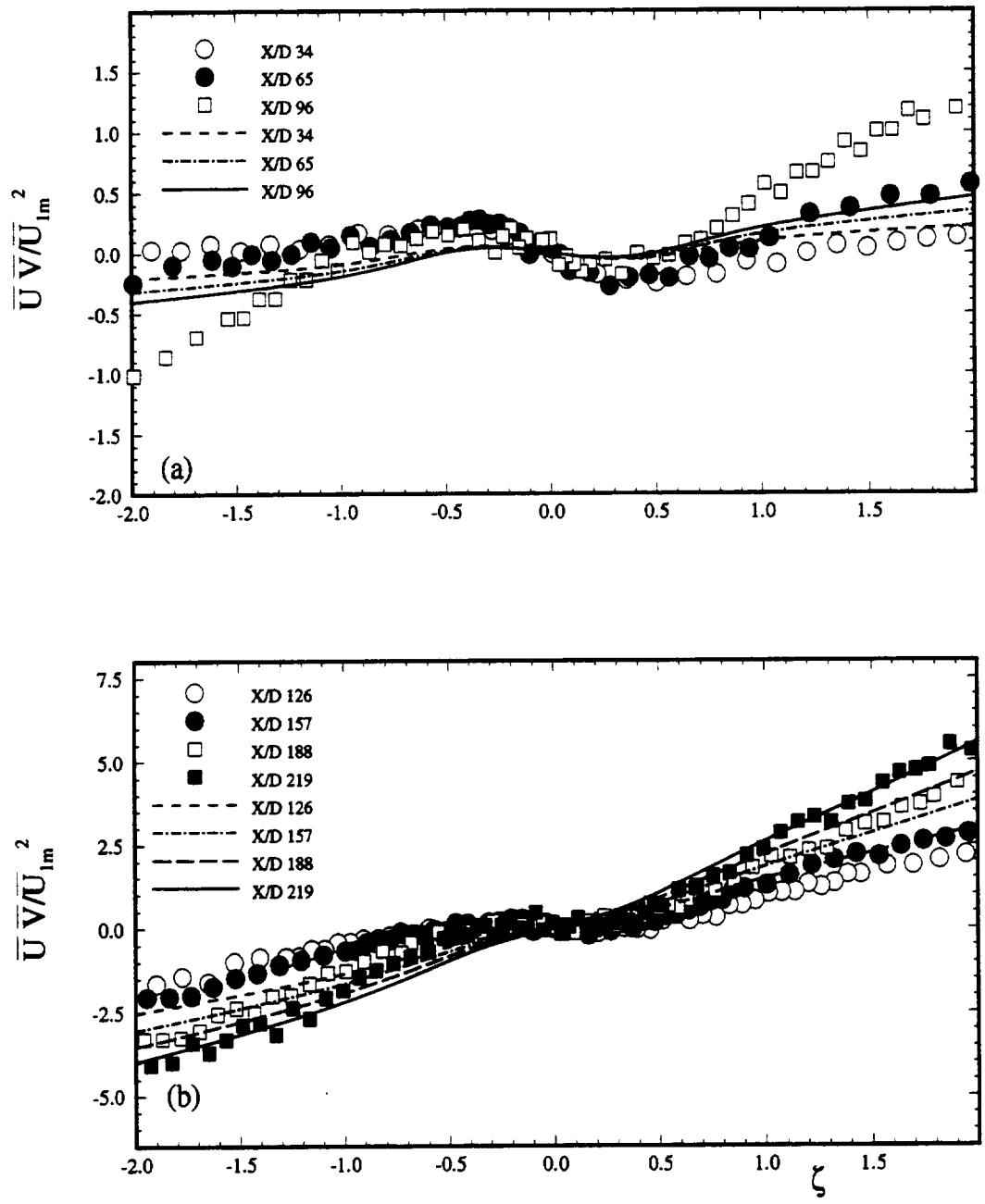


Fig. 52 Partial impulse distribution in curved channel for positive pressure gradient, comparison of theory (lines) and experiment (symbols), (x/d:34-219)

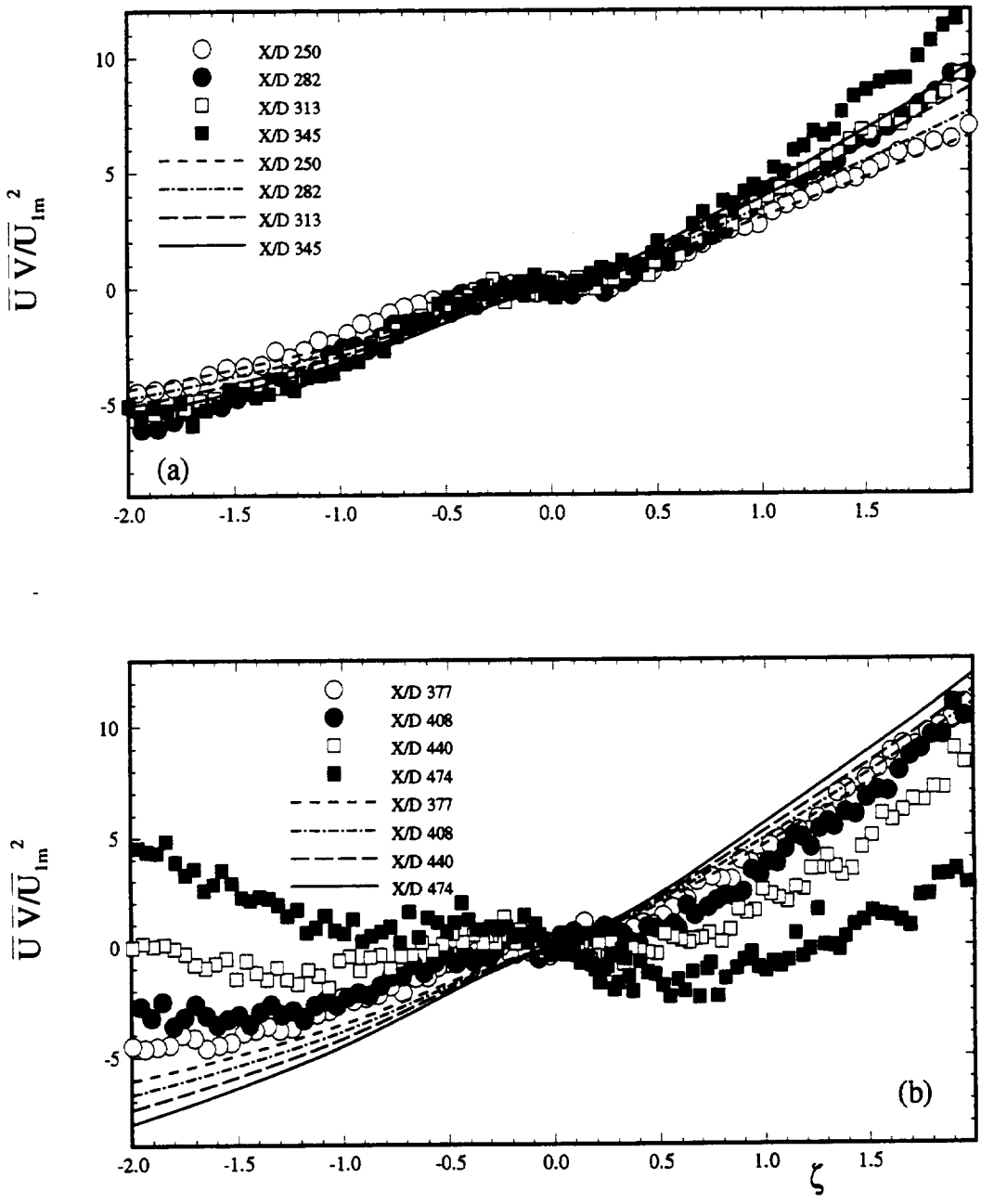


Fig. 53 Partial impulse distribution in curved channel for positive pressure gradient, comparison of theory (lines) and experiment (symbols), (x/d:250-474)

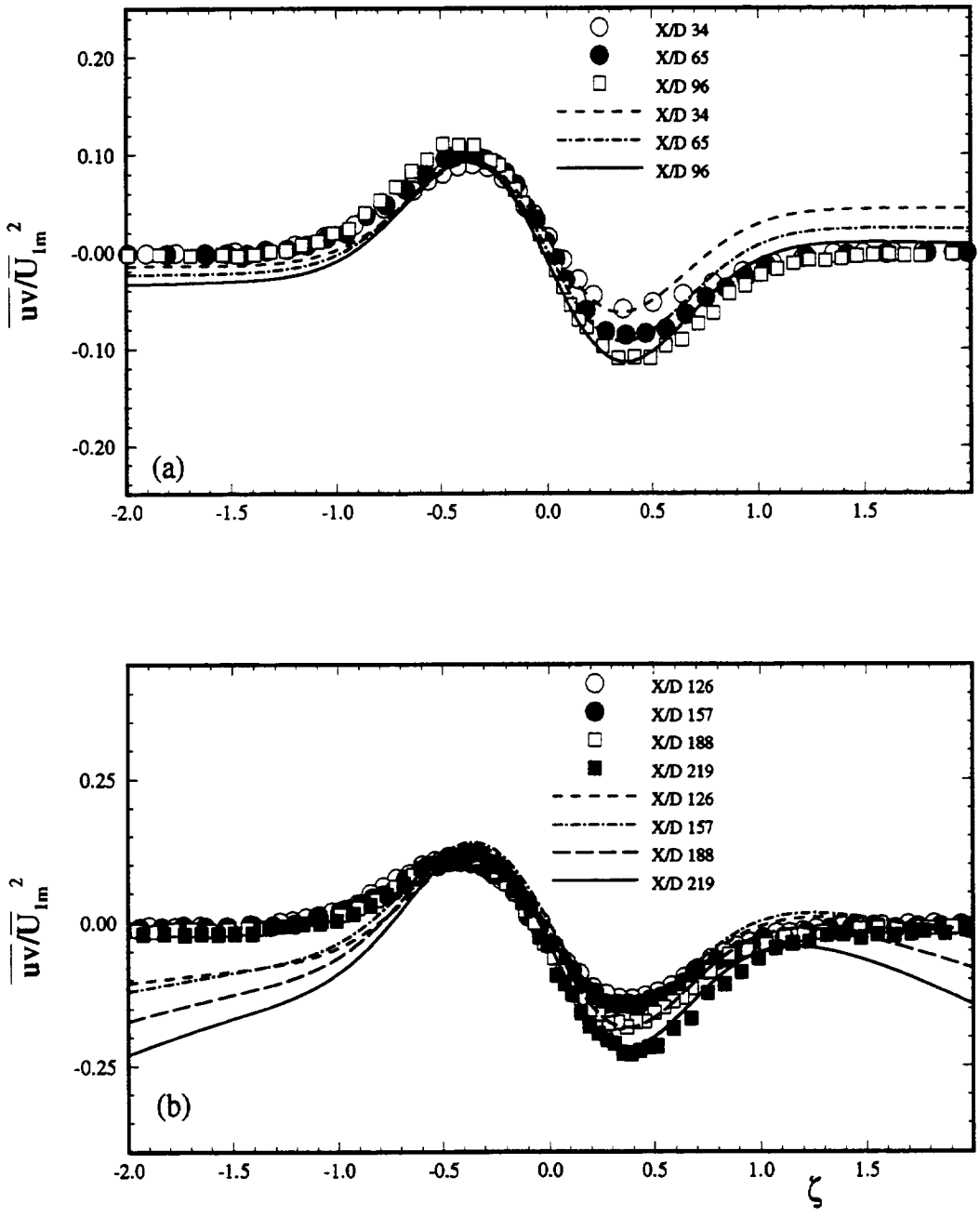


Fig. 54 Reynolds shear stress distribution in curved channel for positive pressure gradient, comparison of theory (lines) and experiment (symbols), (x/d:34-219)

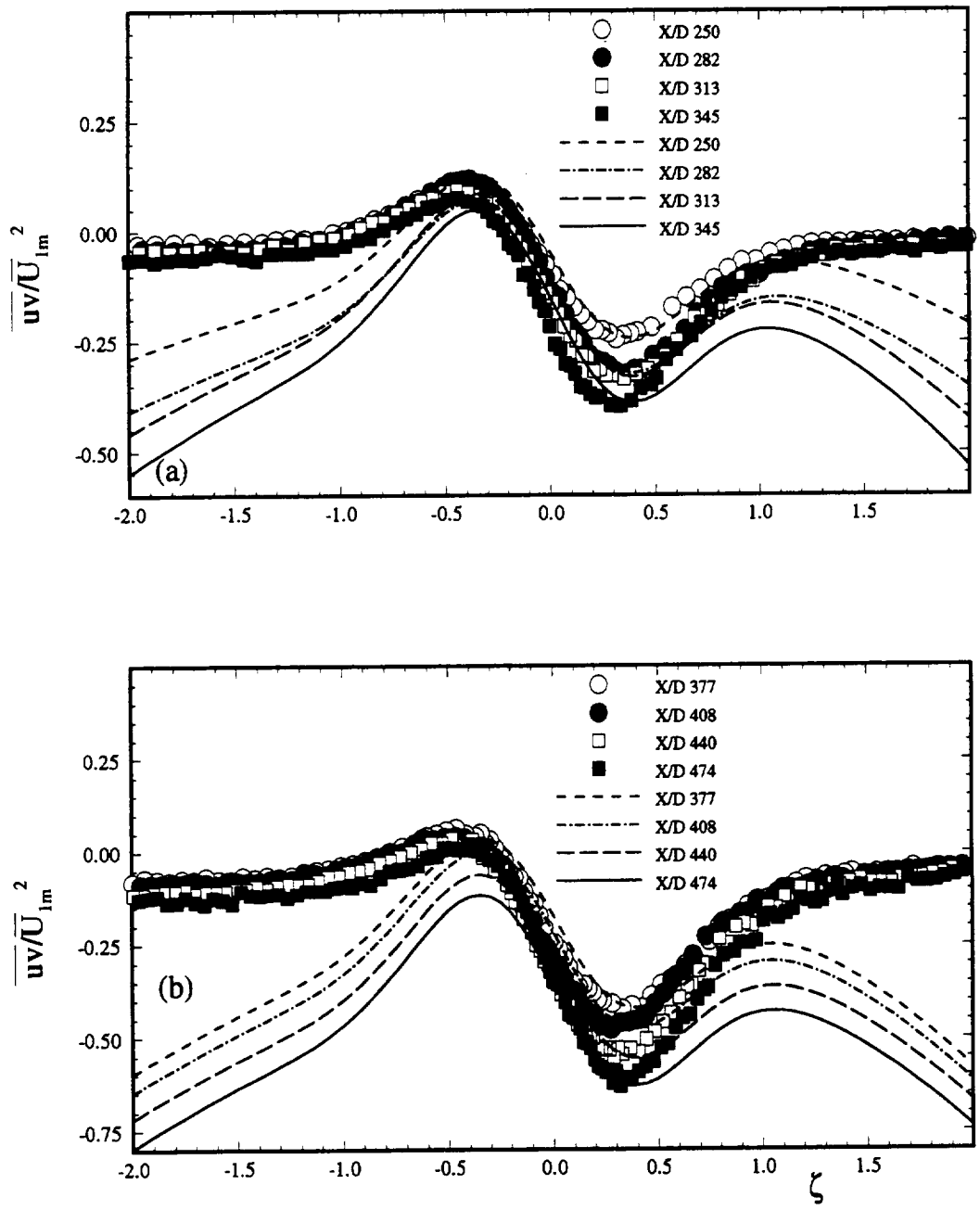


Fig. 55 Reynolds shear stress distribution in curved channel for positive pressure gradient, comparison of theory (lines) and experiment (symbols), (x/d:250-474)

57 and 58. From Fig. 57(a), it is evident that the wake velocity defect is excellently predicted, as has been the case so far for all the cases compared. Figure 57(b) compares mean longitudinal velocity, nondimensionalized with free-stream velocity ($U_{inf}$). Theory is in excellent agreement with the measurements at all streamwise locations. Thus the approximation of potential flow velocity in the vicinity of the wake, i.e. $U_{-} = U_{p_o}(1-\frac{\xi_2}{R})$ is valid while the applicability of the expression for wake velocity defect, $\varphi_1 = e^{-\zeta^2}$, has already been confirmed. The comparison of mean lateral velocity is presented in Fig. 58(a). Initially, there is overprediction up to a x/d of 400, beyond which there is reasonably good agreement between theory and experiment. The mismatch could be due to the nonavailability of pressure distribution. Also, the flow is external with one end open to atmospheric pressure and other end under the influence of a mild pressure gradient. From the mean longitudinal velocity distribution, it is also evident that the flow initially decelerates up to a x/d of 400, beyond which it accelerates. Thus, information regarding the pressure distribution is critical. The comparison between theoretical and experimental Reynolds shear stress distributions is presented in Fig. 58(b). Theory overpredicts the measurements in all cases, though the general tendency is correct. Since the enforced pressure gradient is mild, implementing the expression from a zero pressure gradient case for Reynolds shear stress is justifiable for comparison. It can be concluded from these comparisons that the theory reasonably predicts the situation under investigation.

### 9.6. Periodic Unsteady Wake Development in Curved Channel at Zero Pressure Gradient

In turbomachinery, wake development is associated with unsteadiness due to the mutual interaction between stator and rotor. So, the study of wake development under such conditions is of practical interest. This section deals with the discussion of the

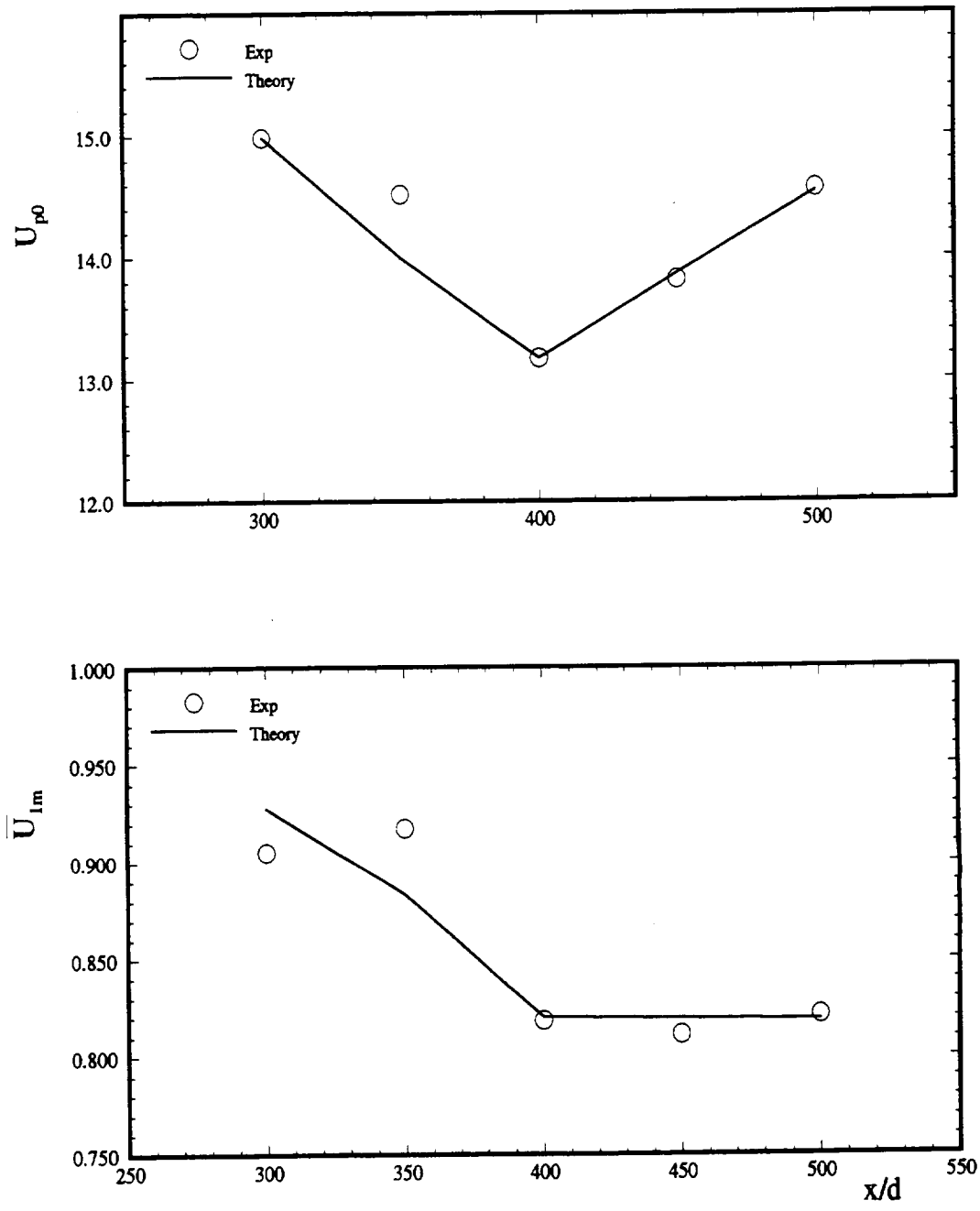


Fig. 56 $U_{p0}$ and $U_{lm}$ from experimental measurements of Nakayama (1987)

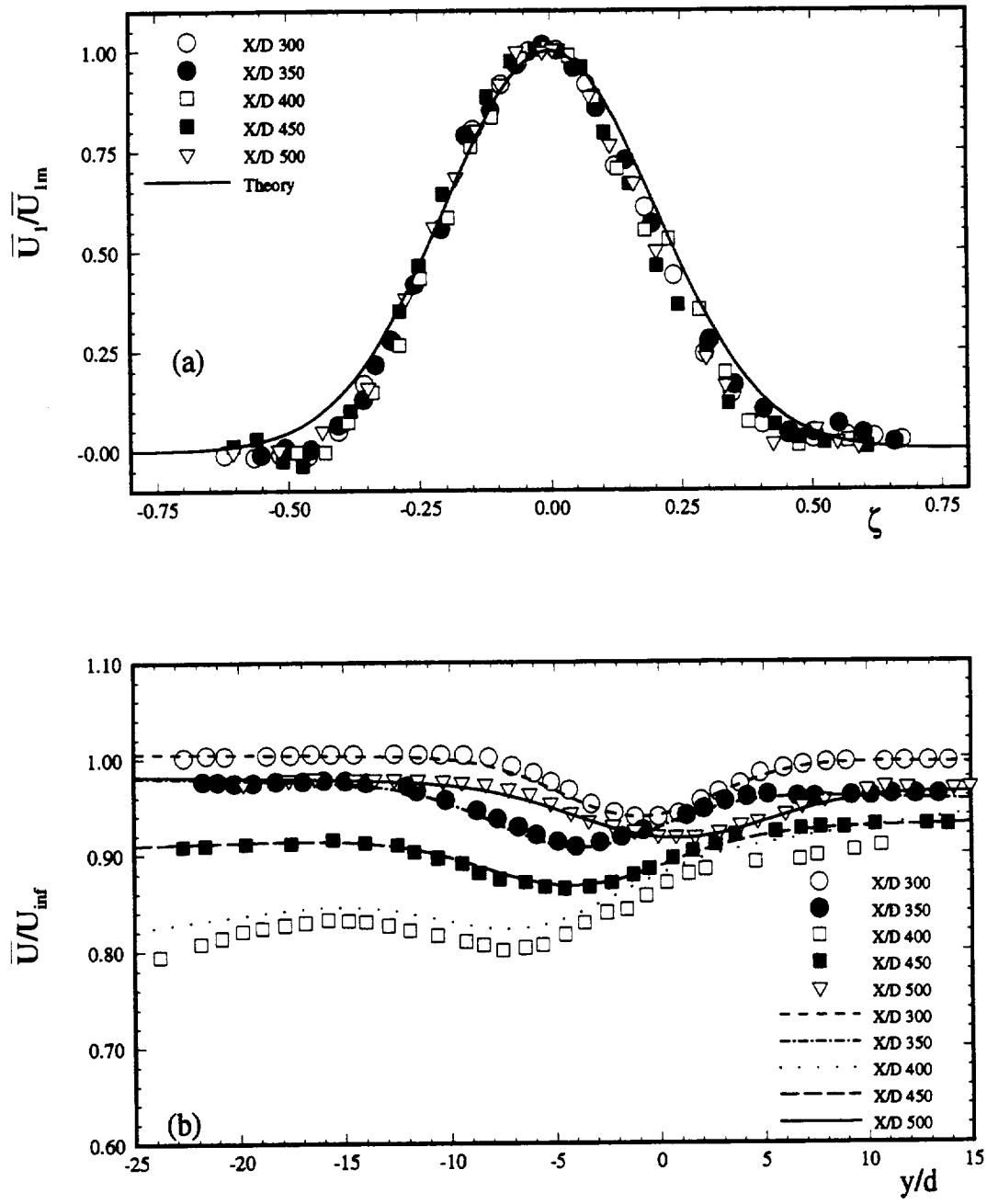


Fig. 57 (a) Nondimensional wake velocity defect and (b) mean longitudinal velocity distribution, theory (lines) compared with measurements (symbols) of Nakayama (1987)

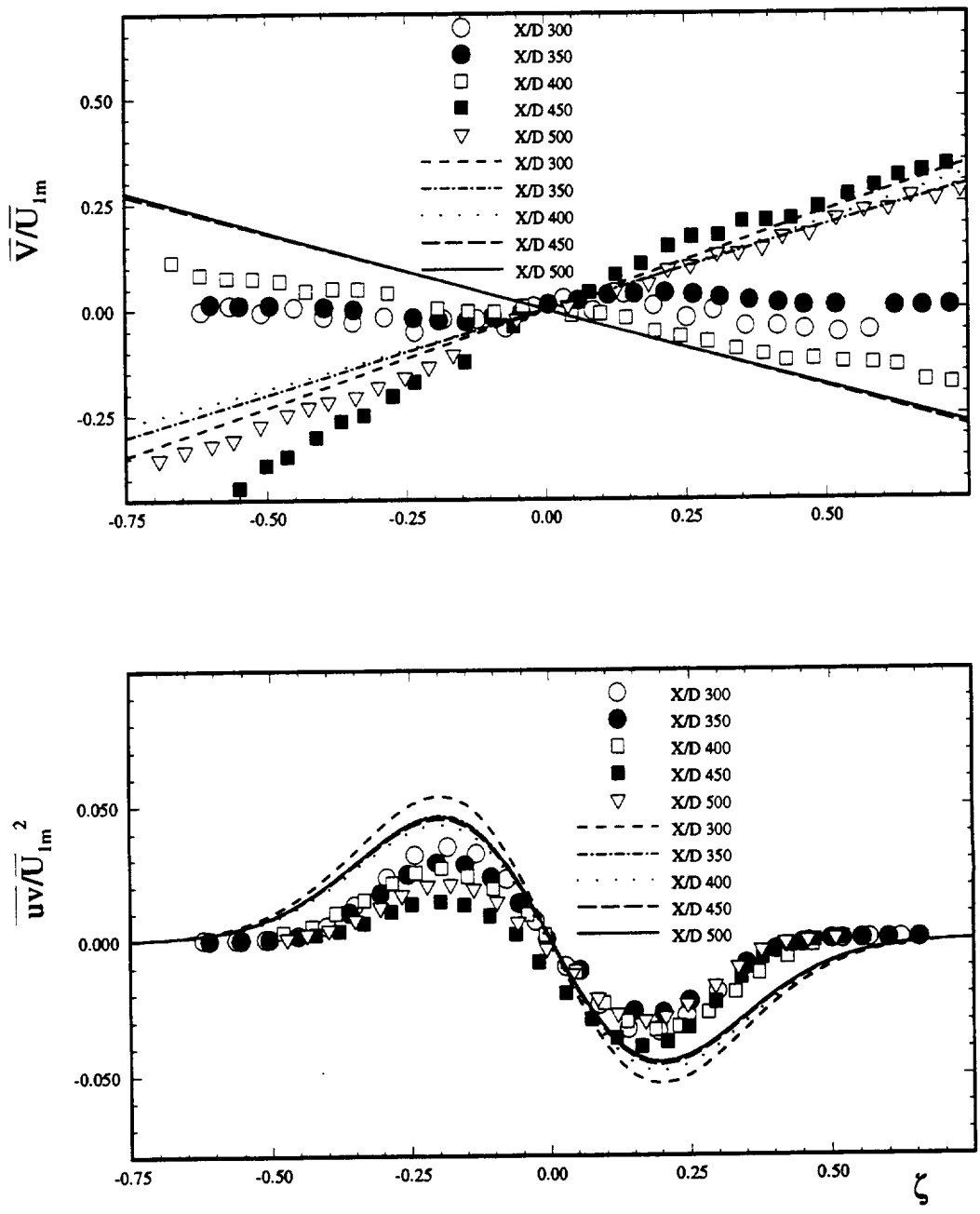


Fig. 58 (a) Mean lateral velocity and (b) Reynolds shear stress distribution, theory (lines) compared with measurements (symbols) of Nakayama (1987)

theoretical comparison with experimental measurements made available from the Turbomachinery Performance Laboratory at Texas A&M University, where periodic unsteady wakes generated by the cylinders of a rotating wake generator at zero pressure gradient are investigated (John, 1993). The wake generator has three cylinders of 1.984 mm diameter each, fixed at an angle of 120° to each other. The instantaneous velocity components obtained in probe coordinates are reduced by phase-averaging. The temporal development of periodic unsteady wake in an absolute frame of reference has been transformed to a curvilinear spatial coordinate system relative to the moving cylinder. Thus, the expressions derived in Chapter 7 for steady wake flow under zero streamwise pressure gradient can be directly used to compare with the experimental data available for the periodic unsteady case.

Figures 59 through 61 show the results of a comparison of the theory with the experimental measurements. All quantities presented are in a relative frame of reference. Figures 59(a,b) and 60(a) show the values of wake width, maximum wake velocity defect, and potential flow velocity at the wake center as a function of streamwise distance from the wake generating body. Figure 60(b) shows the comparison of a nondimensional wake velocity defect. The validity of the expression for $\varphi_{1r}$, i.e.

$$\varphi_{1r} = \frac{\bar{U}_{1r}}{\bar{U}_{1mr}} = e^{-\zeta_r^2}, \quad \zeta_r = \frac{\xi_{2r}}{b}$$

is quite evident considering the excellent match between theory and measurements. The additional subscript "r" denotes that the quantities are in a relative frame of reference. Thus, the similarity of wake velocity defect profiles has been established for the present case as well. The transverse distribution of Reynolds shear stress at different locations downstream of the wake generating body is shown in Fig. 61. The shear stress is nondimensionalized with the square of the maximum wake velocity defect, i.e. $\bar{U}_{1mr}^2$. As discussed earlier, the constant of integration in the expression for shear stress has been

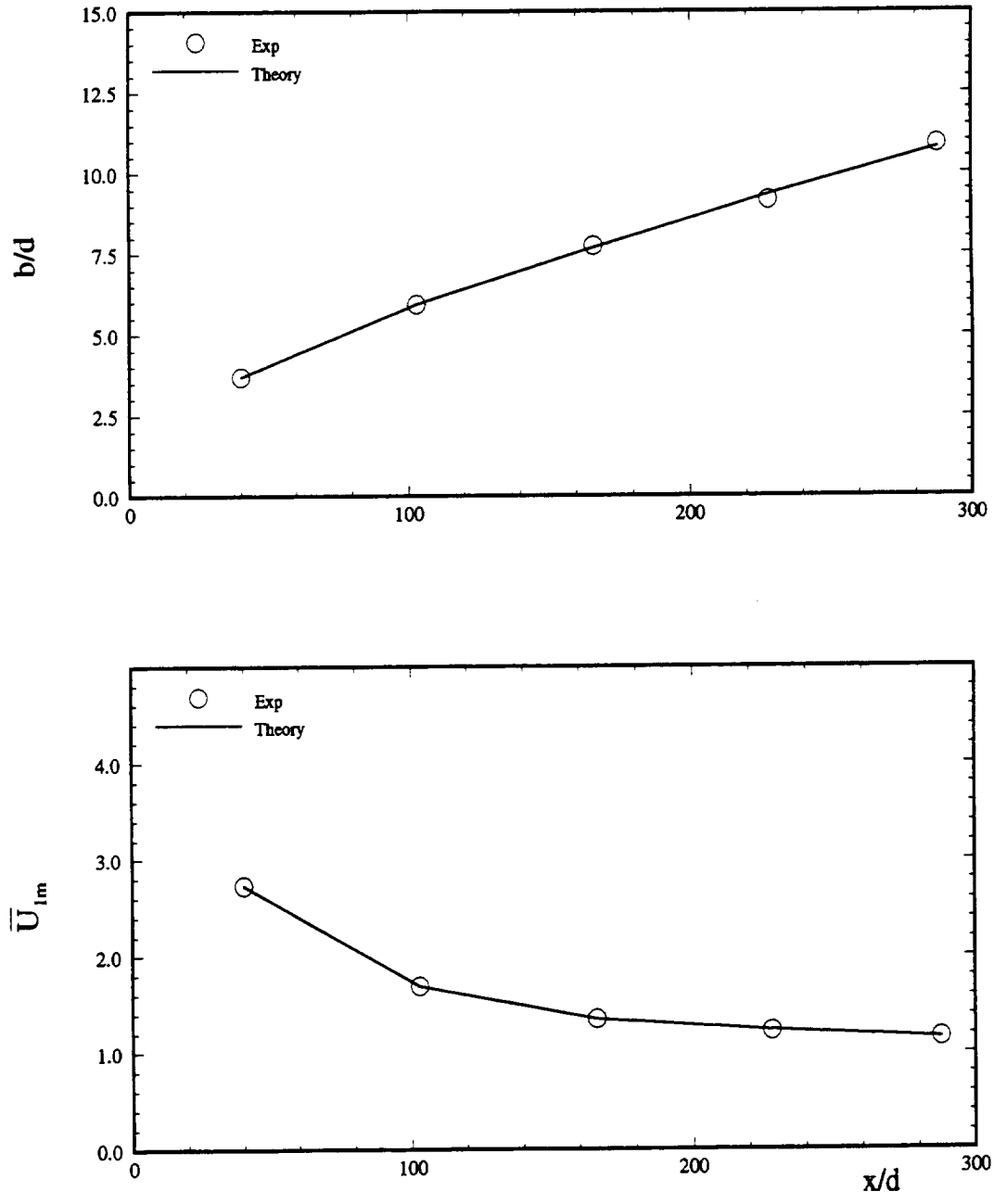


Fig. 59 (a) Nondimensional wake width and (b) $U_{1m}$ in curved channel at zero pressure gradient for unsteady wake

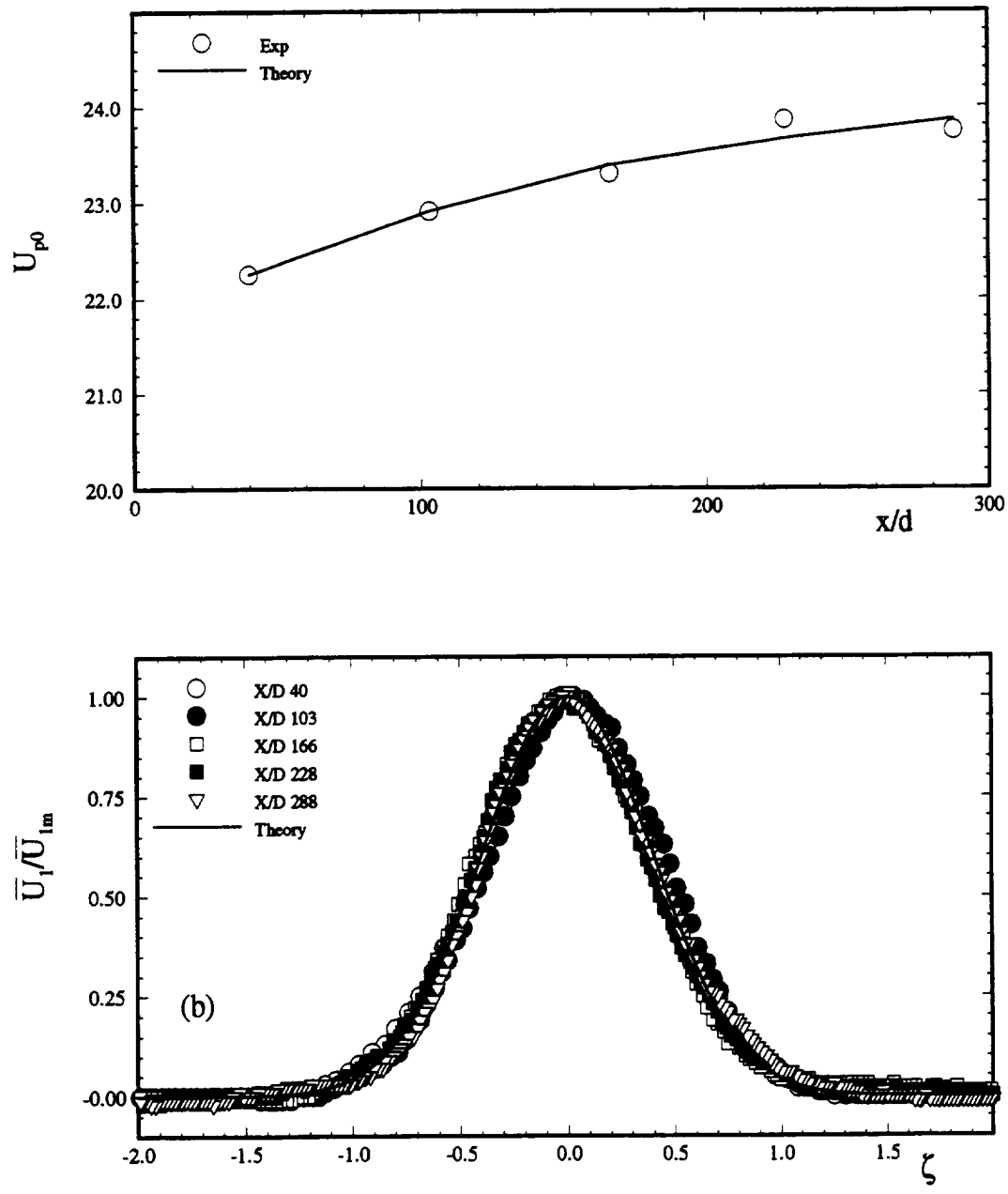


Fig. 60 (a)$U_{p0}$ and (b) dimensionless wake velocity defect distribution in curved channel at zero pressure gradient for unsteady wake, theory (lines) compared with experiment (symbols)

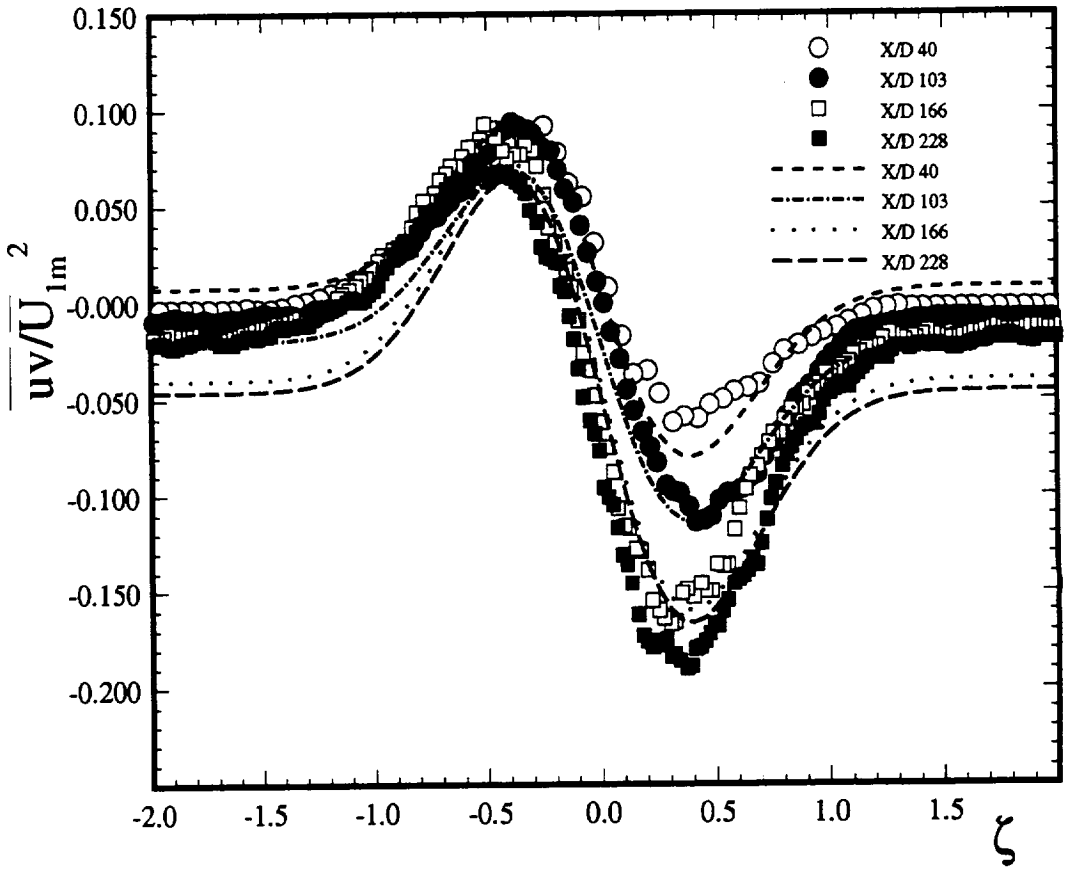


Fig. 61 Reynolds shear stress distribution in curved channel at zero pressure gradient for unsteady wake, theory (lines) compared with experiment (symbols)

evaluated from experimental measurements (Table 5, Appendix) corresponding to the value at $\zeta = 0$. Theory is in good agreement with the experimental measurements for almost all streamwise locations, with the asymmetry in the profiles being predicted quite well. Thus, theory predicted periodic unsteady wake characteristics quite well.

# 10. CONCLUSIONS

The task of predicting the characteristics of two-dimensional turbulent wakes under turbomachinery flow conditions has been undertaken. Comprehensive comparisons of theory with experimental measurements for different locations downstream of a wake generating body have been carried out. The following conclusions can be drawn from the present investigation:

1. The dimensionless wake velocity defect function, $\varphi_1 = e^{-\zeta^2}$, as derived in Chapter 7.2 for straight channel with zero streamwise pressure gradient, is valid for the wake flow under the influence of both the curvature and pressure gradients. Thus, the assumption of similarity in wake velocity defect profiles has been verified.
2. Wake characteristics for zero pressure gradient with and without the presence of streamline curvature are excellently predicted by the theory.
3. The method presented for the calculation of the mean longitudinal turbulent fluctuation impulse, based on Prandtl's theory, for the case of zero streamwise pressure gradient is reasonably valid.
4. The core of the wake region in Reynolds shear stress profiles is well predicted for both the cases of positive and negative pressure gradients.
5. The comparison of theory with the experimental measurements of Nakayama (1987) also verify the general applicability of the developed theory.
6. Excellent match of theory with measurements for periodic unsteady wake development in a curved channel with zero streamwise pressure gradient also verifies the general validity of the theory.

Much better agreement between theory and experiment for wake flow under the influence of a pressure gradient would have been possible had the pressure distribution been measured. In theory, $\partial U_{p_0}/\partial \xi_1$, representative of the pressure gradient, has been implemented by differentiating the expression resulting from the power fit through the

given $U_{p0}$. In turn, $U_{p0}$ has been calculated from a polynomial fit through the potential flow region of mean longitudinal velocity distribution. Thus, there is scope to introduce inaccuracy in obtaining a distribution for pressure gradient. Also, the pressure gradient enforced in the channel is quite large. Better results could have been possible had the pressure gradient been mild. One of the basic assumptions of two dimensionality of the flow within the curved channel may not have been preserved in actual practice. In turbomachinery, the near wake region ($x/d<80$) is of practical interest, and the contributions from the present investigation are useful.

## REFERENCES

Bradshaw, P., 1969, "The Analogy Between Streamline Curvature and Buoyancy in Turbulent Shear Flow," *Journal of Fluid Mechanics*, Vol. 36, pp. 177-191.

Bradshaw, P., 1973, "Effects of Streamline Curvature on Turbulent Flow," *AGARDograph* no. 169.

Coles, D., 1956, "The Law of the Wake in the Turbulent Boundary Layer," *Journal of Fluid Mechanics*, Vol. 1, pp. 138-145.

Doorly, D.J., Oldfield, M.L.G., 1985, "Simulation of Wake Passing in a Stationary Turbine Rotor Cascade," *Journal of Propulsion*, Vol. 1, No. 4, pp. 316-318.

Eifler, J., 1975, "Zur Frage der freien turbulenten Stromungen, insbesondere hinter ruheneden und bewegten Zylindern," Dissertation D-17, Techische Hochschule Darmstadt, Germany.

Gartshore, Ian S., 1967, "Two-Dimensional Turbulent Wakes," *Journal of Fluid Mechanics*, Vol. 30, part 3, pp. 547-560.

Gillis, J. C., Johnston, J. P., 1983, "Turbulent Boundary-Layer Flow and Structure on a Convex Wall and its Redevelopment on a Flat Plate," *Journal of Fluid Mechanics*, Vol. 135, pp. 123-153.

Görtler, H., 1980, "Über den Einflu6 der Wandkümmung auf die Entstehung der Turbulenz," *Zeitschrift für angemandte Mathematik und Mechanik*, Bd. 20, Nr. 3, pp. 138-147.

Hebbar, K. S., 1986, "Mean and Turbulence Measurements in the Boundary Layer and Wake of a Symmetric Aerofoil," *Experiments in Fluids*, Vol. 4, pp. 214-222.

Hill, P. G., Schaub, U. W., Senoo, Y., 1963, "Turbulent Wakes in Pressure Gradients," *Journal of Applied Mechanics*, Transactions of the ASME, Vol. 30, pp. 518-524.

Hoffmann, P. H., Muck, K. C., Bradshaw, P., 1985, "The Effect of Concave Surface on Turbulent Boundary Layers," *Journal of Fluid Mechanics*, Vol. 161, pp. 371-

403.

John, J., 1993, "A Study of the Development of Steady and Periodic Unsteady Turbulent Wakes through Curved Channel at Positive, Zero, and Negative Streamwise Pressure Gradients," Ph.D. Dissertation, Texas A&M University, College Station, Texas.

Koyama, H., 1983, "Effect of streamline Curvature on Laminar and Turbulent Wakes," *Proc. of fourth Symp. on Turbulent Shear Flows*, University of Karlsruhe, Karlsruhe, Germany, pp. 141-155.

Lakshminarayana, B., Raj, R., 1976, "Three-Dimensional Characteristics of Turbulent Wakes Behind Rotors of Axial Flow Turbomachinery," *ASME Journal of Engineering for Power*, Vol. 98, pp. 218-228.

Liu, X., Rodi, W., 1991, "Experiments on Transitional Boundary Layers with Wake-Induced Unsteadiness," *Journal of Fluid Mechanics*, Vol. 231, pp. 229-256.

Muck, K. C., Hoffmann, P. H., Bradshaw, P., 1985, "The Effect of Convex Surface Curvature on Turbulent Boundary Layers," *Journal of Fluid Mechanics*, Vol. 161, pp. 347-369.

Nakayama, A., 1987, "Curvature and Pressure-Gradient Effects on a Small-Defect Wake," *Journal of Fluid Mechanics*, Vol. 175, pp. 215-246.

O' Brien, J. E., Capp, S. P., 1989, "Two-Component Phase-Averaged Turbulent Statistics Downstream of a Rotating Spoked-Wheel Wake Generator," *ASME Journal of Turbomachinery*, Vol. 111, No. 4, pp. 475-482.

Pfeil, H., Eifler, J., 1975a, "Zur Frage der Schubspannungsverteilung für die ebenen freien turbulenten Strömungen," *Forschung*, Ing.-Wes. 41, Nr.4, pp. 105-112.

Pfeil, H., Eifler, J., 1975b, "Messungen im turbulenten Nachlauf des Einzelzylinders," *Forschung*, Ing.-Wes. 41, Nr.5, pp. 137-145.

Pfeil, H., Schröder, T., 1981, "Decay of the Wake Behind a Cylinder Crossing Rapidly the Flow," AIAA 19th Aerospace Science Meeting, AIAA 81-0209.

Ramjee, V., Neelakandan, D., 1989, "Development of Wake of a Rectangular Cylinder in a Curved Stream," *Experiments in Fluids* , Vol. 7, pp. 395-399.

Rayleigh, L., 1916, "On the Dynamics of a Revolving Fluid," *Proceedings of the Royal Society*, London, Series A, Vol. 93, pp.148-154.

Reichardt, H., 1942, "Gesetzmassigkeiten der freien Turbulenz." VDI-Forschungsheft 414.

Savill, A. M., 1983, "The Turbulent Structure of a Highly Curved Two-Dimensional Wake," In: *IUTAM Symposium on complex turbulent flows*. (eds. Dumas, R. & Fulachier, F.) Marseille, Springer: Berlin, Heidelberg, New York, pp. 185-197.

Schlichting, H., 1930, "Uber das ebene Windschattenproblem." Diss. Gottingen, Ing.-Arch.1, 563-571.

Schlichting, H., 1979, *Boundary Layer Theory*, Seventh Edition, McGraw-Hill Publishing Company, New York.

Schobeiri, T., 1976, "Näherungslösung der Navier-Stokes'schen Differentialgleichung für eine zweidimensionale stationäre Laminarströmung konstanter Viskosität in konvexen und konkaven Diffusoren und Düsen," *Zeitschrift fur angewandte Mathematik und Physik*, Vol.27, Fasc. 1.

Schobeiri, T., 1980, "Geschwindigkeits- und Temperaturverteilung in Hamelscher Spiralströmung," *Zeitschrift für angewandte Mathematik und Mechanik*, Vol. 60, pp. 195-200.

Schobeiri, T., 1987, "Establishment of a Research Facility for Investigating the Effects of Periodic Unsteady Inlet Flow, Pressure Gradient and Curvature on Boundary Layer Transition, Wake Development and Heat Transfer," Internal Report, Texas A&M University, College Station, Texas.

Schobeiri, T., 1990a, "Wake Development: Theoretical Handwritten," Internal Report, Texas A&M University, College Station, Texas.

Schobeiri, T., 1990b, "The Influence of Curvature and Pressure Gradient on the Flow Temperature and Velocity Distribution," *International Journal of Mechanical Sciences*, Vol. 32, pp. 851-861.

Schobeiri, T., Pardivala, D., 1992, "Establishment of a Research Facility for

Investigating the Effects of Periodic Unsteady Inlet Flow, Pressure Gradient and Curvature on Boundary Layer Transition, Wake Development and Heat Transfer," Rotating Machinery Transport Phenomenon, Hemisphere Publishing Corp., Washington D.C.

Schobeiri, T., 1993a, "Development of Two-Dimensional Wakes within Curved Channels under Zero Streamwise Pressure Gradient - Part I," Under Preparation.

Schobeiri, T., 1993b, "Development of Two-Dimensional Wakes within Curved Channels under Zero Streamwise Pressure Gradient - Part II," Under Preparation.

Schröder, T., 1985, "Entwicklung des instationären Nachlaufs hinter quer zur Strömungsrichtung bewegten Zylindern und dessen Einfluβ auf das Umschlagverhalten von ebenen Grenzschichten stromabwärts angeordneter Versuchskörper," Dissertation D-17, Technischen Hochschule Darmstadt, Germany.

Thomann, H., 1968, "Effect of Streamwise Wall Curvature on Heat Transfer in a Turbulent Boundary Layer," *Journal of Fluid Mechanics*, Vol. 33, pp. 283.

Townsend, A.A., 1947a, "Measurements in the Turbulent Wake of a Cylinder," *Proceedings of the Royal Society*, London, Series A, Vol. 190, pp. 551-561.

Wattendorf, F.L., 1935, "A Study of the Effect of Curvature on Fully Developed Turbulent Flow," *Proceedings of the Royal Society*, London, Vol. 148, pp. 565-598.

# APPENDIX A

# EXPERIMENTAL DATA IMPLEMENTED IN THEORY

**Table 1: Data from Experiments for Zero Pressure Gradient, Curved Channel**

| x/d | b (mm) | $U_{p0}$ (m/s) | $\bar{U}_{1m}$ (m/s) | R (mm) | $c/\bar{U}_{1m}^2$ |
|---|---|---|---|---|---|
| 34 | 7.44 | 20.02 | 2.598 | 3360 | 0.01323 |
| 65 | 11.27 | 20.07 | 1.734 | -4710 | 0.00367 |
| 96 | 13.78 | 20.12 | 1.392 | -1424 | -0.00648 |
| 126 | 16.76 | 20.51 | 1.217 | -875 | -0.00700 |
| 157 | 19.88 | 20.57 | 1.084 | -672 | -0.02350 |
| 187 | 22.88 | 20.60 | 0.905 | -589 | -0.02000 |
| 218 | 26.13 | 20.38 | 0.846 | -573 | -0.04745 |
| 248 | 27.34 | 18.77 | 0.686 | -603 | -0.04745 |
| 278 | 33.88 | 19.11 | 0.611 | -673 | -0.08146 |
| 309 | 36.92 | 19.11 | 0.540 | -781 | -0.13166 |
| 339 | 33.96 | 19.49 | 0.494 | -924 | -0.20737 |
| 370 | 39.87 | 20.03 | 0.491 | -1092 | -0.25122 |
| 400 | 45.91 | 19.59 | 0.469 | -1279 | -0.24552 |
| 431 | 49.21 | 20.26 | 0.445 | -1489 | -0.30556 |
| 461 | 47.70 | 20.31 | 0.453 | -1704 | -0.33518 |

**Table 2: Data from Experiments for Negative Pressure Gradient, Curved Channel**

| x/d | b (mm) | $\bar{U}_{1m}$ (m/s) | $U_{p0}$ (m/s) | R (mm) | $c/\bar{U}_{1m}^2$ |
|---|---|---|---|---|---|
| 34 | 6.92 | 2.710 | 20.23 | -2632 | -1.67e-2 |
| 65 | 10.76 | 1.826 | 20.78 | -887 | -1.59e-2 |
| 96 | 12.15 | 1.447 | 21.44 | -728 | -1.51e-2 |
| 126 | 14.38 | 1.173 | 22.15 | -738 | -4.88e-3 |
| 156 | 17.16 | 0.946 | 22.82 | -787 | -4.39e-2 |
| 185 | 18.22 | 0.795 | 23.56 | -805 | -9.47e-2 |
| 215 | 20.79 | 0.733 | 24.17 | -776 | -9.34e-2 |
| 244 | 22.40 | 0.648 | 23.78 | -702 | -0.1241 |
| 273 | 24.04 | 0.588 | 24.63 | -654 | -0.1588 |
| 302 | 24.18 | 0.538 | 25.37 | -646 | -0.2118 |
| 331 | 24.22 | 0.522 | 26.06 | -684 | -0.2051 |
| 360 | 26.30 | 0.471 | 26.65 | -770 | -0.2789 |
| 388 | 28.78 | 0.435 | 27.29 | -896 | -0.3233 |

Diameter of wake generating body, d = 1.984 mm

**Table 3: Data from Experiments for Positive Pressure Gradient, Curved Channel**

| x/d | b (mm) | $U_{p0}$ (m/s) | $\bar{U}_{1m}$ (m/s) | R (mm) | $c/\bar{U}_{1m}^2$ |
|---|---|---|---|---|---|
| 34 | 7.06 | 19.27 | 2.793 | -1815 | 1.52e-2 |
| 65 | 10.56 | 19.17 | 1.952 | -1461 | 2.28e-3 |
| 96 | 13.30 | 18.85 | 1.550 | -1179 | -7.71e-3 |
| 126 | 16.13 | 18.00 | 1.311 | -958 | -1.14e-2 |
| 157 | 18.97 | 17.76 | 1.216 | -806 | 5.95e-3 |
| 188 | 22.77 | 17.68 | 1.075 | -707 | -9.44e-3 |
| 219 | 25.00 | 17.37 | 0.954 | -656 | -2.51e-2 |
| 250 | 29.76 | 16.94 | 0.898 | -647 | -3.15e-2 |
| 282 | 33.17 | 17.02 | 0.780 | -673 | -9.16e-2 |
| 313 | 35.28 | 16.63 | 0.778 | -728 | -8.20e-2 |
| 345 | 41.37 | 16.33 | 0.716 | -805 | -0.1241 |
| 377 | 43.03 | 16.34 | 0.698 | -897 | -0.1460 |
| 408 | 48.58 | 15.61 | 0.649 | -1002 | -0.1932 |
| 440 | 51.27 | 15.66 | 0.609 | -1106 | -0.2647 |
| 474 | 56.68 | 15.64 | 0.578 | -1207 | -0.3301 |

Diameter of wake generating body, d = 1.984 mm

**Table 4: Data from Experiments of Nakayama (1987)**

| x/d | $\bar{U}_{1m}$ (m/s) | $U_{p0}$ (m/s) | $y_c$ (mm) | R (mm) |
|---|---|---|---|---|
| 300 | 0.9053084 | 14.9862 | -1.60 | 5882 |
| 350 | 0.9175267 | 14.5159 | -6.30 | 2500 |
| 400 | 0.8184329 | 13.1768 | -10.00 | -465 |
| 450 | 0.8111683 | 13.8188 | -6.40 | -2714 |
| 500 | 0.8212935 | 14.5654 | 1.00 | 3571 |

Diameter of wake generating body, d = 1.6 mm; Free-stream velocity = 15 m/s

**Table 5: Data from Experiments for Unsteady Wake under Zero Pressure Gradient, Curved Channel**

| x/d | b/d | $\bar{U}_{1m}$ (m/s) | $U_{p0}$ (m/s) | $c/\bar{U}_{1m}^2$ |
|---|---|---|---|---|
| 40 | 3.70 | 2.732 | 22.255 | 0.008 |
| 103 | 5.93 | 1.693 | 22.912 | -0.020 |
| 166 | 7.74 | 1.351 | 23.304 | -0.040 |
| 228 | 9.16 | 1.226 | 23.862 | -0.046 |
| 288 | 10.89 | 1.160 | 23.747 | -0.100 |

Diameter of wake generating body, d = 1.984 mm

# APPENDIX B: DATA GENERATION PROGRAMS

## Programs for Zero Pressure Gradient, Curved Channel

```
************************************************************
c      PROGRAM FOR THE LONGITUDINAL MEAN VELOCITY (U)
c      DISTRIBUTION
************************************************************
c opening an output file
      character *64 FILENAME
1     format(A64)
      write(*,*)'enter the output filename:'
      read(*,1)FILENAME

      open(5,file=FILENAME,status='new')

      d=1.984
c reads in the input
      write(*,*)'enter x/d:'
      read(*,*)xd
c
      write(*,*)'enter U_p0:'
      read(*,*)up0
c calculates the wake width, b
      if(xd .lt. 100)then
        b = 0.39112*d*((xd)**(0.598563))/1.772
        db = 0.39112*0.598563*((xd)**(0.598563-1))/1.772
      else
        b = 0.12923*d*((xd)**0.842548)/1.772
        db = 0.12923*0.842548*((xd)**(0.842548-1))/1.772
      endif
c calculates the maximum wake velocity defect, u_1m
      if(xd .lt. 100)then
        u1m = 21.74097*(xd**-0.603475)
      else
        u1m = 1.447473 + 3.0899e-3*xd - 6.0324e-5*(xd**2)
     *                + 1.9791e-7*(xd**3) -
     *                2.3941e-10*(xd**4)
     *                + 8.7410e-14*(xd**5)
      endif
c calculates the radius of curvature
      r = - 1699.27 + 13.2273*xd - 7.10465e-2*(xd**2)
     *          + 1.75099e-4*(xd**3) - 1.42756e-7*(xd**4)
     *          - 6.04952e-11*(xd**5)
c
      do y = -125,125,2.5
      z = y/b
      u = up0*(1-z*b/r) - u1m*exp(-z*z)
      write(5,*)y,u
```

```
      enddo

      stop
      end
************************************************************
************************************************************
C     PROGRAM FOR THE LATERAL VELOCITY (V) DISTRIBUTION
************************************************************
character *64 FILENAME
1     format(A64)
      write(*,*)'enter the output filename:'
      read(*,1)FILENAME

      OPEN(5,FILE=FILENAME,STATUS='NEW')

      d=1.984

      call input(xd,r)
      call wkwidth(xd,d,b,db)
      call uu1m(xd,d,a,u1m,up0)
      call output(xd,d,r,b,db,a,u1m,up0)

      do x = -2.0,2.0,0.05
      z = x*1.772
      g = exp(-z*z)
      t = r/(r+b*z)
c nondimensional (V/U_1m)
      y = -t*db*z*g
      write(5,*)x,y
      enddo

      stop
      end
************************************************************
subroutine input(xd,r)
************************************************************
write(*,*)'enter x/d'
      read(*,*)xd
      r = - 1699.27 + 13.2273*xd - 7.10465e-2*(xd**2)
     *          + 1.75099e-4*(xd**3) - 1.42756e-7*(xd**4)
     *          - 6.04952e-11*(xd**5)
      return
      end
************************************************************
subroutine wkwidth(xd,d,b,db)
************************************************************
if(xd .lt. 100)then
       b = 0.39112*d*((xd)**(0.598563))/1.772
```

```
        db = 0.39112*0.598563*((xd)**(0.598563-1))/1.772
      else
        b = 0.12923*d*((xd)**0.842548)/1.772
        db = 0.12923*0.842548*((xd)**(0.842548-1))/1.772
      endif

      return
      end
*************************************************************
subroutine uu1m(xd,d,a,u1m,up0)
*************************************************************
write(*,*)'enter U_p0:'
      read(*,*)up0
c
      if(xd .lt. 100)then
        u1m = 21.74097*(xd**-0.603475)
      else
        u1m = 1.447473 + 3.0899e-3*xd - 6.0324e-5*(xd**2)
     *                + 1.9791e-7*(xd**3) -
     *                 2.3941e-10*(xd**4)
     *                + 8.7410e-14*(xd**5)
      endif

      a = up0/u1m

      return
      end
*************************************************************
subroutine output(xd,d,r,b,db,a,u1m,up0)
*************************************************************
print*,'x/d=',xd,'   d=',d,'   r=',r
      print*,'b=',b*1.772,'   db=',db
      print*,'b/d=',b*1.772/d
      print*,'u/u_1m=',a,'   u1m=',u1m,' up0=',up0

      return
      end
*************************************************************
*************************************************************
C     PROGRAM FOR REYNOLDS SHEAR STRESS
*************************************************************
character *64 FILENAME
1     format(A64)
      write(*,*)'enter the output filename:'
      read(*,1)FILENAME

      OPEN(5,FILE=FILENAME,STATUS='NEW')
```

```
      d=1.984

      write(*,*)'enter value of const at z=0:'
      read(*,*)const

      call input(xd,r)
      call wkwidth(xd,d,b,db)
      call uu1m(xd,d,a,u1m,up0)
      call output(xd,d,r,b,db,a,u1m,up0)

      do x = -2.0,2.0,0.05
      z = x*1.772
      g = exp(-z*z)
      t = r/(r+b*z)
      term = t*a*db*(-z*g+b*g/r*(1.+z*z))+t*db*z*g*(1-g)
      y = term+const
      write(5,*)x,y
      enddo

      stop
      end
*************************************************************
subroutine input(xd,r)
*************************************************************
write(*,*)'enter x/d'
      read(*,*)xd
      r = - 1699.27 + 13.2273*xd - 7.10465e-2*(xd**2)
     *          + 1.75099e-4*(xd**3) - 1.42756e-7*(xd**4)
     *          - 6.04952e-11*(xd**5)

      return
      end
*************************************************************
subroutine wkwidth(xd,d,b,db)
*************************************************************
if(xd .lt. 100)then
        b = 0.39112*d*((xd)**(0.598563))/1.772
        db = 0.39112*0.598563*((xd)**(0.598563-1))/1.772
      else
        b = 0.12923*d*((xd)**0.842548)/1.772
        db = 0.12923*0.842548*((xd)**(0.842548-1))/1.772
      endif

      return
      end
*************************************************************
subroutine uu1m(xd,d,a,u1m,up0)
*************************************************************
```

```
write(*,*)'enter up0:'
     read(*,*)up0
c
     if(xd .lt. 100)then
       u1m = 21.74097*(xd**-0.603475)
     else
       u1m = 1.447473 + 3.0899e-3*xd - 6.0324e-5*(xd**2)
    *                + 1.9791e-7*(xd**3) -
    *                 2.3941e-10*(xd**4)
    *                + 8.7410e-14*(xd**5)
     endif
c
     a = up0/u1m

     return
     end
*************************************************************
subroutine output(xd,d,r,b,db,a,u1m,up0)
*************************************************************
print*,'x/d=',xd,'   d=',d,'   r=',r
     print*,'b=',b*1.772,'   db=',db
     print*,'b/d=',b*1.772/d
     print*,'u/u_1m=',a,'   u1m=',u1m,' up0=',up0

     return
     end
*************************************************************
*************************************************************
c    PROGRAM FOR THE LONGITUDINAL FLUCTUATION IMPULSE
*************************************************************
character *64 FILENAME
1    format(A64)
     write(*,*)'enter the output filename:'
     read(*,1)FILENAME

     open(5,file=FILENAME,status='new')

     d=1.984

     write(*,*)'enter x/d:'
     read(*,*)xd
c calculation of radius of curvature
     r = - 1699.27 + 13.2273*xd - 7.10465e-2*(xd**2)
    *          + 1.75099e-4*(xd**3) - 1.42756e-7*(xd**4)
    *          - 6.04952e-11*(xd**5)
c calculation of wake width
     if(xd .lt. 100)then
       b = 0.39112*d*((xd)**(0.598563))/1.772
```

```
        db = 0.39112*0.598563*((xd)**(0.598563-1))/1.772
      else
        b = 0.12923*d*((xd)**0.842548)/1.772
        db = 0.12923*0.842548*((xd)**(0.842548-1))/1.772
      endif
c
      a2 = 1.50
c
      do x = -2,2,0.05
      z = x*1.772
      t = r/(r+z*b)
      psi = t*(1.0+b/r*z+a2*z*z)*exp(-z*z)
      write(5,*)x,psi
      enddo

      stop
      end
*****************************************************************
```

**Programs for Positive Pressure Gradient, Curved Channel**

```
*****************************************************************
c   -   PROGRAM FOR THE LONGITUDINAL MEAN VELOCITY (U)
c       DISTRIBUTION
*****************************************************************
c opening an output file
      character *64 FILENAME
1     format(A64)
      write(*,*)'enter the output filename:'
      read(*,1)FILENAME

      open(5,file=FILENAME,status='new')

      d=1.984
c reads in the input
      write(*,*)'enter x/d:'
      read(*,*)xd
c
      if(xd .lt. 100)then
        up0 = 20.71391*(xd**-0.019894)
        dup0 = 20.71391*-0.019894*(xd**-1.019894)/d
      else
        up0 = 32.21922*(xd**-0.116591)
        dup0 = 32.21922*-0.116591*(xd**-1.116591)/d
      endif
c calculates the wake width
      if(xd .lt. 100)then
        b = 0.412923*d*(xd**0.611281)/1.772
        db = 0.412923*0.611281*(xd**(0.611281-1))/1.772
```

```
      else
        b = 0.076865*d*(xd**0.955126)/1.772
        db = 0.076865*0.955126*(xd**(0.955126-1))/1.772
      endif
c calculates the maximum wake velocity defect
      if(xd .lt. 100)then
        u1m = 20.59*(xd**-0.565849)
        du1m = 20.59*-0.565849*(xd**-1.565849)/d
      else
        u1m = 28.9309*(xd**-0.632416)
        du1m = 28.9309*-0.632416*(xd**-1.632416)/d
      endif
c calculated the radius of curvature
      r = -3377.81 + 53.29529*xd - 0.435468*(xd**2)
     *           + 1.7222e-3*(xd**3) - 3.22e-6*(xd**4)
     *           + 2.2493e-9*(xd**5)
c
      do y = -125,125,2.5
      z = y/b
      u = up0*(1-z*b/r) - u1m*exp(-z*z)
      write(5,*)y,u
      enddo

      stop
      end

**************************************************************
**************************************************************
C     PROGRAM FOR THE LATERAL VELOCITY (V) DISTRIBUTION
**************************************************************
character *64 FILENAME
1     format(A64)
      write(*,*)'enter the output filename:'
      read(*,1)FILENAME

      OPEN(5,FILE=FILENAME,STATUS='NEW')

      d = 1.984
      pi = 4.0*atan(1.0)
      sfac = sqrt(pi)/2.0

      call input(xd,r)
      call wkwidth(xd,d,b,db)
      call uu1m(xd,d,b,a,u1m,up0,dup0,du1m)
      call output(xd,d,r,b,db,a,u1m,up0,dup0,du1m)

      do x = -2.0,2.0,0.05
      z = x*1.772
```

```
      g = exp(-z*z)
      t = r/(r+b*z)
      vr = z*b/r
c nondimensional (V/U_1m)
      y = -t*b/u1m*dup0*z*(1.-vr/2) - t*db*(z*g-sfac*erf(z))
     *          + t*b/u1m*du1m*sfac*erf(z)
      write(5,*)x,y
      enddo

      stop
      end
**************************************************************
subroutine input(xd,r)
**************************************************************
write(*,*)'enter x/d'
      read(*,*)xd
c
      r = -3377.81 + 53.29529*xd - 0.435468*(xd**2)
     *          + 1.7222e-3*(xd**3) - 3.22e-6*(xd**4)
     *          + 2.2493e-9*(xd**5)

      return
      end
**************************************************************
subroutine wkwidth(xd,d,b,db)
**************************************************************
if(xd .lt. 100)then
        b = 0.412923*d*(xd**0.611281)/1.772
        db = 0.412923*0.611281*(xd**(0.611281-1))/1.772
      else
        b = 0.076865*d*(xd**0.955126)/1.772
        db = 0.076865*0.955126*(xd**(0.955126-1))/1.772
      endif

      return
      end
**************************************************************
subroutine uu1m(xd,d,b,a,u1m,up0,dup0,du1m)
**************************************************************
if(xd .lt. 100)then
        up0 = 20.71391*(xd**-0.019894)
        dup0 = 20.71391*-0.019894*(xd**-1.019894)/d
      else
        up0 = 32.21922*(xd**-0.116591)
        dup0 = 32.21922*-0.116591*(xd**-1.116591)/d
      endif
c
      if(xd .lt. 100)then
```

```
        u1m = 20.59*(xd**-0.565849)
        du1m = 20.59*-0.565849*(xd**-1.565849)/d
      else
        u1m = 28.9309*(xd**-0.632416)
        du1m = 28.9309*-0.632416*(xd**-1.632416)/d
      endif
c
      a = up0/u1m

      return
      end
*************************************************************
subroutine output(xd,d,r,b,db,a,u1m,up0,dup0,du1m)
*************************************************************
print*,'x/d=',xd,'   d=',d,'   r=',r
      print*,'b=',b*1.772,'   db=',db
      print*,'   dup0=',dup0,'   b/d=',b*1.772/d
      print*,'u/u_1m=',a,'   u1m=',u1m,' up0=',up0
      print*,'du1m=',du1m

      return
      end
*************************************************************
*************************************************************
c     PROGRAM FOR REYNOLDS SHEAR STRESS
*************************************************************
character *64 FILENAME
1     format(A64)
      write(*,*)'enter the output filename:'
      read(*,1)FILENAME

      OPEN(5,FILE=FILENAME,STATUS='NEW')

      d = 1.984
      pi = 4.0*atan(1.0)
      sfac = sqrt(pi)/2.0

      write(*,*)'enter value of shear stress at z=0:'
      read(*,*)uvatz0
c
      call input(xd,r)
      call wkwidth(xd,d,b,db)
      call uu1m(xd,d,b,a,u1m,up0,dup0,du1m)
      call output(xd,d,r,b,db,a,u1m,up0,dup0,du1m)
c
      do x = -2.0,2.0,0.05
      z = x*1.772
      g = exp(-z*z)
```

```
      t = r/(r+b*z)
      vr = z*b/r
c
      term1 = -t*up0/(u1m**2)*dup0*b*z*vr/2.*(1.-vr/3.)
      term2 = -t*up0/u1m*db*(z*g-b*g/r*(2.+z*z)
     *           - sfac*erf(z)*(1.+vr))
      term3 = t*db*(z*g*(1.-g)-sfac*erf(z)*(1.-g))
      term4 = t*up0/(u1m**2)*du1m*b*
     *           (b*g/r+sfac*erf(z)*(1.+vr))
      term5 = t*b/u1m*dup0*(2.*sfac*erf(z)
     *           + b*g/r*(1.+0.5*z*z)-z*g)
      term6 = -t*b/u1m*du1m*(sfac*erf(z)*(2.-g))
      const = uvatz0 - 2.*a*db*b/r - up0/(u1m**2)*du1m*b*b/r
     *           - b/u1m*dup0*b/r
      y = term1+term2+term3+term4+term5+term6+const
      write(5,*)x,y
      enddo

      write(5,*)'const=',const

      stop
      end
**************************************************************
subroutine input(xd,r)
**************************************************************
write(*,*)'enter x/d'
      read(*,*)xd
c
      r = -3377.81 + 53.29529*xd - 0.435468*(xd**2)
     *           + 1.7222e-3*(xd**3) - 3.22e-6*(xd**4)
     *           + 2.2493e-9*(xd**5)

      return
      end
**************************************************************
subroutine wkwidth(xd,d,b,db)
**************************************************************
if(xd .lt. 100)then
        b = 0.412923*d*(xd**0.611281)/1.772
        db = 0.412923*0.611281*(xd**(0.611281-1))/1.772
      else
        b = 0.076865*d*(xd**0.955126)/1.772
        db = 0.076865*0.955126*(xd**(0.955126-1))/1.772
      endif

      return
      end
**************************************************************
```

```
subroutine uu1m(xd,d,b,a,u1m,up0,dup0,du1m)
************************************************************
if(xd .lt. 100)then
       up0 = 20.71391*(xd**-0.019894)
       dup0 = 20.71391*-0.019894*(xd**-1.019894)/d
     else
       up0 = 32.21922*(xd**-0.116591)
       dup0 = 32.21922*-0.116591*(xd**-1.116591)/d
     endif
c
     if(xd .lt. 100)then
       u1m = 20.59*(xd**-0.565849)
       du1m = 20.59*-0.565849*(xd**-1.565849)/d
     else
       u1m = 28.9309*(xd**-0.632416)
       du1m = 28.9309*-0.632416*(xd**-1.632416)/d
     endif
c
     a = up0/u1m

     return
     end
************************************************************
subroutine output(xd,d,r,b,db,a,u1m,up0,dup0,du1m)
************************************************************
print*,'x/d=',xd,'   d=',d,'   r=',r
     print*,'b=',b*1.772,'   db=',db
     print*,'   dup0=',dup0,'   b/d=',b*1.772/d
     print*,'u/u_1m=',a,'   u1m=',u1m,' up0=',up0
     print*,'du1m=',du1m

     return
     end
************************************************************
```

**Programs for Negative Pressure Gradient, Curved Channel**

```
************************************************************
c      PROGRAM FOR THE LONGITUDINAL MEAN VELOCITY (U)
c      DISTRIBUTION
************************************************************
c opening an output file
     character *64 FILENAME
1    format(A64)
     write(*,*)'enter the output filename:'
     read(*,1)FILENAME

     open(5,file=FILENAME,status='new')
```

```
      d=1.984
c reads in the input
      write(*,*)'enter x/d:'
      read(*,*)xd
c
      if(xd .lt. 100)then
        up0 = 16.65487*(xd**0.054489)
      else
        up0 = 9.301764*(xd**0.1769854)
      endif
c calculates the wake width
      b = 0.476759*d*(xd**0.569376)/1.772
      db = 0.476759*0.569376*(xd**(0.569376-1))/1.772
c calculates the maximum wake velocity defect
      if(xd .lt. 100)then
        u1m = 22.8643*(xd**-0.604982)
        du1m = -22.8643*0.604982*(xd**(-1.604982))/d
      else
        u1m = 69.42161*(xd**-0.8492)
        du1m = -69.42161*0.8492*(xd**-1.8492)/d
      endif
c calculated the radius of curvature
      r = -0.7011e+3 - 0.30234e+1*xd + 0.22708e-1*(xd**2)
     *           - 0.41328e-4*(xd**3)
c
      do y = -125,125,2.5
      z = y/b
      u = up0*(1-z*b/r) - u1m*exp(-z*z)
      write(5,*)y,u
      enddo

      stop
      end

************************************************************
************************************************************
C     PROGRAM FOR THE LATERAL VELOCITY (V) DISTRIBUTION
************************************************************
character *64 FILENAME
1     format(A64)
      write(*,*)'enter the output filename:'
      read(*,1)FILENAME

      OPEN(5,FILE=FILENAME,STATUS='NEW')

      d = 1.984
      pi = 4.0*atan(1.0)
      sfac = sqrt(pi)/2.0
```

```
      call input(xd,r)
      call wkwidth(xd,d,b,db)
      call uu1m(xd,d,b,a,u1m,up0,dup0,du1m)
      call output(xd,d,r,b,db,a,u1m,up0,dup0,du1m)

      do x = -2.0,2.0,0.05
      z = x*1.772
      g = exp(-z*z)
      t = r/(r+b*z)
      vr = z*b/r
c nondimensional (V/U_1m)
      y = -t*b/u1m*dup0*z*(1.-vr/2) - t*db*(z*g-sfac*erf(z))
     *           + t*b/u1m*du1m*sfac*erf(z)
      write(5,*)x,y
      enddo

      stop
      end
*************************************************************
subroutine input(xd,r)
*************************************************************
write(*,*)'enter x/d'
      read(*,*)xd
c
      r = -0.7011e+3 - 0.30234e+1*xd + 0.22708e-1*(xd**2)
     *           - 0.41328e-4*(xd**3)

      return
      end
*************************************************************
subroutine wkwidth(xd,d,b,db)
*************************************************************
b = 0.476759*d*(xd**0.569376)/1.772
      db = 0.476759*0.569376*(xd**(0.569376-1))/1.772

      return
      end
*************************************************************
subroutine uu1m(xd,d,b,a,u1m,up0,dup0,du1m)
*************************************************************
if(xd .lt. 100)then
        up0 = 16.65487*(xd**0.054489)
        dup0 = 16.65487*0.054489*(xd**(0.054489-1))/d
      else
        up0 = 9.301764*(xd**0.1769854)
        dup0 = 9.301764*0.1769854*(xd**(0.1769854-1))/d
      endif
```

```
c
      if(xd.lt.100)then
        u1m = 22.8643*(xd**-0.604982)
        du1m = -22.8643*0.604982*(xd**(-1.604982))/d
      else
        u1m = 69.42161*(xd**-0.8492)
        du1m = -69.42161*0.8492*(xd**-1.8492)/d
      endif
c
      a = up0/u1m

      return
      end
*****************************************************************
subroutine output(xd,d,r,b,db,a,u1m,up0,dup0,du1m)
*****************************************************************
print*,'x/d=',xd,'    d=',d,'    r=',r
      print*,'b=',b*1.772,'    db=',db
      print*,'    dup0=',dup0,'    b/d=',b*1.772/d
      print*,'u/u_1m=',a,'    u1m=',u1m,' up0=',up0
      print*,'du1m=',du1m

      return
      end
*****************************************************************
*****************************************************************
c     PROGRAM FOR REYNOLDS SHEAR STRESS
*****************************************************************
character *64 FILENAME
1     format(A64)
      write(*,*)'enter the output filename:'
      read(*,1)FILENAME

      OPEN(5,FILE=FILENAME,STATUS='NEW')

      d = 1.984
      pi = 4.0*atan(1.0)
      sfac = sqrt(pi)/2.0

      write(*,*)'enter value of shear stress at z=0:'
      read(*,*)uvatz0
c
      call input(xd,r)
      call wkwidth(xd,d,b,db)
      call uu1m(xd,d,b,a,u1m,up0,dup0,du1m)
      call output(xd,d,r,b,db,a,u1m,up0,dup0,du1m)
c
      do x = -2.0,2.0,0.05
```

```
      z = x*1.772
      g = exp(-z*z)
      t = r/(r+b*z)
      vr = z*b/r
c
      term1 = -t*up0/(u1m**2)*dup0*b*z*vr/2.*(1.-vr/3.)
      term2 = -t*up0/u1m*db*(z*g-b*g/r*(2.+z*z)
     *          - sfac*erf(z)*(1.+vr))
      term3 = t*db*(z*g*(1.-g)-sfac*erf(z)*(1.-g))
      term4 = t*up0/(u1m**2)*du1m*b*
     *          (b*g/r+sfac*erf(z)*(1.+vr))
      term5 = t*b/u1m*dup0*(2.*sfac*erf(z)
     *          + b*g/r*(1.+0.5*z*z)-z*g)
      term6 = -t*b/u1m*du1m*(sfac*erf(z)*(2.-g))
      const = uvatz0 - 2.*a*db*b/r - up0/(u1m**2)*du1m*b*b/r
     *          - b/u1m*dup0*b/r
      y = term1+term2+term3+term4+term5+term6+const
      write(5,*)x,y
      enddo

      write(5,*)'const=',const

      stop
      end
**************************************************************
subroutine input(xd,r)
**************************************************************
write(*,*)'enter x/d'
      read(*,*)xd
c
      r = -0.7011e+3 - 0.30234e+1*xd + 0.22708e-1*(xd**2)
     *      - 0.41328e-4*(xd**3)

      return
      end
**************************************************************
subroutine wkwidth(xd,d,b,db)
**************************************************************
      b = 0.476759*d*((xd)**(0.569376))/1.772
      db = 0.476759*0.569376*((xd)**(0.569376-1))/1.772

      return
      end
**************************************************************
subroutine uu1m(xd,d,b,a,u1m,up0,dup0,du1m)
**************************************************************
if(xd .lt. 100)then
       up0 = 16.65487*(xd**0.054489)
```

```
        dup0 = 16.65487*0.054489*(xd**(0.054489-1))/d
      else
        up0 = 9.301764*(xd**0.1769854)
        dup0 = 9.301764*0.1769854*(xd**(0.1769854-1))/d
      endif
c
      if(xd.lt.100)then
        u1m = 22.8643*(xd**-0.604982)
        du1m = -22.8643*0.604982*(xd**(-1.604982))/d
      else
        u1m = 69.42161*(xd**-0.8492)
        du1m = -69.42161*0.8492*(xd**-1.8492)/d
      endif
c
      a = up0/u1m

      return
      end
*****************************************************************
subroutine output(xd,d,r,b,db,a,u1m,up0,dup0,du1m)
*****************************************************************
print*,'x/d=',xd,'   d=',d,'   r=',r
      print*,'b=',b*1.772,'   db=',db
      print*,'   dup0=',dup0,'   b/d=',b*1.772/d
      print*,'u/u_1m=',a,'   u1m=',u1m,' up0=',up0
      print*,'du1m=',du1m
      return
      end
*****************************************************************
```

# REPORT DOCUMENTATION PAGE

Form Approved
OMB No. 0704-0188



| 1. AGENCY USE ONLY (*Leave blank*) | 2. REPORT DATE | 3. REPORT TYPE AND DATES COVERED |
|---|---|---|
| | January 1996 | Final Contractor Report |

**4. TITLE AND SUBTITLE**

Prediction of Characteristics of Two Dimensional Turbulent Wakes Under the Influence of Streamline Curvature and Zero, Positive, and Negative Pressure Gradients, Part II

**5. FUNDING NUMBERS**

WU-505-90-52
G-NAG3-1256

**6. AUTHOR(S)**

M.T. Schobeiri and K.R. Pappu

**7. PERFORMING ORGANIZATION NAME(S) AND ADDRESS(ES)**

Texas A&M University
Department of Mechanical Engineering
College Station, Texas 77843

**8. PERFORMING ORGANIZATION REPORT NUMBER**

E-10098

**9. SPONSORING/MONITORING AGENCY NAME(S) AND ADDRESS(ES)**

National Aeronautics and Space Administration
Lewis Research Center
Cleveland, Ohio 44135-3191

**10. SPONSORING/MONITORING AGENCY REPORT NUMBER**

NASA CR-198449

**11. SUPPLEMENTARY NOTES**

Project Manager, Barbara L. Lucci, Internal Fluid Mechanics Division, NASA Lewis Research Center, organization code 2630, (216) 433-5902.

**12a. DISTRIBUTION/AVAILABILITY STATEMENT**

Unclassified - Unlimited
Subject Category 34

This publication is available from the NASA Center for Aerospace Information, (301) 621-0390.

**12b. DISTRIBUTION CODE**

**13. ABSTRACT** (*Maximum 200 words*)

The development of a wake flow downstream of a cylindrical rod within a curved channel under turbomachinery flow conditions (streamline curvature, and zero, positive and negative pressure gradients) has been investigated theoretically. The theoretical framework is based on the equations of continuity and motion that are transformed into an orthogonal curvilinear coordinate system. These equations describing the wake phenomenon are solved for mean velocities, and Reynolds normal and shear stresses. The theory also describes the straight wake as a special case, for which the radius of curvature approaches infinity. To demonstrate its general validity, the theory has been compared with experimental measurements made available from the Turbomachinery Performance Laboratory at Texas A&M University as well as from the current literature.

| 14. SUBJECT TERMS | 15. NUMBER OF PAGES |
|---|---|
| Wake flow; Curvature; Pressure gradient | 158 |
| | 16. PRICE CODE: A08 |

| 17. SECURITY CLASSIFICATION OF REPORT | 18. SECURITY CLASSIFICATION OF THIS PAGE | 19. SECURITY CLASSIFICATION OF ABSTRACT | 20. LIMITATION OF ABSTRACT |
|---|---|---|---|
| Unclassified | Unclassified | Unclassified | |

National Aeronautics and
Space Administration

**Lewis Research Center**
21000 Brookpark Rd.
Cleveland, OH 44135-3191